

**Water Vapor in the Tropical Upper Troposphere:
On the Influence of Deep Convection**

Inaugural-Dissertation
zur
Erlangung des Doktorgrades
der Mathematisch-Naturwissenschaftlichen Fakultät
der Universität zu Köln

vorgelegt von
Susanne Nawrath
aus Köln

Köln 2002

Berichterstatter: Prof. Dr. P. Speth
Prof. Dr. D. Kley

Tag der mündlichen Prüfung: 22. Mai 2002

Abstract

Water vapor is one of the most important trace gases in the atmosphere. It has significant impact on climate, chemistry, and the energy budget. Of particular interest is the water vapor distribution in the upper troposphere, especially in the tropics.

The major source of water vapor for the tropical upper troposphere is deep convection. The dynamically as well as radiatively induced subsidence, on the other hand, balances the convective motion and transports relatively dry air downwards. The net effect of both processes is not well understood, due to a lack of reliable measurements in this region.

In this work the water vapor content of the upper tropical troposphere and the mechanisms responsible for the water vapor distribution are studied with an extensive dataset of in-situ measurements of the relative humidity. The measurements were carried out on board commercial aircraft in the scope of the EU project MOZAIC (**M**easurements of **O**zone and **W**ater Vapor by **A**irbus In-Service **A**ir**C**raft).

A climatological view on the measured parameters over the tropical Atlantic ocean shows that the humidity is highly variable on all temporal and spatial scales. The humidity distribution in the tropics, with its bimodal shape, differs strongly from the distribution in the subtropics or midlatitudes. In addition, a more detailed analysis of the processes influencing the water vapor distribution in areas of subsidence is performed. The convective origin of the measured air is traced with backward trajectories, and convective clouds are identified independently with Meteosat satellite measurements of the cloud top temperature.

It is found that the convective origin of the measured air lies relatively close to the location of the measurement especially in the inner tropics. In particular, the meridional exchange is very weak. In the subsiding convective outflow the relative humidity decreases more slowly than it would be expected from radiative transfer models for solely radiatively induced subsidence under clear-sky conditions. The occurrence of supersaturation with respect to ice indicates a significant influence of subvisible cirrus clouds on the radiation budget in the vicinity of deep convective towers. After about one day of advection away from the convective cloud the mean relative humidity stays almost constant. This is likely due to small-scale mixing processes, as suggested by the mean development of the simultaneously measured ozone concentration.

Kurzzusammenfassung

Wasserdampf ist eines der wichtigsten atmosphärischen Spurengase. Sein Einfluss auf das Klima, die Chemie und den Energiehaushalt ist bedeutend. Von besonderem Interesse ist dabei die Wasserdampfverteilung in der oberen Troposphäre insbesondere in den Tropen.

Die wichtigste Wasserdampfquelle für die tropische obere Troposphäre ist tropische Konvektion. Ihr wirkt das grossräumige Absinken entgegen, das seine Ursache sowohl in der Dynamik als auch im Strahlungshaushalt hat. Es gleicht die konvektive Aufwärtsbewegung aus und transportiert dabei relativ trockene Luft nach unten. Über den Netto-Effekt dieser beiden Prozesse ist wenig bekannt, vorallem wegen eines Mangels an zuverlässigen Messungen in dieser Region.

In dieser Arbeit werden der Wasserdampfgehalt und die Mechanismen, die für die Wasserdampfverteilung in der oberen tropischen Troposphäre verantwortlich sind, mithilfe einer grossen Menge an in-situ Feuchtemessungen untersucht. Die Messungen wurden auf Linienflugzeugen im Rahmen des EU Projektes MOZAIC durchgeführt (**M**eamurements of **O**zone and **W**ater Vapor by **A**irbus In-Service **A**ir**C**raft; Messungen von Ozon und Wasserdampf auf Airbus Linienflugzeugen).

Eine Klimatologie der gemessenen Parameter über dem tropischen Atlantik zeigt, dass die Feuchte auf allen zeitlichen und räumlichen Skalen sehr variabel ist. Die bimodale Verteilung der Feuchte in den Tropen unterscheidet sich ausserdem deutlich von der Verteilung in den Sub-Tropen oder mittleren Breiten. Ausserdem wurden die Prozesse, die die Wasserdampfverteilung in den Gebieten mit absinkender Luft bestimmen, genauer untersucht. Der konvektive Ursprung der Luft wurde dabei mithilfe von Rückwärts-Trajektorien zurückverfolgt und die konvektiven Wolken wurden unabhängig davon mit Meteosat Satelliten-Messungen der Wolkenoberflächentemperatur identifiziert.

Es zeigt sich, dass der konvektive Ursprung insbesondere in den inneren Tropen relativ nah an den Messungen liegt. Besonders der meridionale Austausch ist sehr schwach. In der Luftströmung, die die konvektiven Wolken verlässt und dabei absinkt, nimmt die relative Feuchte langsamer ab, als es aus Ergebnissen von Strahlungsmodellen erwartet würde, die ein rein strahlungsbedingtes Absinken unter wolkenlosen Bedingungen voraussetzen. Das Auftreten von Eis-Übersättigung deutet darauf hin, dass optisch dünne Cirrus Wolken in der Nähe der konvektiven Türme einen bedeutenden Einfluss auf den Strahlungshaushalt haben. Nach etwa einem Tag Advektion von der konvektiven Wolke bleibt die relative Feuchte fast konstant. Dafuer sind sehr wahrscheinlich kleinskalige Mischungsprozesse die Ursache, worauf die mittlere Entwicklung der gleichzeitig gemessenen Ozonkonzentration hinweist.

Contents

| | |
|------------------------------------------------------|------------|
| Abstract | iii |
| Kurzzusammenfassung | iv |
| List of Abbreviations | vii |
| 1 Introduction | 1 |
| 2 Water Vapor | 5 |
| 2.1 Circulation in the Tropics | 5 |
| 2.2 The Greenhouse Effect | 7 |
| 2.3 Ozone over the Tropical Atlantic Ocean | 10 |
| 2.4 Deep Convection | 11 |
| 2.5 Previous Studies | 12 |
| 3 The MOZAIC Project | 15 |
| 4 Climatology of MOZAIC Data | 19 |
| 4.1 Flight Characteristics | 19 |
| 4.2 Relative Humidity Distribution | 22 |
| 4.3 Seasonal Variability | 24 |
| 4.4 Mean Latitudinal Variability | 26 |
| 4.5 Interannual Variability | 28 |
| 4.6 Comparison with ECMWF | 29 |
| 4.7 Ozone Variability | 32 |
| 5 Origin of the Water Vapor | 35 |
| 5.1 Concept for Tracing the Origin | 35 |
| 5.2 Trajectories by Meteo France | 36 |
| 5.3 Cloud Top Temperature | 40 |
| 5.4 Sea Surface Temperature | 43 |
| 5.5 Tracing Convective Clouds | 45 |
| 5.6 The Origin of the Measured Air | 47 |
| 5.6.1 Trajectory Length and Field of View | 47 |

| | | |
|----------|---------------------------------------------------|------------|
| 5.6.2 | Identifying Source Regions | 49 |
| 5.6.3 | Distance Between Measurement and Cloud | 50 |
| 6 | Convection | 53 |
| 6.1 | The Vicinity of Convective Clouds | 54 |
| 6.1.1 | Variability with Altitude | 55 |
| 6.1.2 | Seasonal Variability | 58 |
| 6.1.3 | Ozone Variability | 61 |
| 6.1.4 | Influence of SST | 63 |
| 6.2 | Advection Away From Convective Regions | 67 |
| 6.2.1 | Development of Humidity | 68 |
| 6.2.2 | Development with Spatial Distance | 71 |
| 6.2.3 | Development of Ozone | 73 |
| 7 | Processes in Convective Outflow | 75 |
| 7.1 | Introduction | 75 |
| 7.2 | Subsidence During Large-Scale Advection | 77 |
| 7.3 | Analysis of Processes | 80 |
| 7.3.1 | Comparison with Model Results | 80 |
| 7.3.2 | The First Half of the First Day | 83 |
| 7.3.3 | The Second Half of the First Day | 84 |
| 7.3.4 | The Second Day | 84 |
| 7.4 | Conclusion | 85 |
| 8 | Summary and Outlook | 87 |
| A | Additional Graphs | 91 |
| | Bibliography | 94 |
| | Danksagung/Acknowledgements | 105 |
| | Zusammenfassung | 107 |

List of Abbreviations

| | |
|---------|----------------------------------------------------------------------------|
| AVHRR | Advanced Very High Resolution Radiometer |
| CCM2 | Community Climate Model Version 2 |
| CDS | Climate Data Set |
| corir | corrected infrared count |
| CTT | Cloud Top Temperature |
| DLR | Deutsches Zentrum für Luft- und Raumfahrt |
| ECMWF | European Centre for Medium-Range Weather Forecasts |
| ERBE | Earth radiation buget experiment |
| INDOEX | Indian Ocean Experiment |
| ITCZ | Innertropical Convergence Zone |
| MARF | Meteorological Archive and Retrieval Facility |
| MJO | Madden-Julian Oscillation |
| MLS | Microwave Limb Sounder |
| MOZAIC | Measurement of Ozone and Water Vapor by Airbus In-Service Aircraft |
| N.H. | Northern Hemisphere |
| OLR | Outgoing Long-Wave Radiation |
| POLINAT | Pollution from Aircraft Emissions in the North Atlantic Flight Corridor |
| PV | Ertel's Potential Vorticity |
| SHADOZ | Southern Hemisphere Additional Ozonesondes |
| SST | Sea Surface Temperature |
| UARS | Upper Atmosphere Research Satellite |

Chapter 1

Introduction

In the last decades the public has become more and more aware of the issue of climate change and the anthropogenically enhanced greenhouse effect. For the understanding and prediction of the future evolution of the climate system, water vapor and clouds are the strongest sources of uncertainty (Stocker et al., 2001).

Water vapor is also the most important contributor to the natural greenhouse effect of the Earth's atmosphere (e.g., Raval and Ramanathan (1989); Held and Soden (2000)). It is called 'greenhouse effect' as the atmosphere is permeable to the incoming solar radiation, but holds the infrared terrestrial radiation back like a glasshouse. Water vapor and clouds are the main contributors together with several other trace gases like carbon dioxide and methane.

The anthropogenic enhancement of the greenhouse effect leads to a change in the radiative balance of the Earth-atmosphere system that could result in a rise of the mean surface temperature. It is mainly triggered by carbon dioxide emissions from fossil fuel burning since the industrial revolution. The direct effect of the rising CO₂ concentration in the atmosphere is small, though. It is significantly enhanced by the so-called water vapor feedback. As the atmosphere gets warmer its capability of holding water vapor increases exponentially with temperature. It can therefore absorb more radiation and is warmed further. With the help of model simulations this positive feedback effect is estimated to amplify the initial radiative forcing by about a factor of two (e.g., Manabe and Wetherald (1967); Held and Soden (2000)). The tropics are the region with the largest greenhouse effect which is strongly correlated with the surface temperature (Raval and Ramanathan, 1989). The water vapor feedback is also stronger in warmer regions as the saturation water vapor pressure increases with temperature (Clausius-Clapeyron relation). Over the warmest areas of the oceans, even an unstable amplification of the greenhouse effect is possible, the so-called 'supergreenhouse effect' (Ramanathan and Collins, 1991). The fact that there is an upper limit on the sea surface temperatures measured currently and that paleoclimatic records are interpreted to point at a relatively stable sea surface

temperature in the tropics in history gives indication for other (negative) feedback effects that act to stabilize the surface temperature.

There is a vivid ongoing discussion about possible negative feedback mechanisms involving the interaction between the sea surface temperature, tropical deep convection, and the water vapor distribution in the tropical upper troposphere. Lindzen (1990) proposed a drying effect of higher reaching deep convection at higher sea surface temperatures leading to less moisture in the subsiding regions outside the convection, which would allow more energy to be emitted to space due to a weaker greenhouse effect. Ramanathan and Collins (1991), on the other hand, suggest their 'Thermostat-Hypothesis' from finding a shielding effect of the enhanced deep convection against incoming solar radiation. Pierrehumbert (1995) favors lateral transport of energy into drier regions, and Lindzen et al. (2001) propose a regulating mechanism based on an increase of the relative area of dry regions in the tropics with increasing surface temperature. The importance of the dry regions for global climate is also stressed by Spencer and Braswell (1997) as well as the fact that there is little known about these regions due to a lack of measurements. Balloon soundings are mainly taken from land stations, but the largest area of the tropics is covered by oceans which are also the main source of water vapor. The few satellite measurements of upper tropospheric water vapor are not very reliable as well, and they cannot provide the resolution necessary to study small-scale phenomena like convection (e.g., Chen et al. (1999); Jensen et al. (1999)).

One of the key questions regarding the dryness of the tropics in the clear sky areas outside deep convection is to what extent deep convection influences the humidity of the surrounding air. Although less than 1% of the tropics are covered by deep convective clouds (Riehl, 1979), they are the main water vapor source for the tropical upper troposphere (Betts, 1990). Therefore, the development of the relative humidity during the transport away from these clouds is of particular interest. It is assumed to be influenced mainly by radiative cooling resulting in subsidence and adiabatic warming. There have been several previous studies of the processes influencing the humidity during the transport of the air away from the convection. All of them have been done with the help of satellite humidity measurements. Udelhofen and Hartmann (1995), Salathé and Hartmann (1997), and Soden (1998) use the U.S. meteorological geostationary satellite GOES 6.7 μ m channel brightness temperatures. These have only a very low vertical resolution as the derived relative humidity values represent an average over the layer between 550 and 200 hPa with the largest contribution from around 400hPa. Therefore, they can not resolve the altitude region with the strongest sensitivity of outgoing long-wave radiation against changes in the relative humidity, between 300hPa and 200hPa. The Upper Atmosphere Research Satellite (UARS) Microwave Limb Sounder (MLS) measurements used by McCormack et al. (2000) have a better vertical resolution (215 ± 25 hPa), but only a limited horizontal resolution with a horizontal footprint of approximately 100×200 km² (per-

pendicular and parallel to the line of sight, respectively) (Read et al., 2001). An additional limitation of all satellite measurements is that the humidities have to be retrieved from a measured brightness temperature and are not measured directly. Neither the GOES, nor the MLS vertical resolution allows to draw conclusions from the derived mean relative humidity on the specific humidity, as the specific humidity depends strongly on temperature and varies by more than one order of magnitude in the pressure range from 190hPa to 240hPa (MLS pressure range).

For this thesis, measurements in the scope of the MOZAIC project (**M**asurement of **O**zone and **W**ater Vapor by **A**irbus **I**n-service **A**ir**C**raft) (Marenco et al., 1998) are used to study the humidity in the tropical upper troposphere over the Atlantic ocean. The question how the relative humidity in the upper troposphere is influenced by convection is addressed with the help of backward trajectories calculated from European Centre for Medium-Range Weather Forecasts (ECMWF) analysis to determine the distance to the convective cloud from which the air parcel the measurement is taken in originates. And the convective clouds are identified with the help of Meteosat satellite cloud top temperature data.

The MOZAIC project provides a database of reliable and quasi-continuous in-situ measurements starting in August 1994. Relative humidity, temperature and ozone are measured onboard five commercial aircraft of major European airlines during scheduled flights. Most measurements are taken at cruise altitude between 300hPa and 200hPa on distinct pressure levels and the measurement coordinates are the exact position parameters of the aircraft. The exactly measured pressure and temperature allow to determine the specific humidity from the relative humidity measurements. A dataset with measurements every minute along the aircraft path is used corresponding to a horizontal resolution of 15km. After a discussion of the theoretical background in chapter 2, the MOZAIC project will be presented in chapter 3 and the obtained water vapor measurements in chapter 4 to provide a general idea of the humidity distribution in the region of interest. In chapter 5 the method developed to trace the convective origin of the measured water vapor in the tropical upper troposphere with the help of a trajectory analysis and additional satellite data of cloud top temperatures is explained. It is assumed that the air in the upper tropical troposphere must have been transported upwards in a convective cloud and is advected from there. Backward trajectories are necessary to find the convective cloud the air originates, and the clouds are identified with the help of satellite data. This way, the length of time the air parcel undergoes radiative cooling and subsidence during the transport from the cloud to the aircraft is determined. The sea surface temperature at the determined location of the convective cloud is also considered regarding its influence on the convection. Chapter 6 gives an overview over the humidity measurements and other parameters in different distances from the convection. In chapter 7 the processes influencing the humidity along the trajectory during the transport away from the convection are discussed. With the help of a

conceptual model the vertical velocity along every trajectory is calculated and a radiative cooling rate is determined. The comparison of this radiative cooling rates with values found in the literature allows to draw conclusions about the relevant processes.

Chapter 2

Water Vapor in the Tropical Upper Troposphere

In this chapter the processes influencing the humidity of the air that is detrained from convective clouds and transported into the dry regions are put into their theoretical and scientific context. Factors influencing the water vapor distribution in the tropical upper troposphere are considered and the importance of this distribution for the climate system is stressed. In addition, previous work concerned with this problem is discussed.

2.1 Circulation in the Tropics

The tropics are particularly important for global climate because by far most of the solar short-wave radiation is absorbed in this part of the world which covers half of the Earth's surface. This absorption is only partly balanced by local emission of long-wave radiation to space while at the poles there is an excess of emission relative to the weaker solar insolation. Through the necessary poleward transport of energy and momentum the global circulation of the atmosphere and oceans is driven (e.g., Speth and Madden (1987); Curry and Webster (1999)).

Deep convection in the equatorial region in the innertropical convergence zone (ITCZ) moves latent heat and moisture to the upper troposphere very efficiently. It is the main part of the mean tropical meridional circulation, the so-called Hadley circulation, which consists of two closed loops symmetrical to the equator with convection in the ITCZ, an upper tropospheric poleward flow, subsiding air in the subtropical anticyclone region, and a near surface equatorwards return flow by the trade winds. Viewed in detail, this circulation is much more complex, though. The ITCZ is defined as the area close to the equator with the lowest pressure and the highest surface temperatures where the tropical trade winds from both hemispheres converge (Riehl, 1979). It is also the region with the strongest convective activi-

ty, where precipitation exceeds evaporation significantly, and where the outgoing long-wave radiation (OLR) has a local minimum due to the surface radiation being trapped in the deep convective clouds. Over the continents, the ITCZ almost follows the latitude with the highest solar zenith angle, but can reach further poleward for example during monsoon over the Indian subcontinent. Over the western Pacific ocean warmpool it can be split into two branches, while it remains rather stable over the eastern Pacific and the Atlantic ocean. There, it is located between the equator and 10°N during the whole year (Waliser and Gautier, 1993). Waliser and Somerville (1994) review possible reasons for this and present results from a study with a simplified, linearized model showing that the preferred location of the ITCZ is not necessarily related to the SST maximum, but can be explained at least partly from shallow water theory. The convective activity inside the ITCZ is not uniform around the globe. There are clusters with stronger deep convection indicated by clouds which can reach up to the tropopause at 18km. These clusters seem to move along the ITCZ, with the formation of new convective clouds in another area as the older clouds are decaying, while other parts are virtually free of clouds (Riehl, 1979). Deep convection is also influenced by planetary-scale wave-like phenomena on different frequency bands called Madden-Julian oscillation (MJO), which are most pronounced in the Pacific region but also found over the Atlantic ocean (Madden and Julian, 1971, 1994; Vincent et al., 1998). The strong convective upward flow that is concentrated in narrow towers, the so-called hot towers, covering less than 1% of the area of the tropics (Riehl, 1979) is balanced by a large-scale subsiding motion due to radiative cooling of the moist air in the surrounding which suppresses the formation of deep convective towers there.

The part of the Hadley circulation that differs most from the historical concept and the zonal mean is the upper tropospheric flow. There is no poleward upper tropospheric flow that is as strong as the trade winds and a sinking motion only in the subtropical anticyclones. The actual flow is only very weakly directed poleward but over a greater altitude range as the trade winds. In addition, in the whole area between the ITCZ and the subtropics and in parts of the ITCZ, where there is no convection, the air is radiatively cooling and subsiding (Held and Soden, 2000).

Superimposed on the meridional Hadley circulation there is an important zonal circulation system which is called Walker circulation (e.g., Hastenrath (1991); Philander (1990)) (figure 2.1). It consists of rising branches over the continents and the Pacific warmpool and subsidence over the oceans. Its most discussed part is the Southern Oscillation over the Pacific Ocean. When this part breaks down every few years it leads to El Niño events. Over the Atlantic Ocean the Walker Circulation induces subsidence over the western coastal area of Africa and rising motion over the Amazon basin. The schematic view of the Walker circulation along the equator shows that the rising branches of the circulation are connected to the continents.

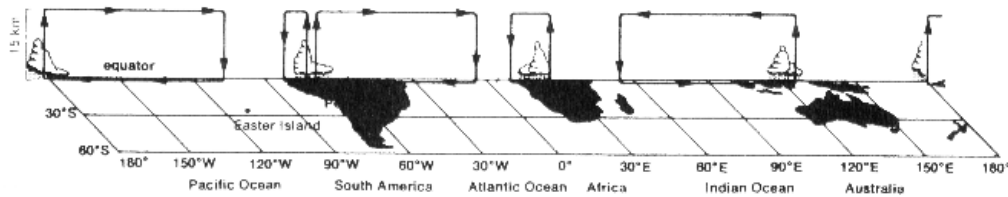


Figure 2.1: Schematic view of the Walker circulation at the equator (from Newell (1979)).

2.2 The Greenhouse Effect and its Regulation

The temperature of the Earth and its atmosphere is determined by the difference of the energy amount of solar short-wave radiation reaching and terrestrial long-wave radiation leaving the Earth's surface. The globally averaged amount of energy from the solar incoming short-wave radiation reaching the Earth-atmosphere system is 342Wm^{-2} (figure 2.2). Without the greenhouse effect the Earth's surface would be in radiative balance at a mean temperature of -19°C . The actual mean temperature of about 14°C is obtained mainly through the radiative effects of water vapor and clouds (Baede et al., 2001). The long-wave emission from the surface is absorbed and warms the atmosphere which then reemits it to space. The energy amount emitted decreases with decreasing temperature of the emitter (Stefan-Boltzmann law, $W = \sigma T^4$) and thus the energy emitted by the upper troposphere is lower than that emitted by the Earth's surface. This allows the surface to be warmer than it would be without the atmosphere. The warming effect is largest if the radiation is absorbed and reemitted at higher altitudes with lower temperature. This is why the warming effect of water vapor in the upper troposphere and thin cirrus clouds, which do not reflect much solar radiation but reemit long-wave radiation at very low temperatures, is the highest (Arking, 1991). This effect is called the natural greenhouse effect as the atmosphere is permeable to the incoming solar radiation but holds the infrared radiation back like a glasshouse. Water vapor and clouds provide approximately 80% of the greenhouse effect, with minor contributions by several other trace gases like carbon dioxide and methane (Curry and Webster, 1999) (figure 2.2). The anthropogenic enhancement of the greenhouse effect is mainly triggered by carbon dioxide emissions through fossil fuel burning since the industrial revolution. The larger absorption of infrared emission reduces the amount of energy that is emitted to space and could be balanced by a warming of the Earth-atmosphere system. The direct effect of the rising CO_2 concentration in the atmosphere is small, though. It is significantly enhanced by the so-called water vapor feedback. As the atmosphere gets warmer it is capable to hold more water vapor as the saturation vapor pressure increases exponentially with temperature (Clausius-Clapeyron), can absorb more radiation and is thus warmed further. Without any regulating mechanism this

solely thermodynamical control of the water vapor content could result in a runaway greenhouse effect (Raval and Ramanathan, 1989; Ramanathan and Collins, 1991). Several observations have led to the conclusion that a regulating mechanism must be present in the atmosphere. First, an upper threshold for the sea surface temperature (SST) is observed, although it would be expected that a solely positive feedback would lead to a further enhancement of the surface temperature (Graham and Barnett, 1987). The second phenomenon is the relative stability of the tropical sea surface temperature during the last glaciation. Paleoclimatic records of foraminifera assemblages (CLIMAP, 1976) were interpreted in a way, that the surface temperature in the tropics was no more than about 1°C cooler, although the snowline record shows a lower snowline that is consistent with a temperature reduction by 5°C in the mid-troposphere (Sun and Lindzen, 1993b). Only more recent data indicate that the surface in the tropics may as well have been cooler during the last glacial maximum by approximately 5°C (Guilderson et al., 1994; Stute et al., 1995).

There is a controversial discussion in the scientific community about possible stabilizing feedback mechanism. Lindzen (1990) raised the question whether the possible climate change was lower than expected from calculations with climate models, due to a possible negative feedback related to the convective activity in the tropics. The main mechanism for a negative feedback would be the enhanced drying of the surrounding atmosphere if the convective towers reach higher altitudes and thus lower

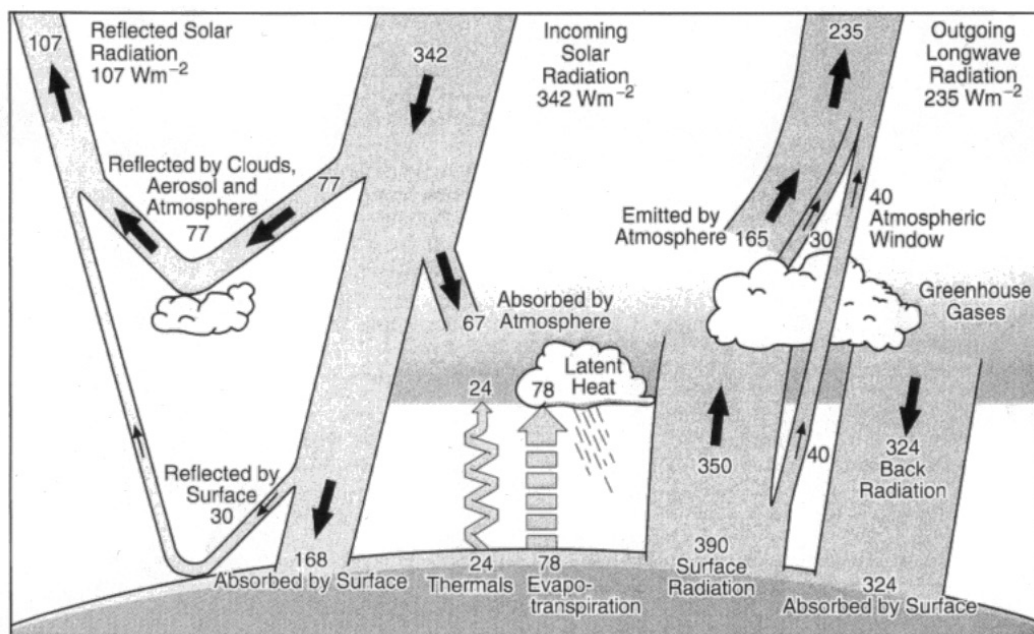


Figure 2.2: Earth radiation budget illustrating the natural greenhouse effect (from Kiehl and Trenberth (1997)).

temperatures so that more water vapor freezes out. One of the best known and most discussed theories about such a negative feedback is the so-called 'Thermostat-Hypothesis' by Ramanathan and Collins (1991). From the study of radiation budget observations with the Earth radiation budget experiment (ERBE) (e.g., Harrison et al. (1990)) they propose that under warming conditions there is enhanced cumulonimbus convective activity which leads to a higher altitude, wider spreading, and greater thickness of the cirrus anvils in the upper troposphere. These anvils then reflect more solar radiation and thus shield the surface from further warming. This hypothesis was opposed by several researchers with different explanations, e.g. Fu et al. (1992) and Pierrehumbert (1995). While the former present evidence from satellite data that the cloud anomalies are not connected to SST anomalies, the latter deduced from a simple model of the tropical troposphere, that the warming and cooling effects from clouds almost cancel out, but lateral heat transport from convective regions into dry regions with efficient radiative cooling could be sufficient to prevent a runaway greenhouse. Wallace (1992) argues similarly, that the uniform temperature distribution in the tropics hints to an effective lateral transport which would allow for a rapid redistribution of locally enhanced water vapor concentrations. Very recently, from observations of clouds and water vapor Lindzen et al. (2001) found evidence for a similar mechanism, the increase of dry, clear-sky area and the decrease of humid and cloudy areas with increasing SST. They call it 'Iris effect' as this mechanism would be able to regulate the greenhouse effect depending on the surface temperature as the iris of an eye can adapt to different light conditions. These theories are based on the fact that the absorption and emission of long-wave radiation is most sensitive to changes in the water vapor concentration in the tropical upper troposphere where the background specific humidity is very low (Spencer and Braswell, 1997). Moreover, they propose a primarily dynamical control of the upper tropospheric humidity in the tropics with moistening through deep convection interacting with the sea surface temperature and drying through convectively or radiatively induced subsidence.

The interaction between deep convection and the SST as a possible key to negative feedback has been the subject of many studies (e.g., Bony et al. (1995, 1997); Chiang et al. (2001); Gadgil et al. (1984); Hartmann and Michelsen (1993); Inamdar and Ramanathan (1994, 1998); Lau et al. (1997); Newell et al. (1997); Raval and Ramanathan (1989); Stephens (1990)). The minimum threshold temperature necessary but not sufficient for the formation of deep convection is approximately 300K (Gadgil et al., 1984; Graham and Barnett, 1987). At higher SST deep convection can still be suppressed by the above mentioned large-scale phenomena, namely the Walker circulation or the MJO. Graham and Barnett (1987) showed, for example, that the highest sea surface temperatures which are found coincide with areas of diminished convection whereas strongest convection would be expected. They argue that these high SSTs are only possible in areas with for other reasons diminished convective activity as the latter acts to regulate the SST. This result is supported

by findings from Waliser et al. (1993). Deep convection can possibly be regulated in another way. Kley et al. (1999) proposed that large amounts of dry air may be laterally entrained in deep convective towers and restrain their strength. These regulating processes make it difficult to obtain unequivocal results concerning the interaction between water vapor and the sea surface temperature.

2.3 Ozone over the Tropical Atlantic Ocean

In their above mentioned study Kley et al. (1999) take advantage of the fact that the marine boundary layer over the remote ocean is ozone depleted (Winkler, 1988). Due to low NO_x levels ($< 10\text{ppt}$) ozone is destroyed in a photolytic reaction:



Typical ozone mixing ratios over the remote tropical ocean range between 10 and 20 ppbv (Thompson et al., 2002). If the ozone depleted air is lifted rapidly in a deep convective motion into the upper troposphere its ozone content will stay low as the lifetime of ozone in the upper troposphere increases with the decreasing water vapor concentrations to about 100 days. This way, air from convective origin can be identified by its low ozone content for several days and the magnitude of the ozone concentration can provide insight into mixing processes with surrounding air (Kley et al., 1996, 1997). Low mixing ratios near 20 ppbv indicate transport of undiluted boundary layer air into the upper troposphere and higher mixing ratios can originate either from entrainment during the convective motion or from mixing processes after the air is detrained from the cloud.

An important source of ozone for the tropical upper troposphere is biomass burning in the tropical rainforests particularly during the dry season. For the southern hemisphere tropical Atlantic ocean the source region is the South American continent during austral spring (Anderson, 1996; Thompson et al., 1996). Jacob et al. (1996) propose from an analysis of aircraft observations during the TRACE A expedition in 1992 that ozone is produced in the continental NO_x emissions that are lifted to the upper troposphere. It is then transported over the Atlantic ocean where the ozone is destroyed as it subsides into regions with high humidities and low NO_x concentrations. The mass exchange between the upper and the lower troposphere can be understood within the scope of the Walker circulation (figure 2.1).

2.4 Deep Convection, Subsidence, and their Influence on Water Vapor in the Tropical Upper Troposphere

Deep convection is the major source of water vapor for the tropical upper troposphere (Betts, 1990). Very large amounts of water vapor are transported upwards in deep convective towers. This water vapor condenses and partly rains out. The low temperatures in the upper tropical troposphere around -80°C result in a decrease of the saturation vapor pressure by several orders of magnitude compared to the level at the ground. This way all the air that reaches the upper troposphere in the convective towers has a very low specific humidity but is still saturated and can contain hydrometeors. Moistening of the surrounding air is possible by detrainment from the clouds at every altitude (Betts, 1990).

Zhu et al. (2000) found from measurements of the Microwave Limb Sounder (MLS) on board the Upper Atmosphere Research Satellite (UARS) that the moisture in the upper troposphere is most likely increased mainly by intensified local convection. The water vapor that is detrained in the upper troposphere is transported away from the areas of active convection with the large-scale circulation. During this transport the air emits long-wave radiation and is therefore cooled. As described by the hydrostatic energy equation the cooler air sinks to lower altitudes, is adiabatically warmed, and the relative humidity decreases unless there are other humidity sources. Possible sources are evaporating hydrometeors that either precipitate from the anvil of the cloud (Sun and Lindzen, 1993a) or are also detrained from the convective cloud. The narrow deep convective towers form cirrus cloud anvils that can cover much larger areas as the tower itself. The ice water content of the outer detraining anvils is not very high so that the evaporation does not have a large impact on the humidity. Sherwood (1999) showed that thin cirrus clouds can have a much larger impact through their radiative effect. As the cloud particles absorb more long-wave radiation than the surrounding air, the radiative cooling is slower and the air does not subside as fast as the surrounding air. This way it stays at higher altitude and colder temperature and preserves a higher relative humidity. Dobbie and Jonas (2001) find from a modeling study that the lifetime of cirrus clouds of different thicknesses is increased if radiative effects are considered. They also show that significant inhomogeneity can arise inside cirrus clouds due to the influence of solar as well as infrared radiation.

Subsidence occurs mainly in the subtropical anticyclones but also in the inner tropics and in the ITCZ outside convective regions (Held and Soden, 2000). It is partly induced by convection, but mainly through radiative cooling to space, and together with the poleward flux balances the upward mass and energy flux taking place in deep convective hot towers resulting in the Hadley circulation. During the subsid-

ing motion the air is warmed adiabatically so that the relative humidity drops as the specific humidity stays constant. This can lead to extreme low relative humidities increasing the amount of outgoing long-wave radiation by allowing more energy from lower levels to be emitted to space (Spencer and Braswell, 1997). That way the greenhouse effect in these areas is diminished.

2.5 Previous Studies

There have been several modeling studies concerning the water vapor distribution in the upper troposphere at greater distances from convection (Pierrehumbert, 1998; Pierrehumbert and Roca, 1998; Dessler and Sherwood, 2000). They show that the water vapor distribution modeled by following the large-scale advection starting in convective regions is in good agreement with satellite measurements of upper tropospheric humidities. Factors of uncertainty for these studies are the low resolution and limited reliability of the satellite measurements. Nadir sounding instruments provide a relatively high horizontal resolution, but their vertical resolution is limited as the measurements are influenced by the whole air column. Limb scanning instruments provide a higher vertical resolution and a relatively high resolution perpendicular to the scanning direction, but not in this direction. Another source of uncertainty can be the algorithm to derive water vapor concentrations or humidities (Read et al., 2001). These algorithms have to include assumptions about the state of the atmosphere and other boundary conditions which influence the quality of the result. Unfortunately, apart from the water vapor measurements that have to be derived from satellite brightness temperature measurements, there have been only balloon measurements mainly taken from land stations while the largest area of the tropics is covered by oceans. Besides, there are inconsistencies between different kinds of radiosondes when compared to satellite measurements (Soden and Lanzante, 1996) and the soundings are not very accurate in the upper troposphere due to the low water vapor concentrations (Elliott and Gaffen, 1991). Satellite water vapor measurements are also only possible under cloud free conditions (Soden and Lanzante, 1996). This lack of measurements is often regretted by researchers dealing with the study of the climate system (e.g., Clark et al. (1998)). The drawbacks of the use of satellite measurements of water vapor also affect the studies directly concerned with the processes influencing the humidity during the transport of the convective outflow away from the cloud. Udelhofen and Hartmann (1995) look at the GOES $6.7\mu\text{m}$ humidities relative to the distance from the nearest convective cloud. They find a rather fast decrease of humidity with distance. A study with UARS MLS data and additional trajectories and cloud data by McCormack et al. (2000) shows similar results. In the study of Salathé and Hartmann (1997) the humidity in drier regions at some distance from the convective area is modeled relatively well just by assuming that the relative humidity is decreased by subsidence induced adiabatic

warming during its transport from the convective to the dry region. Soden (1998), who tracks the convective outflow by following water vapor structures from GOES data, finds that the drying is slower in the vicinity of convective clouds than farther away. For the interpretation in all these studies it is assumed that there are no mixing processes and no other sources of humidity during the large-scale transport. There are also model studies of radiative cooling rates and the resulting decrease in relative humidity. Mapes (2001) relaxes an initially constant relative humidity profile by radiative cooling (figure 2.3). The temperature profile is taken from measurements over the tropical Pacific ocean and the radiative heating rates were calculated with version 2 of the Community Climate Model (CCM2) (e.g., Hack et al. (1993); Kiehl et al. (1994)). He finds that an atmosphere at a constant relative humidity over all altitudes dries very fast especially in the upper troposphere between 300hPa and 200hPa where the relative humidity drops to 40% after only one day of radiative cooling. Other authors (Doherty and Newell, 1984; Clough et al., 1992; Hartmann et al., 2001) find similar radiative cooling rates.

This thesis is concerned with the aforementioned subjects. But instead of satel-

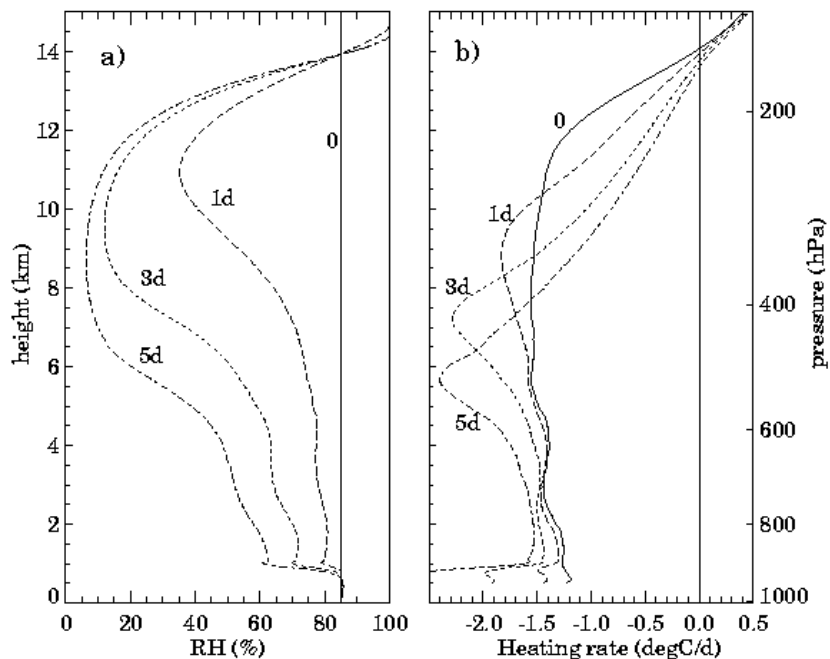


Figure 2.3: Relative humidity and radiative heating rates from a radiative model with a fixed temperature profile. The initially constant relative humidity of 85% (with respect to ice below 0°C) is relaxed solely by radiative cooling (from Mapes (2001)).

lite measurements of water vapor the first available high quality quasi-continuous in-situ measurements of water vapor in the upper troposphere are used. These data originate from the MOZAIC project, which will be described in more detail in the next chapter. They provide a much better horizontal and vertical resolution than satellite measurements and are quality controlled. For the study of the processes during the advection away from the convection they are brought together with trajectories calculated from ECMWF wind fields and satellite cloud top temperature measurements (figure 2.4). A conceptual model is applied to analyse the processes of interest.

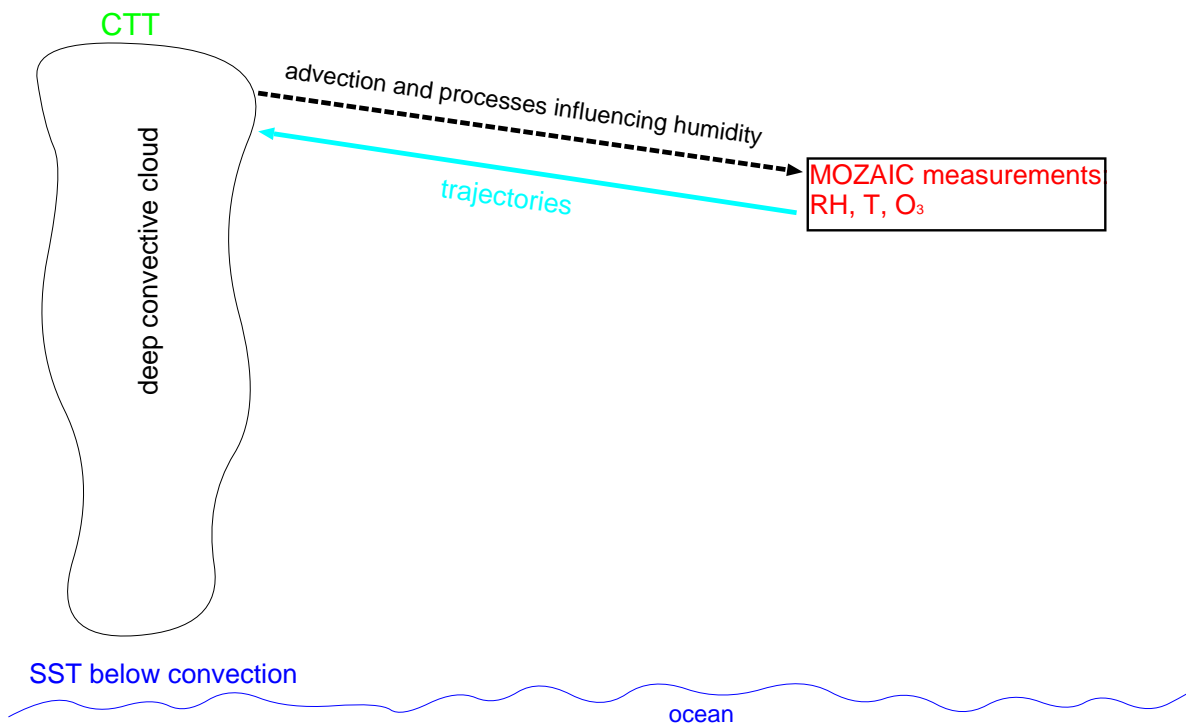


Figure 2.4: Concept for tracing the convective origin of the air. MOZAIC measurements are taken at different (spatial and temporal) distances from convective clouds. The distance to the originating cloud is determined by following a backward trajectory to the closest cloud that is identified from satellite derived cloud top temperatures.

Chapter 3

The MOZAIC Project

The MOZAIC project is a multinational initiative, sponsored by the European Commission and major European airlines (Air France, Austrian Airlines, Lufthansa, and Sabena) to measure ozone and water vapor (through measurements of relative humidity and temperature) from five commercial Airbus A340 aircraft on scheduled flights. For the ozone instruments as well as the coordination of the project CNRS Toulouse, France, is responsible and the water vapor measurements are carried out by Forschungszentrum Jülich, Germany. The measurements started in August 1994 and since then more than 15,000 flights with more than 100,000 flight hours were made starting from Europe to destinations in North America, South America, Asia, and Africa (figure 3.1). This provides a quasi-global coverage for more than 6 years (Marenco et al., 1998).

The instruments were especially designed to allow an almost maintenance-free automatic operation. For the water vapor measurements two sensors, a capacitive Vaisala Humicap-H relative humidity sensor and a Pt100 temperature sensor, are mounted together inside a Rosemount housing, model 102 BX. In this housing the air from outside the local boundary of the aircraft is adiabatically compressed, producing a temperature raise of up to about 30°C depending on the flight velocity. Therefore, the measured RH is much smaller than that of the ambient air, that has to be computed with the help of the velocity measurement provided by the aircraft (Helten et al., 1998). The ozone analyser is a Dasibi dual-beam UV absorption instrument (Thermo-Electron, model 49-103). A detailed description is given by Thouret et al. (1998).

To ensure the quality of the measurements the devices are calibrated regularly. For this purpose, each humidity sensor is replaced during regular maintenance of the aircraft approximately every month or every 500 hours of flight, and sent to Jülich afterwards. Before and after each change the sensors are placed in an environmental simulation chamber where humidity, temperature and pressure can be controlled (Smit et al., 2000) to calibrate them against an accurate Lyman- α fluores-

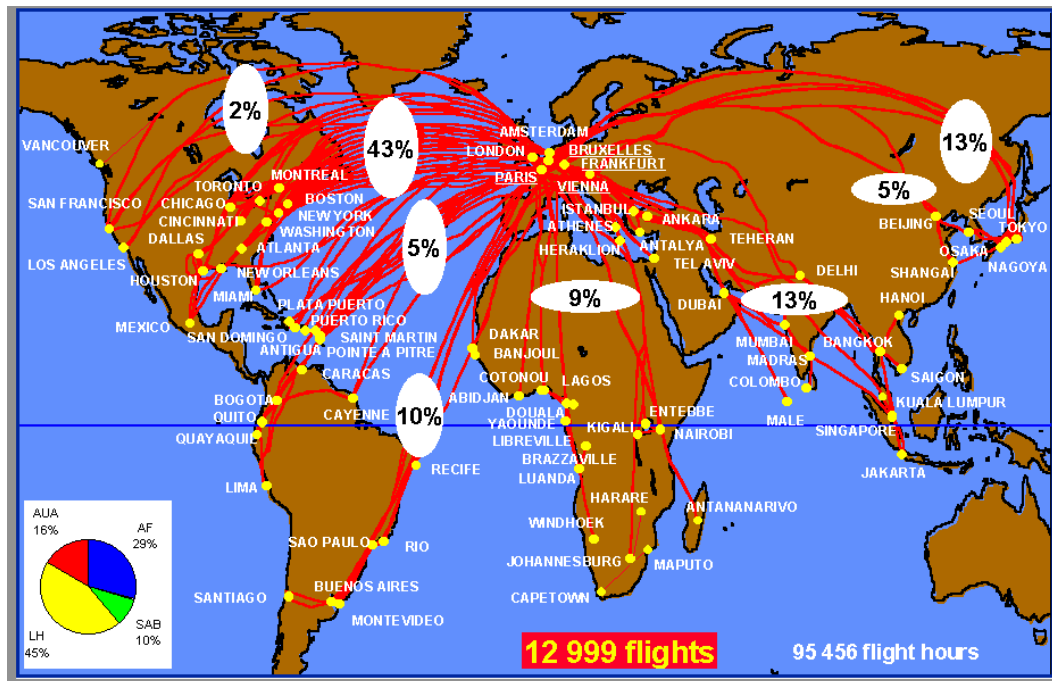


Figure 3.1: Map of the MOZAIC flight coverage, September 1994–December 1999. The pie-chart in the lower left corner shows the fraction of flights for the four participating airlines.

cence hygrometer (Kley and Stone, 1978; Kley et al., 1979) under realistic in-flight conditions. The mean of the pre- and post-flight calibration coefficients is used to calculate the humidity values from the raw data. From the calibration, the accuracy is determined. All data are evaluated for consistency prior to their release on the MOZAIC database (Helten et al., 1998). The uncertainty of the relative humidity measurements depends on the outside air temperature. At cruise altitude the total uncertainty lies between $\pm 4\%$ RH at about 10km and $\pm 7\%$ RH at about 13km. The temperature sensor is replaced and checked in the chamber simultaneously. Besides, the temperature measurements that are carried out routinely on every aircraft are recorded together with the MOZAIC measurements and thus provide an independent basis for comparison. This was done for all measurements from the beginning until the end of 1997. The comparison showed a good agreement within the combined uncertainties of both measurements. For data with the highest relative humidity validity values, meaning that they are considered reliable, more than 98% of the temperature measurements differ by less than 1K and less than 0.35% by more than 2K. In addition to the continuously applied quality control, in-situ comparison with other instruments has been carried out several times, e.g., 1997 with a cryogenic frost-point hygrometer on board the DLR research aircraft Falcon in the scope of the POLINAT campaign. The water vapor mixing ratios differed by less than 5% for measurements taken during the period of closest approach of

both aircraft (Helten et al., 1999). The ozone instruments are exchanged every year to be checked and re-calibrated against a laboratory reference instrument (Thouret et al., 1998). The ozone inlet lines are also checked every year. Furthermore, the instrument is calibrated regularly during aircraft operation on ground and during flight with the help of an internal ozone generator. The ozone measurements are compared with the other MOZAIC instruments on a routine basis several times a year when the flight schedule allows it. Comparison with other instruments like in the above mentioned POLINAT campaign also showed good agreement.

The measurements are recorded every 4 seconds, and the evaluation is done for this raw data set. The data set used for this study is averaged to give a value every minute during the flight in cruise altitude. This corresponds to a distance of about 15km between two data points, which means that 7-8 samples per degree of latitude belong to one single flight and are taken within 8 minutes. Therefore, they are not completely independent. This has to be kept in mind when looking at mean values. Only data points that are flagged for high reliability are taken into account. In addition to the measured relative humidity with respect to liquid water, the MOZAIC database provides the water vapor mixing ratio calculated from the relative humidity, temperature and pressure with the help of the Goff-Gratch formula (Goff and Gratch, 1946) for the saturation water vapor pressure.

$$e(T) = \exp(A/T + B + C T + D T^2 + E \ln T) \quad (3.1)$$

The parameters A to E for the vapor pressure with respect to liquid water are $A = -6096.9385$, $B = 21.2409642$, $C = -2.711193 \cdot 10^{-2}$, $D = 1.673952 \cdot 10^{-5}$, and $E = 2.433502$.

The mixing ratio is referred to as 'specific humidity' in this work as these quantities differ by less than 0.1% in the upper troposphere. The relative humidity with respect to ice is also calculated with the help of the Goff-Gratch formula. The parameters A to E for the vapor pressure with respect to ice are $A = -6024.5282$, $B = 29.32707$, $C = 1.0613868 \cdot 10^{-2}$, $D = -1.3198825 \cdot 10^{-5}$, and $E = -0.49382577$. As in the upper troposphere the temperature is always below 0°C, the relative humidity with respect to ice is used in this work exclusively, even if it is addressed as 'relative humidity'. If the relative humidity with respect to water is meant, it is mentioned explicitly.

Chapter 4

Climatology of MOZAIC Data over the Tropical Atlantic Ocean

As the focus of this thesis will be on processes related to convection over a tropical ocean, the data that were measured above the tropical Atlantic ocean are used for the analysis of the influence of convection on the surrounding air later in this work. For this region a climatological overview of the data measured by the MOZAIC aircraft is given in this chapter. After a description of the flight characteristics, the measured relative humidity distribution is discussed as well as the latitudinal, seasonal and interannual variability of all measured parameters. In addition, the measured humidities are compared with humidities from ECMWF analysis that are available in the MOZAIC database interpolated to the MOZAIC data points.

4.1 Flight Characteristics

As the MOZAIC project is based on aircraft of European airlines, all long-range flights either start or end in Europe and reach all continents except Australia. The only tropical ocean that is covered regularly is the tropical Atlantic by flights mainly to and from São Paulo and Rio de Janeiro. The flight tracks of these flights are all located in a narrow corridor with a width of about 10° longitude (figure 4.1). The actual flight tracks do not vary during the year within this corridor. There are around 10-20 flights per month from the beginning of the MOZAIC project until today but with a considerable gap of several month during 1995 when non of the airlines served Brazil with their MOZAIC aircraft. The month with the largest number of flights is January 1998 with 30 flights. The flights are not spread regularly over each month so that weekly means are not possible, but regularly enough to allow monthly means. The tropical Atlantic is covered by these flights between about 5°S (longitude range: 40°W to 30°W) and 30°N (longitude range: 20°W to 10°W). Except for a few flights with instrument failures all others cover the whole latitude range, although the coverage in midlatitudes is a bit lower due to some aircraft flying

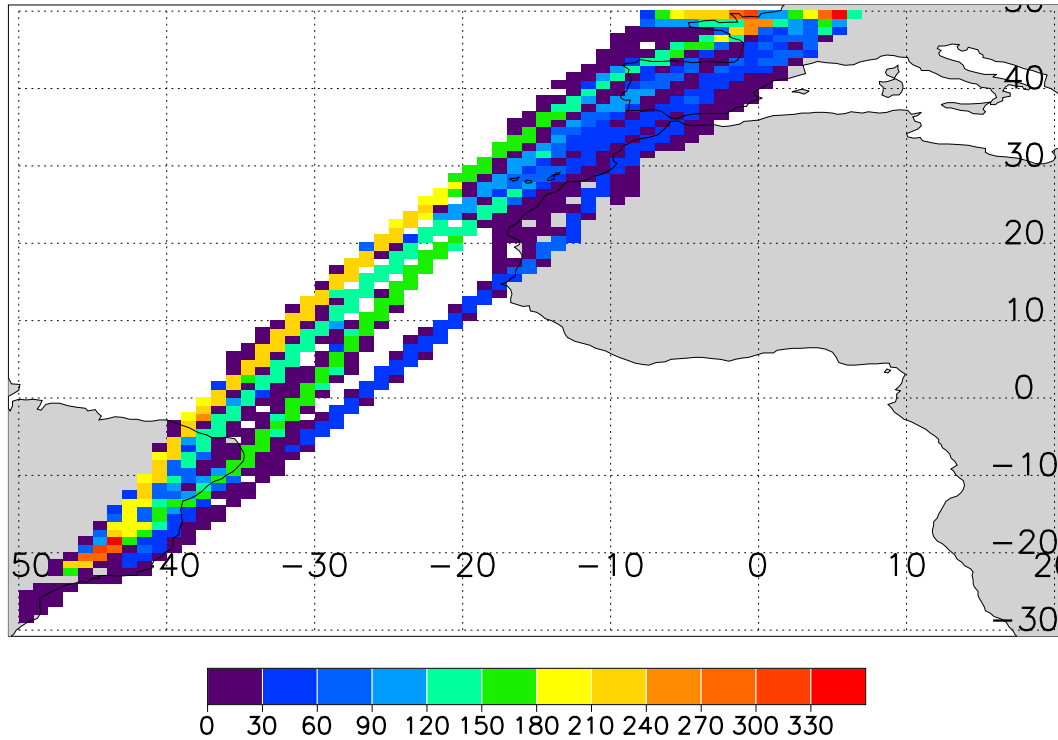


Figure 4.1: Number of flights per $1^\circ \times 1^\circ$ box. September 1994 to June 2000, only flights between Europe and South America are shown.

above the tropopause and only tropospheric measurements being used. To exclude stratospheric measurements that are possible at cruise altitude outside the tropics, Ertel's Potential Vorticity (PV) is used, which is calculated for every one minute data record from ECMWF analysis by Meteo France and included in the MOZAIC database. The criterion chosen is $|PV| < 2$. This threshold may be too low and also exclude some tropospheric measurements, but will not allow any measurements of stratospheric air in the dataset (Duhnke et al., 1998). It corresponds to a threshold of 100ppbv ozone. South of 5°S more than 75% of all flights are above the South American continent. Only measurements at cruise altitude are taken which lies between 9 and 12km. In this altitude range the aircraft fly on 5 distinct pressure levels centered around 288hPa, 262 hPa, 238hPa, 217hPa, and 197hPa due to flight security constraints. The data taken include some measurements from in-flight ascents and descents with a range of 2hPa, but the actual variability per pressure level is lower than 2hPa. The two most prominent pressure levels are 238hPa and 262hPa with about one third of all measurements each (Figure 4.2). This results in a very good coverage on these two very narrow pressure ranges providing a very high vertical resolution, but restricts the opportunity for the study of height dependent features.

The latitudinal coverage is not uniform for single pressure levels. The 238hPa level

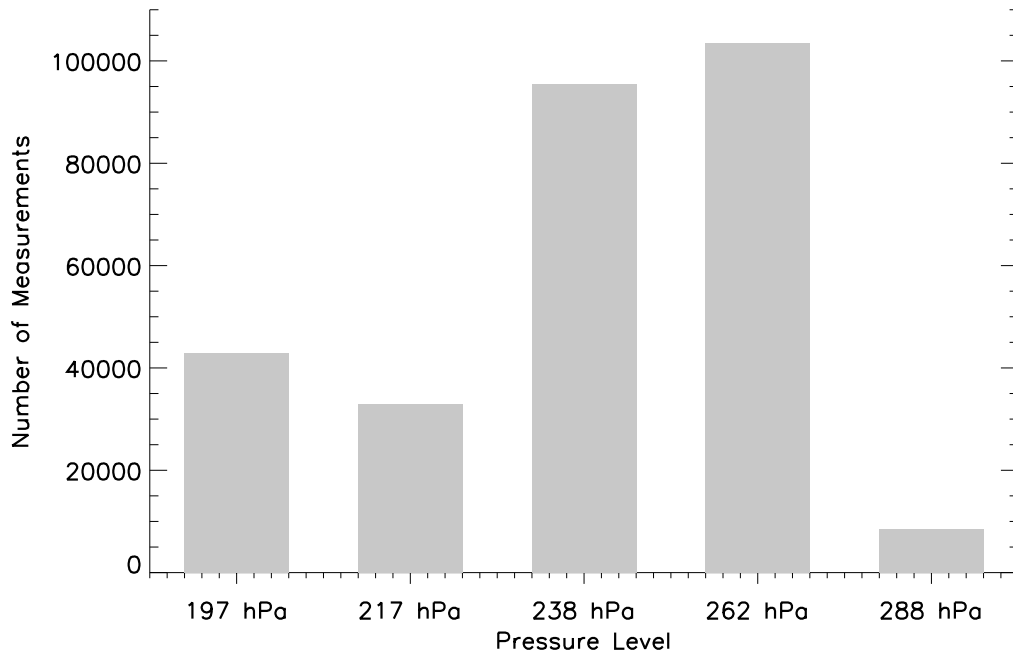


Figure 4.2: Number of measurements by pressure level from September 1994 to June 2000 on flights between Europe and South America.

is mainly used between 5°S and 30°N , while the 262hPa level is used between 20°S and 15°N and north of 30°N (Figure 4.3). Over the South American continent the 262hPa level is used most and the 197hPa and 238hPa levels equally often. The large number of measurements near 50°N corresponds to the location of the main airports used. In these latitude bins not only flights to South America are included in the sampling region, but also some of the more frequent flights to North America.

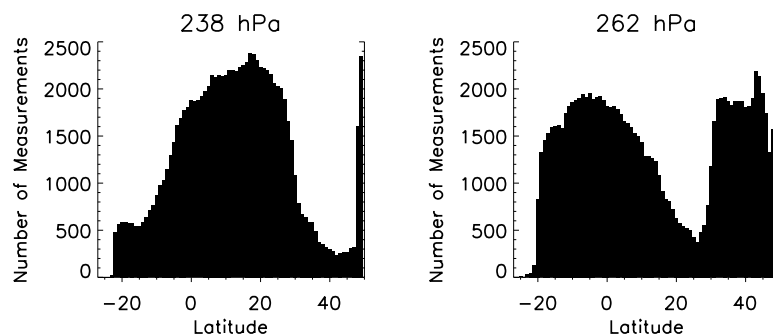


Figure 4.3: Number of measurements by latitude for the most prominent pressure levels from September 1994 to June 2000 on flights between Europe and South America.

As the temperature does not vary by more than a few tenths of a degree on one pres-

sure level inside the tropics and the difference in temperature between the different pressure levels is several degrees, these pressure levels have to be distinguished for a climatology of temperature and specific humidity. The two main pressure levels, 238hPa and 262hPa, are chosen for the climatological analysis below as they provide the best data coverage.

4.2 Relative Humidity Distribution

The distribution of relative humidity is somewhat bimodal so that the mean value is not the mode (Fig. 4.4). Besides the main mode around 20% relative humidity, there is a lower secondary peak near the saturation level.

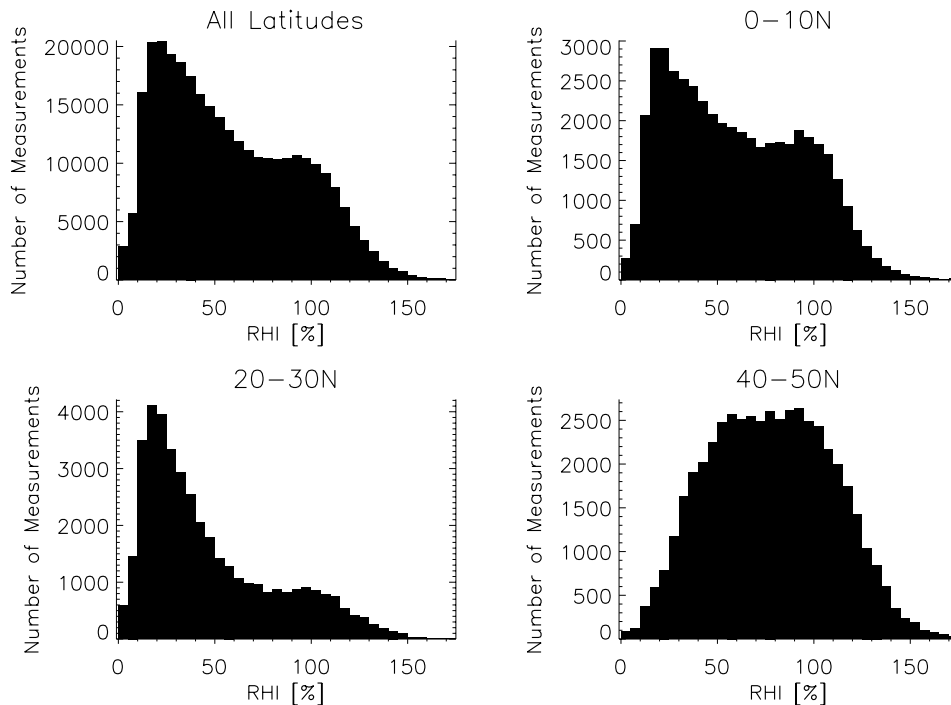


Figure 4.4: Histograms of the relative humidity with respect to ice (RHI) for different latitude bands from September 1994 to June 2000 for measurements taken on flights to and from South America on all pressure levels.

Differences in the mean value are due to variations in the proportion of these peaks throughout the entire tropical measurement region. That means that higher mean relative humidities arise from a higher peak at saturation and fewer measurements of dry air. Only in midlatitudes the number of measurements at very low relative humidities is negligible and the number of measurements of relative humidities over ice in the middle range is increased leading to a virtually unimodal distribution.

What is striking is the high fraction of measurements above ice-saturation. This was also observed from other measurement platforms (e.g. Heymsfield et al. (1998), Jensen et al. (1999)). Gierens et al. (2000) find a connection between the occurrence of ice-supersaturation and subvisible cirrus clouds.

The relative humidity with respect to liquid is presented in figure 4.5. The shape of

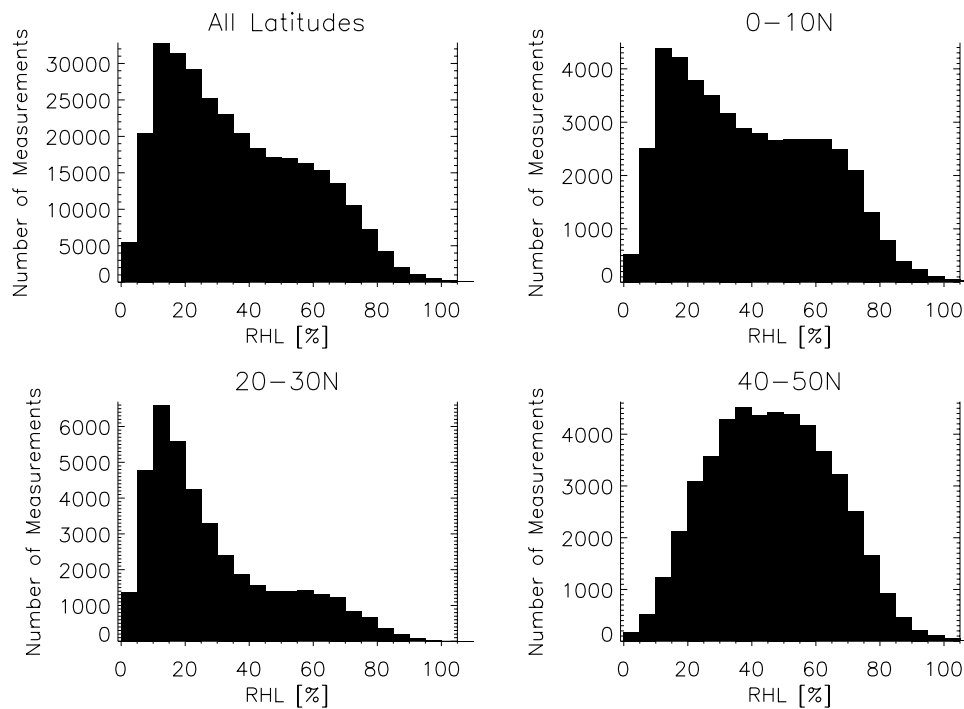


Figure 4.5: Histograms of the relative humidity with respect to liquid (RHL) for different latitude bands from September 1994 to June 2000 for measurements taken on flights to and from South America.

the distributions is similar, but no supersaturation is found. The observed supersaturation with respect to ice with relative humidities exceeding 150% is not caused by evaporation of ice crystals in the inlet system. Although this could happen due to the temperature at the sensor being higher than the temperature outside the inlet (see chapter 3), the ice water content of cirrus clouds at 10-12 km altitude is typically below 0.005gm^{-3} (Liou, 1992) and thus much smaller than the gaseous water vapor content with values above 0.04gm^{-3} ($\hat{=}$ 0.12g/kg at 238hPa and 229K). In addition, theoretical estimates (H. G. J. Smit, private communication) have shown that even at larger ice water contents the traveling time of the air parcels between intake and sensor is too short for evaporation of ice crystals to give a considerable contribution to the gaseous amount. The relative humidities with respect to liquid water never exceed the saturation level of 100%. This is in accordance with the physics of undercooled water which would predict homogeneous nucleation at rela-

tive humidities exceeding 100-101% with respect to liquid water (Pruppacher, 1997).

4.3 Seasonal Variability

Figure 4.6 shows the temporal variation by latitude of relative humidity over ice. The measurements are averaged by month and latitude (1°). The panel covers more

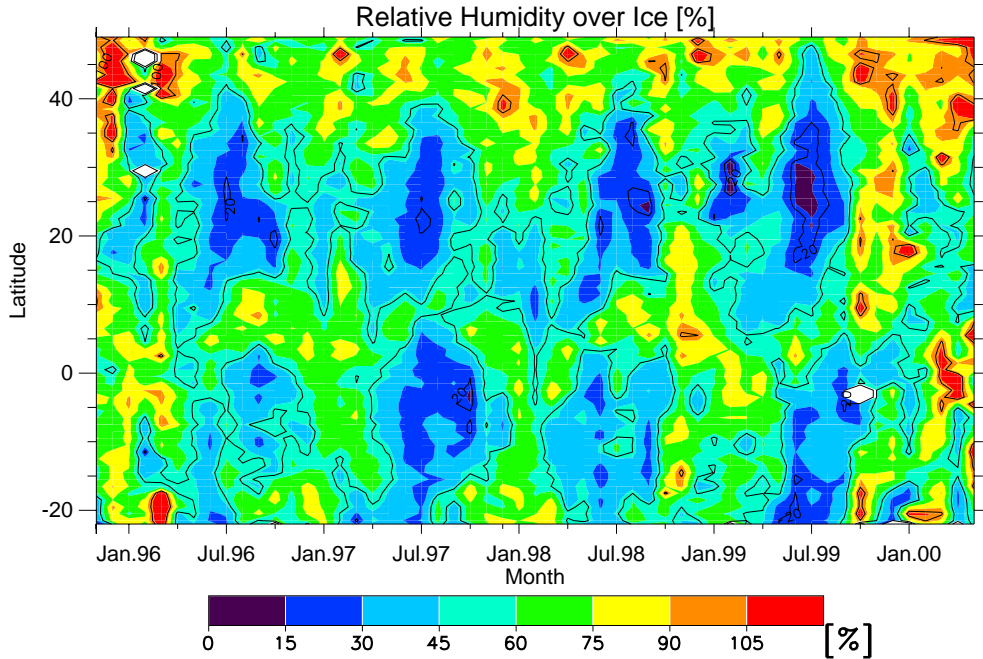


Figure 4.6: Relative humidity with respect to ice from November 1995 to May 2000. Monthly mean by latitude averaged over all pressure levels.

than 4 years of continuous monthly mean data. This range of time is chosen because of a data gap over the Atlantic in 1995, so that a longer timeseries would not be continuous although the measurements started in August 1994. High humidities associated with the ITCZ (Waliser and Gautier, 1993) meander latitudinally roughly between the equator and 10°N following the solar zenith. North and south of it there is a relatively dry region which is driest every year in July and somewhat moister in January on both sides of the ITCZ and thus of the equator but generally slightly moister on the southern hemisphere. These features might be related to the location of the flight corridor. The aircraft fly mainly above the South American continent south of the equator and fly very close to or partly above the African continent and the Sahara desert at around 30°N . Over South America the ITCZ moves much farther to the south in southern hemisphere summer than it does over the Atlantic.

In figure 4.7 specific humidity and temperature are shown correspondingly, but for these parameters only one pressure level can be taken at once. The 262hPa level is

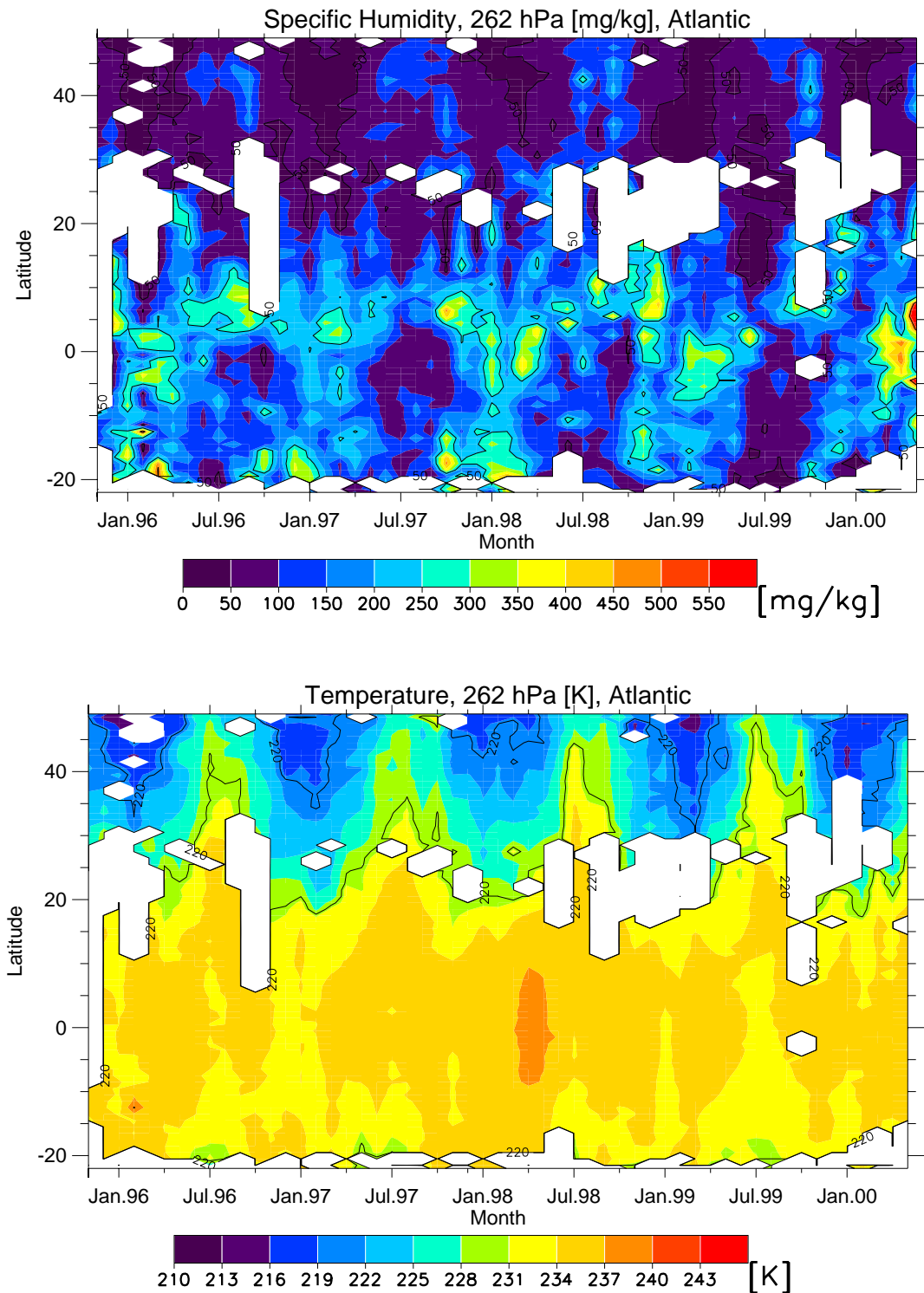


Figure 4.7: Specific humidity and temperature from November 1995 to May 2000. Monthly mean by latitude for pressure level 262hPa. For the 238hPa level see appendix.

chosen as it provides the best coverage. The 238hPa level is presented in the appendix for comparison and for the coverage of those latitudes that are not covered well in the 262hPa pressure level. The specific humidity is highest in the ITCZ and in austral summer during the rainy season over South America with values up to about 400 mg/kg. Monthly mean specific humidities below 50 mg/kg occur only rarely in this area. North of 10°N it is much lower with a seasonal variation north of 30°N ranging between about 200 mg/kg in summer and below 50 mg/kg in winter, corresponding to the temperature variation as the relative humidity stays almost constant or at least does not show seasonal variation. South of 20°N where the temperature does only vary by a few degrees throughout all latitudes during the whole time span the variation of the specific humidity is mainly determined by the variation of the relative humidity. The higher specific humidity in the rainy season 1997/1998 seems to be related to higher temperatures, though, as the relative humidity is higher in the two other rainy seasons. This temperature maximum is likely related to the 1997/1998 El Niño (Giannini et al., 2001), but there is also indication of interannual variations in the Atlantic ocean-atmosphere system independent of El Niño (Handoh and Bigg, 1999; Tseng and Mechoso, 2001).

4.4 Mean Latitudinal Variability

Figure 4.8 shows a comparison of the mean latitudinal variations on the different pressure levels. The numbers presented are mean values from September 1994 to June 2000 for all pressure levels and in 1 degree latitude bins. The number of measurements given by the orange dashed line has to be divided by 8 to give a lower bound for the number of individual flights included in each bin. The other parameters shown are: specific humidity in g/kg (black), relative humidity with respect to ice in % (blue), and temperature in K (green). From the number of measurements it is clear, that only the 238hPa and 262hPa levels provide a good coverage. The other pressure levels show a significant amount of measurements only around 20°S, 20°N, and 50°N for 197hPa, 217hPa, and 288hPa, respectively.

For all pressure levels the latitudinal distributions of relative humidity are similar in the run of the curve and also in the absolute value. Therefore, means can be taken for all pressure levels together. The relative humidity is almost constant at about 50% south of the equator. It has a slight maximum directly north of the equator (60%), where the ITCZ is located over the Atlantic ocean, and a minimum (40%) near 20°N. From there it increases up to more than 80% in midlatitudes.

Temperature and specific humidity also have a similar course on all pressure levels, but with different absolute values. The pressure levels are separated by a temperature difference of about 5K. Between 20°S and 30°N the temperature varies by

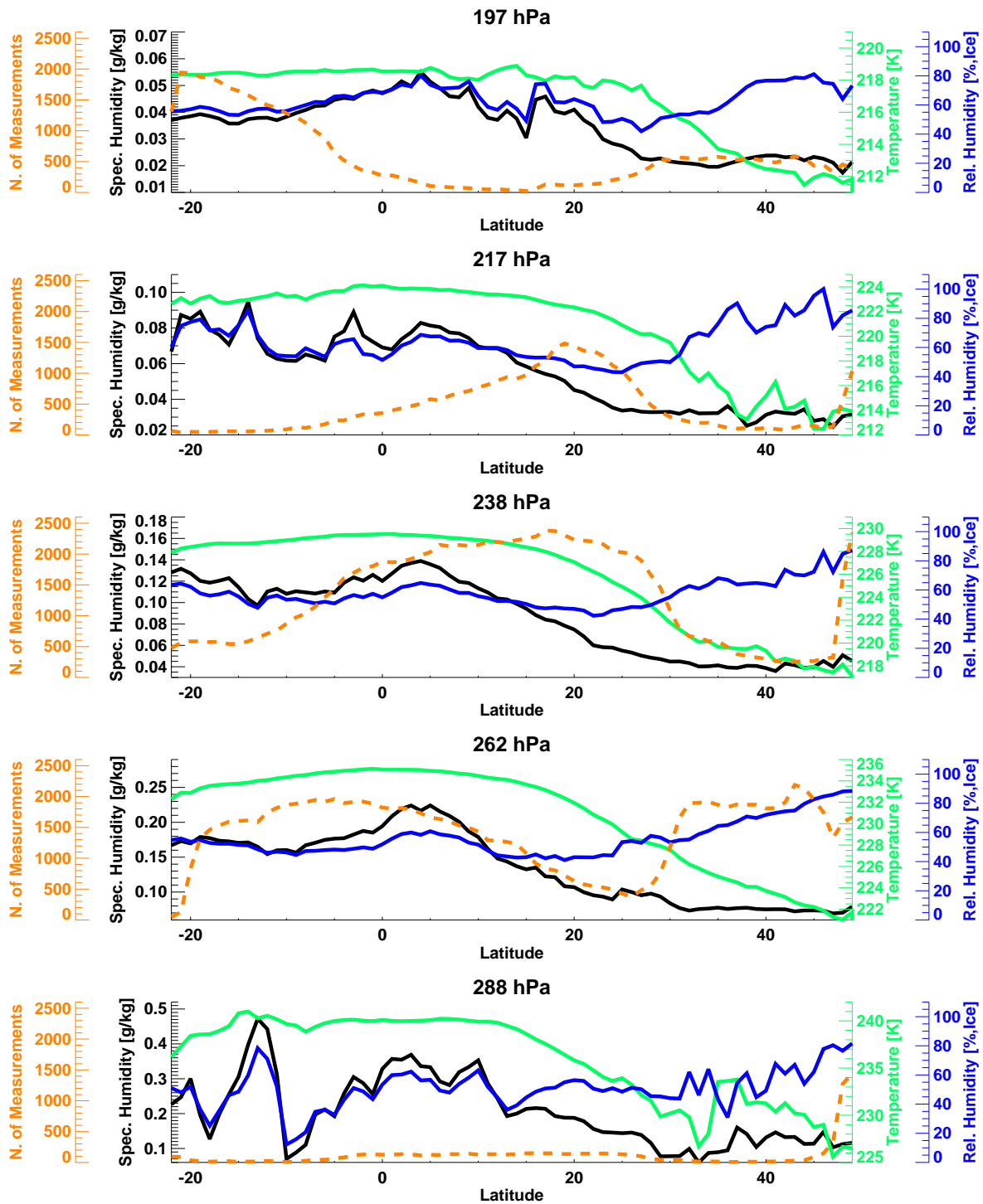


Figure 4.8: Latitudinal mean from September 1994 to June 2000 for all pressure levels of main parameters: specific humidity in g/kg (black), relative humidity with respect to ice in % (blue), temperature in K (green), and number of measurements (orange, dashed).

less than a degree on each pressure level, but falls off from there by about 10°C into northern midlatitudes with the sharpest decrease between 20°N and 30°N . The specific humidity has a maximum in the ITCZ and is almost constant throughout the southern hemisphere region. Towards the north it decreases at lower latitudes than the temperature and stays almost constant on a low level north of about 30°N .

In general, the mean latitudinal distributions are asymmetrical to the equator. The mean location of the ITCZ shows up rather clearly in the humidity data, and south of the equator most parameters show little latitudinal variations up to São Paulo and Rio de Janeiro where the MOZAIC flights start or end. To some degree this could be related to the limitation of the flight corridor and its location mainly above the South American continent. The high variability on the less sampled pressure levels can be explained with the high atmospheric variability.

4.5 Interannual Variability

In order to illustrate the degree of interannual variability for the different parameters, the latitude band between the equator and 10°N is chosen, because it is the main area of interest in this work (figure 4.9). The mean over this latitude band

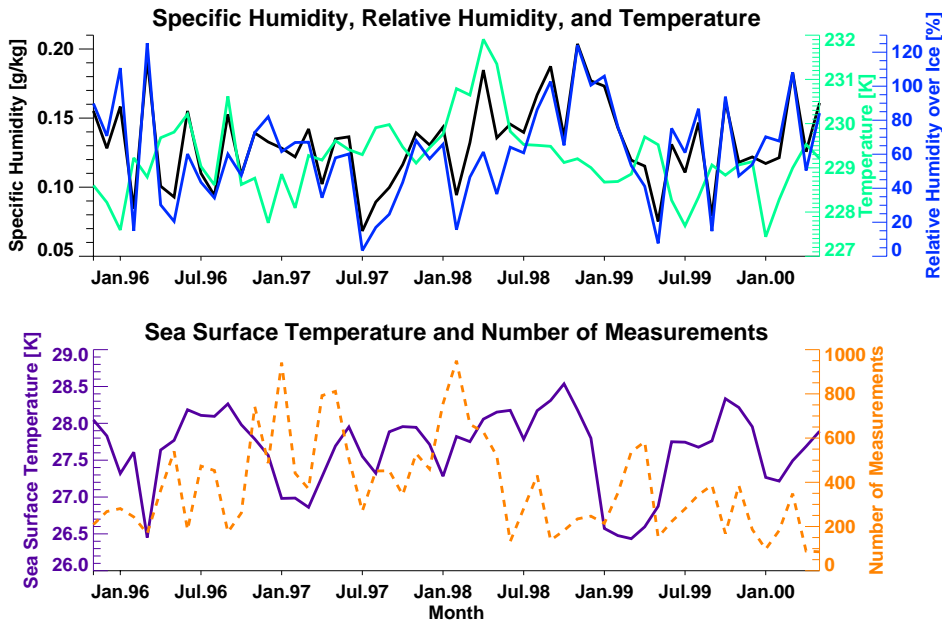


Figure 4.9: Monthly mean for measurements taken between the equator and 10°N at 238hPa. Specific humidity (black), temperature (green), and relative humidity (blue) in the top panel. Sea surface temperature (purple), and number of measurements (orange, dashed) in the bottom panel.

always includes the ITCZ and is therefore not sensitive to latitudinal variations of its location. This latitude band is best covered in the 238 hPa pressure level. Although monthly mean values are shown, no seasonal cycle is visible. The temperature maximum in March 1998 was already discussed in section 4.3. This maximum is followed by a maximum in humidity approximately 6 months later, characterized by high humidities in the whole latitude band from the equator to 10°N and even further to the north (figure 4.6). The number of measurements included in every monthly mean is shown in the bottom panel in orange. It varies from 100 single measurements in some month of the year 2000 up to almost 1000 per month in January 1997 and February 1998. In general, the number of measurements is higher in the northern hemisphere winter, due to the greater demand for flights from Europe to Brazil during that season. The interannual variability in the number of measurements is explainable with the individual choice of the airlines whether a MOZAIC aircraft is used on a certain route. The sea surface temperature plotted purple in the bottom panel is the Reynolds SST analysis (section 5.4) taken at the point directly below the aircraft.

4.6 Comparison with ECMWF

Together with the original flight data there are also specific humidities and temperatures from ECMWF analysis included in the MOZAIC database. The ECMWF analysis is produced operationally from different meteorological measurements (e.g., ground-based, aircraft, and satellite measurements) with the help of a 4-dimensional variational assimilation model (Rabier et al., 2000; Mahfouf and Rabier, 2000; Klinker et al., 2000). The analysis used has a horizontal resolution of T213 spectral truncation corresponding to approximately 0.5 degrees. The vertical resolution was 31 levels until March, 8th 1999, 50 levels from March, 9th 1999 to October 10th 1999 and 60 levels afterwards. The time resolution is 6 hours (at 00, 06, 12, and 18 GMT). The analysis data are interpolated on the aircraft trajectory at the given measurement coordinates. A 3-dimensional cubic interpolation is used in space and a linear interpolation in time.

The temperature of the ECMWF analysis agrees quite well with the MOZAIC measurements. The mean of the difference for all measurements of MOZAIC and ECMWF temperature is $0.05 \pm 0.97\text{K}$ and for 98% of all measurements $|T_{MOZAIC} - T_{ECMWF}| < 2\text{K}$.

From the ECMWF specific humidities relative humidities with respect to ice are calculated with the help of equation 3.1. Figure 4.10 shows histograms of this relative humidities corresponding to the MOZAIC histograms in figure 4.4. The distributions of the relative humidity with respect to ice from the ECMWF specific humidity shows virtually no supersaturation. In the inner tropical latitude band between the

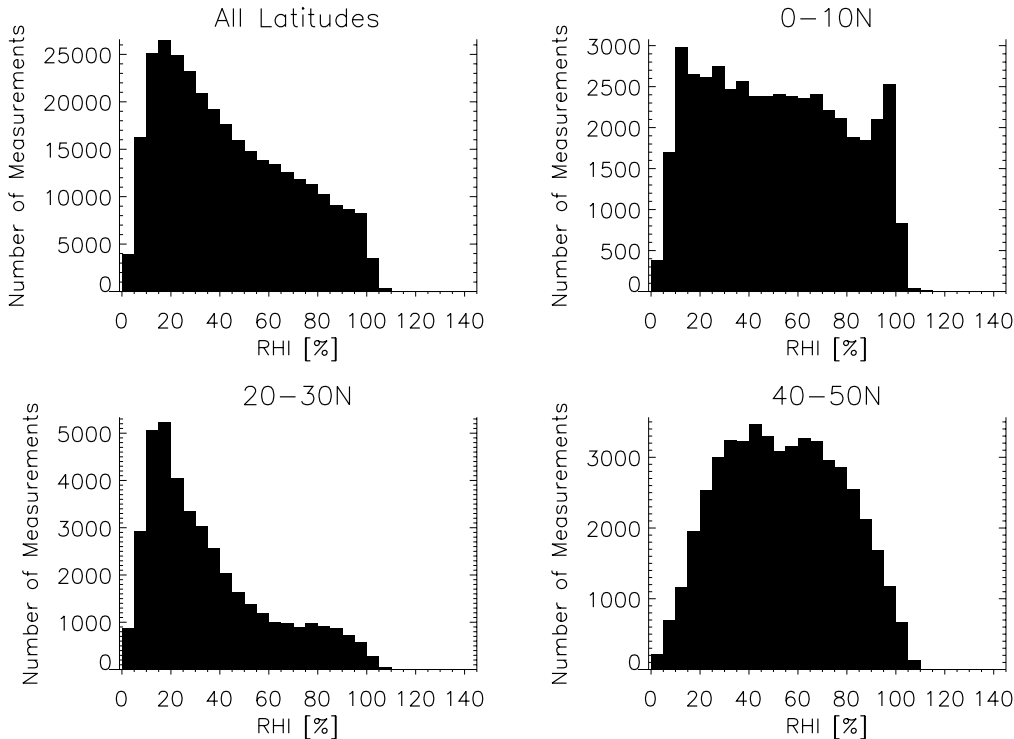


Figure 4.10: Histograms of the relative humidity with respect to ice (RHI) from September 1994 to June 2000 calculated from ECMWF specific humidities interpolated to MOZAIC measurement coordinates on flights to and from South America for different latitude bands on all pressure levels.

equator and 10°N all relative humidity values occur almost equally often. For further comparison figure 4.11 includes two panels corresponding to the ones in figures 4.6 and 4.7 showing the specific humidity on the 262 hPa pressure level and also the relative humidity calculated from the ECMWF specific humidity. Although the general features of both specific humidities are similar, the ECMWF specific humidity is lower than the MOZAIC specific humidity throughout the whole domain except for the ITCZ in 1998 where it is slightly higher. Especially the amplitude of the midlatitude seasonal variation north of 30°N is lower in the ECMWF data. Furthermore, they have much less structure although the means were taken from data at the same points. But as the MOZAIC data are in-situ measurements and the ECMWF data are interpolated from analysed fields with a restricted resolution the latter provide much smoother monthly and latitudinal mean values.

The relative humidity plot (figure 4.11, bottom) is provided to give a complete coverage with a mean from all pressure levels. Mean relative humidities are about 20% lower than MOZAIC relative humidities almost everywhere. An analysis of the reasons for the discrepancies between measured and analysed fields requires a detailed

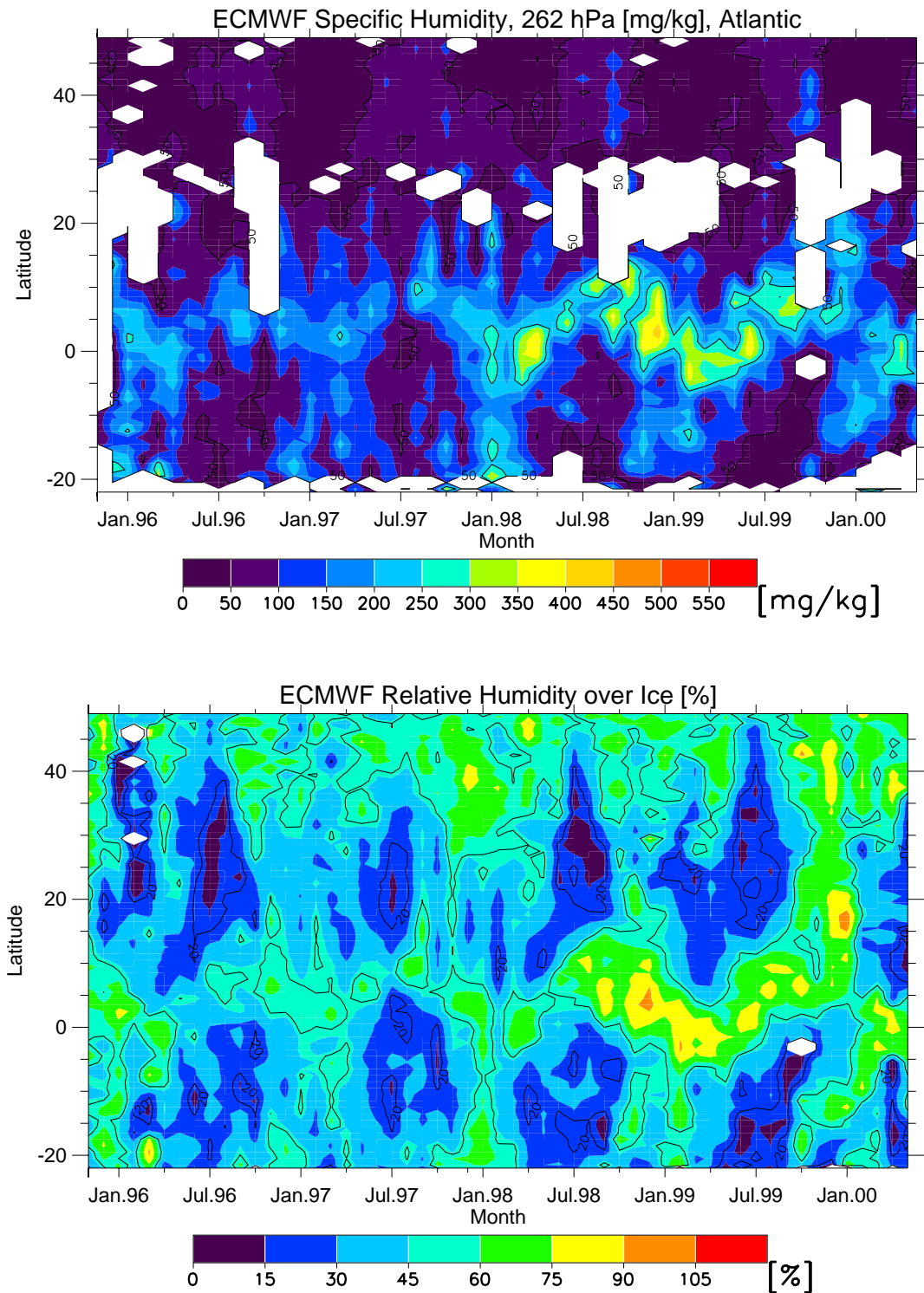


Figure 4.11: Relative and specific humidity from ECMWF. Specific humidity interpolated to MOZAIC coordinates at 262hPa, relative humidity calculated from ECMWF specific humidity averaged over all pressure levels.

view at the data assimilation and modeling applied to the ECMWF analysis. Certainly, one reason is the lower resolution as compared to the in-situ measurements. Another one is the uncertainty in the ECMWF vertical wind fields, as the relative humidity is influenced by vertical motions significantly. Especially in the remote areas of the tropics the amount of in-situ data included in the assimilation process is low, and vertical winds that are not measured directly from satellites have to be derived from the assimilation model. Convection and radiative cooling are included in the model but partly linearized (Mahfouf, 1999; Mahfouf and Rabier, 2000). Besides, the comparison shows that ice-supersaturation is obviously prevented in the model.

4.7 Ozone Variability

The MOZAIC ozone measurements (figure 4.12) can be used to identify the convective origin of air in the upper troposphere (section 2.3). The ozone mixing ratio

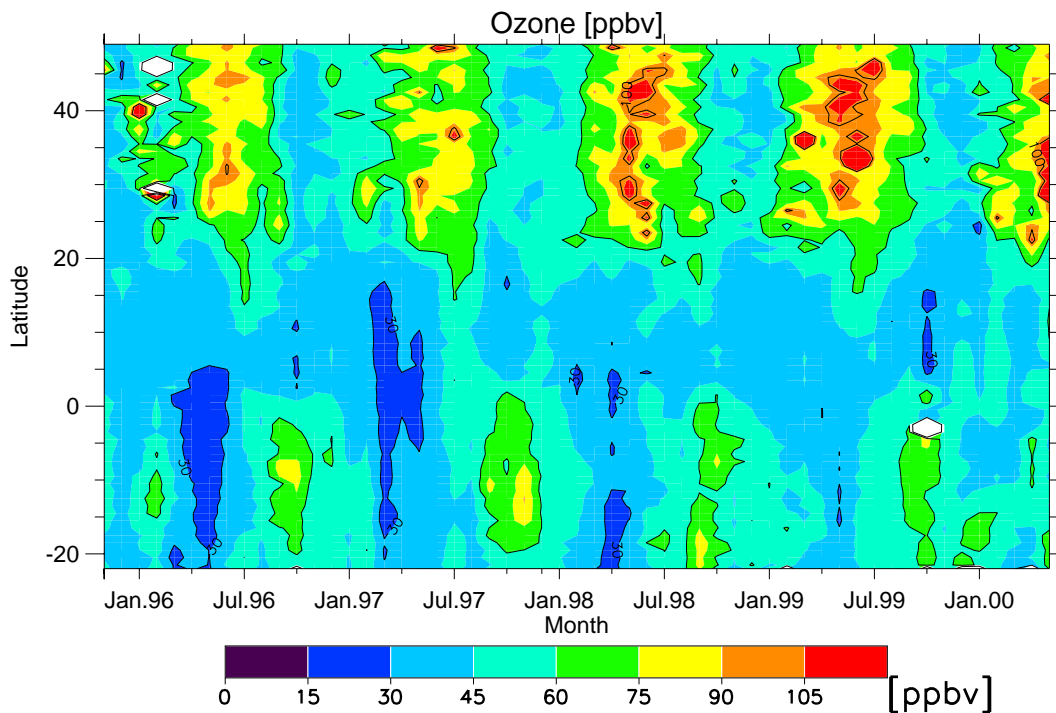


Figure 4.12: Monthly mean ozone mixing ratio averaged over all pressure levels for different latitude bands from September 1994 to June 2000. The measurements are taken on flights to and from South America (Corresponding to figure 4.6).

is lowest between the equator and 10°N ($< 40\text{ppbv}$) and also between the wet and the dry season south of the equator. This is due to the lifting of ozone depleted air from the remote marine boundary layer by deep convection (see section 2.3).

The reason for the higher values in southern hemisphere spring is most likely the biomass burning. North of 20°N there is a rather uniform seasonal variation with higher values in spring/summer and the lowest in late fall.

Chapter 5

Tracing the Convective Origin of the Water Vapor

In this chapter, the datasets that are needed to trace the convective origin of the air measured by the MOZAIC aircraft are described and their limitations discussed. There is also a detailed description of the method that was developed to trace convective clouds along trajectories and a presentation of some general features of the trajectories.

5.1 Concept for Tracing the Origin

By far most of the water vapor reaches the tropical upper troposphere by convection. As the temperature near the tropical tropopause is very low, most of the water vapor condenses eventually and a significant part of it rains out immediately inside the convective cloud and thus deposits its latent heat there. The rest is detrained from the cloud and, eventually, evaporates again. The detrainment happens mainly near the cloud top, but detrainment is possible at every altitude especially in mesoscale convective clusters with stratiform clouds and lower convective clouds in addition to the deep convective towers. From there the moist air is transported with the large-scale flow and leaves the convective area eventually. In a clear sky regime this air undergoes radiative cooling and subsides into warmer parts of the troposphere. If no mixing occurs the air keeps its original low water vapor content and the relative humidity is lowered through adiabatic warming.

The MOZAIC aircraft will usually encounter the detrained air some time after it has left the immediate convection, although they could still be inside or very close to the anvil of the convective cloud. Due to processes possibly influencing the relative humidity along the way, it is necessary to know how far the aircraft was from the originating cloud at the time the sample was taken to interpret the measured relative humidity correctly. This is achieved by using backward trajectories that are

calculated by Meteo France from ECMWF analysis wind fields. These trajectories lose their validity as soon as they encounter deep convection, though. The ECMWF model should be able to identify mesoscale convective systems, but it is not able to resolve deep convective towers and the strong vertical winds in their vicinity. In the tropics satellite data have the largest influence on the analysis, but they are mainly useful for large-scale features (Bouttier and Kelly, 2001). While the horizontal wind fields can be calculated from pressure fields quite reliably, the vertical winds vary much stronger on smaller scales. This is no problem for the analysis in this work, as the intention of the use of trajectories is to find the closest deep convective cloud anyway, but the location of this cloud with a low cloud top temperature indicating deep convection has to be identified with an independent dataset. For this purpose, additional satellite observations of the cloud top temperature from the Eumetsat CDS (Climate Data Set) are used in this analysis.

Another feature of interest is the sea surface temperature (SST) underlying the detected convective cloud. If the SST influences the properties of the convective tower and the convective tower influences the water vapor distribution in the surrounding air, it is crucial to know the convective tower the air originates from and the underlying SST to find out something about the interaction between the SST and upper tropospheric water vapor. Therefore, another independent dataset, Reynolds SST analysis, is used. A detailed description of the different datasets used is given in this chapter. The method used for tracing the convective origin is described in section 5.5.

5.2 Trajectories by Meteo France

In the scope of the MOZAIC project Meteo France, the French weather service, is responsible for keeping the database up to date and providing additional meteorological information for users of the database. Maybe the most important parameter provided is the PV, which is used to distinguish tropospheric from stratospheric air outside the inner tropics, independent of the ozone content that is to be analysed (section 4.1). As opposed to the specific humidity data that are interpolated from the ECMWF analysis, the PV is derived with the help of backward trajectories to obtain a better resolution (Simon, 2000). For this purpose 3-D trajectories are calculated from ECMWF wind fields (same ECMWF analysis as described in section 4.6) starting at every MOZAIC one minute data point and going backward in time. A trajectory length of two days was shown to provide a good agreement between ozone and PV small scale structures without requiring excessive amounts of computer time.

The coordinates time, latitude, longitude, pressure, and also the temperature that is interpolated from the ECMWF analysis at the point of the MOZAIC measure-

ment are included in the Meteo France trajectory data for every MOZAIC data point. The spatial coordinates plus temperature of the trajectory at the times of the ECMWF analysis to at least two days backward in time complete each data record (figure 5.1). These routinely calculated trajectories are used for the analysis

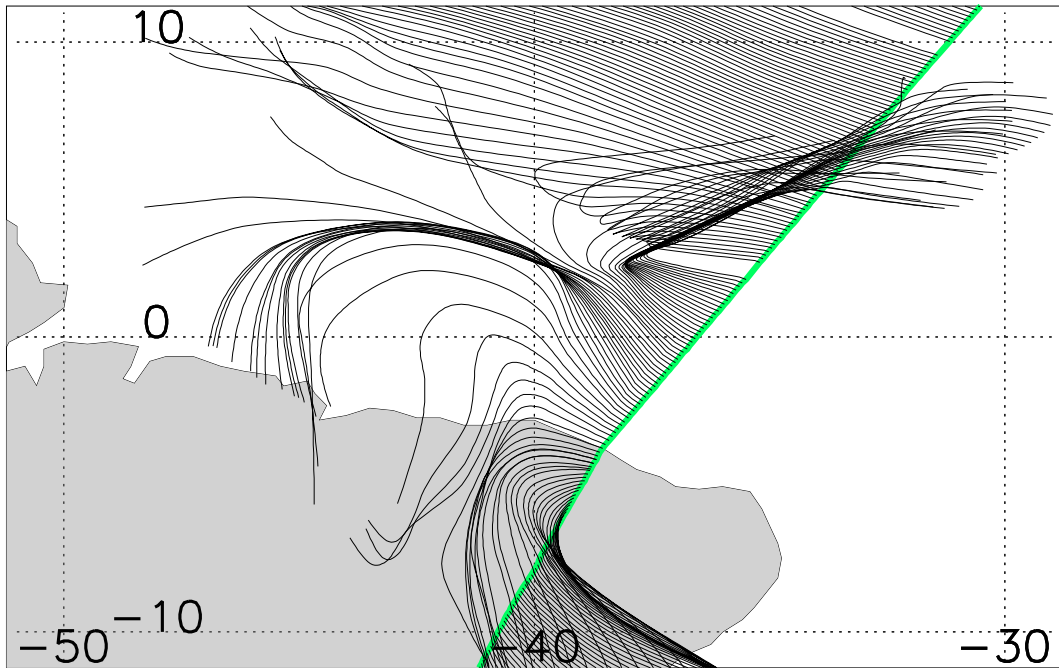


Figure 5.1: Example for 2-day-trajectories at every given measurement point along the flight track (green). The flight went from Paris to São Paulo starting on November 28th 1997. The part of the flight track that is shown crossing the equator from north to south off the coast of South America was covered on November 29th approximately between 5 and 8 UTC.

in the scope of this thesis. The advantage is that these trajectories are readily available from the MOZAIC database. Drawbacks are that the length of the trajectories is limited to two days, although this is not a problem in the inner tropics, as 80% of the trajectories encounter a deep convective cloud within these two days (see also section 5.6). In addition, the low time resolution is a limitation. The trajectories are calculated every 15min from interpolated 6h ECMWF wind fields, but the location is only stored and available in the MOZAIC database at the same 6h intervals the ECMWF analysis is available. This was resolved by applying an interpolation to the available coordinates to obtain an apparent time resolution of 30 min. A comparison between the interpolated trajectories and trajectories of higher resolution showed good agreement. The latter were calculated for several flights in May 1997 at the Royal Netherlands Meteorological Institute (KNMI) in De Bilt, The Netherlands, with the locally developed trajectory model TRAJKS (Scheele et al., 1996) to test the applicability of the tracing method.

The accuracy of the trajectories depends mainly on the quality of the wind fields used for their calculation. Uncertainties depending on the interpolation of the wind fields are usually avoided in case studies by calculating a group of trajectories starting at several points close to the point of interest. For this study the calculation of trajectories every 15km along the aircraft trajectory allows the statistical analysis of trajectories that are located more closely to each other than the resolution of the wind field, to exclude random errors based on the interpolation procedure.

Approximately half of all trajectories show a rising motion prior to the measurement even in cloud free areas. A case study indicated that this behavior originates probably from unrealistic vertical motion in the ECMWF analysis that were used to calculate these trajectories (figure 5.2). The vertical movement of the trajectory is completely undisturbed by high clouds being present most of the time, although the local temperature of the trajectory is higher than the cloud top temperature indicating that the trajectory would be inside the cloud. Instead, the trajectory rises slowly toward the measurement.

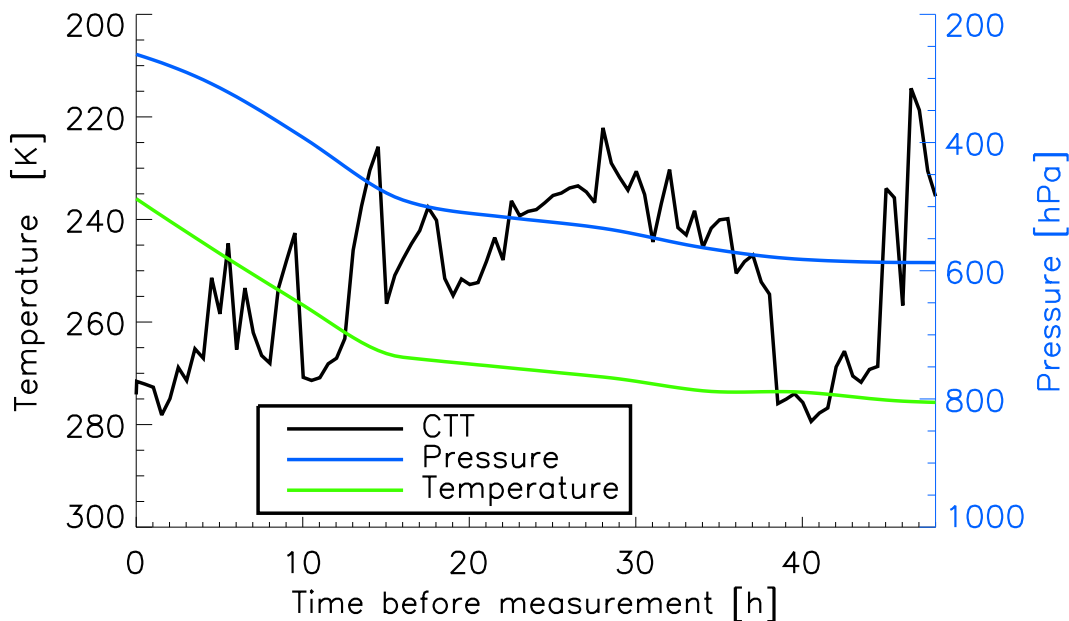


Figure 5.2: Example for CTT, pressure, and temperature along one trajectory. The backward trajectory starts on December, 12th 1998 at 22:01 UTC from a MOZAIC measurement at 3.11°N , 29.46°W . In this plot the trajectory is calculated from left to right away from the aircraft, but the wind direction is from right to left. The criteria for a deep convective cloud (section 5.5) are fulfilled at about 13h before the measurement.

The upward motion is connected to a mesoscale convective cluster that is detectable from satellite OLR measurements. This radiation is lowest in convective region

where the surface radiation is trapped by the convective clouds. In the dry regions with a weak greenhouse effect the OLR is highest. The globally averaged OLR is 235 W/m^2 (figure 2.2) with typical values in the tropics ranging between 300 W/m^2 for clear and dry conditions to below 160 W/m^2 from deep convective clouds. The OLR is often used for the study of convection (e.g., Graham and Barnett (1987); Waliser and Gautier (1993)), although it is not only influenced by clouds but also by the water vapor content and the surface temperature in clear conditions. In the case study (figure 5.3) the MOZAIC aircraft is close to a mesoscale cloud system (see also 5.4).

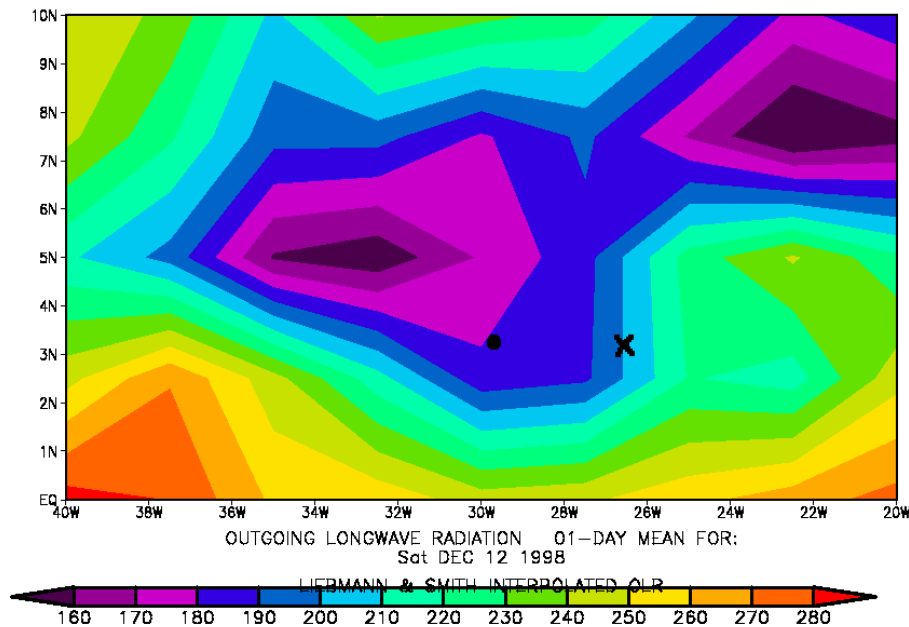


Figure 5.3: Outgoing long-wave radiation in W/m^2 on December, 12th 1998. The dot indicates the position of the MOZAIC aircraft and the cross the location of the convective cloud. The trajectory runs on a straight line between these two points. Source: NOAA-Cires/Climate Diagnostics Center homepage <http://www.cdc.noaa.gov/>

The convective cloud upwind of the MOZAIC aircraft is located outside of the mesoscale cluster and not resolved in the daily mean OLR data. The trajectory rises slowly from 464hPa at the cloud to 262hPa at the aircraft. It can be concluded that the vertical path of these trajectories is unrealistic. As 80% of the trajectories do not leave the 200hPa to 300hPa range and the vertical gradients in the horizontal wind fields are small, the horizontal path is assumed to be realistic, though. In order to find out the real vertical movement for an analysis of the processes influencing the

humidity along the trajectory additional assumptions are made which are described in chapter 7.

5.3 Cloud Top Temperature

The cloud top temperature data used for the trajectory analysis are provided by Eumetsat, the organization responsible for the reception, processing, dissemination, and archiving of the Meteosat satellite data (Eumetsat, 1999). These satellites are a series of geostationary satellites for meteorological purposes. Usually, there are several Meteosat satellites in orbit at any given time. The main operational satellite is always positioned above 0° longitude (figure 5.4) while the others are either in a parking position, or placed somewhere else for additional service.

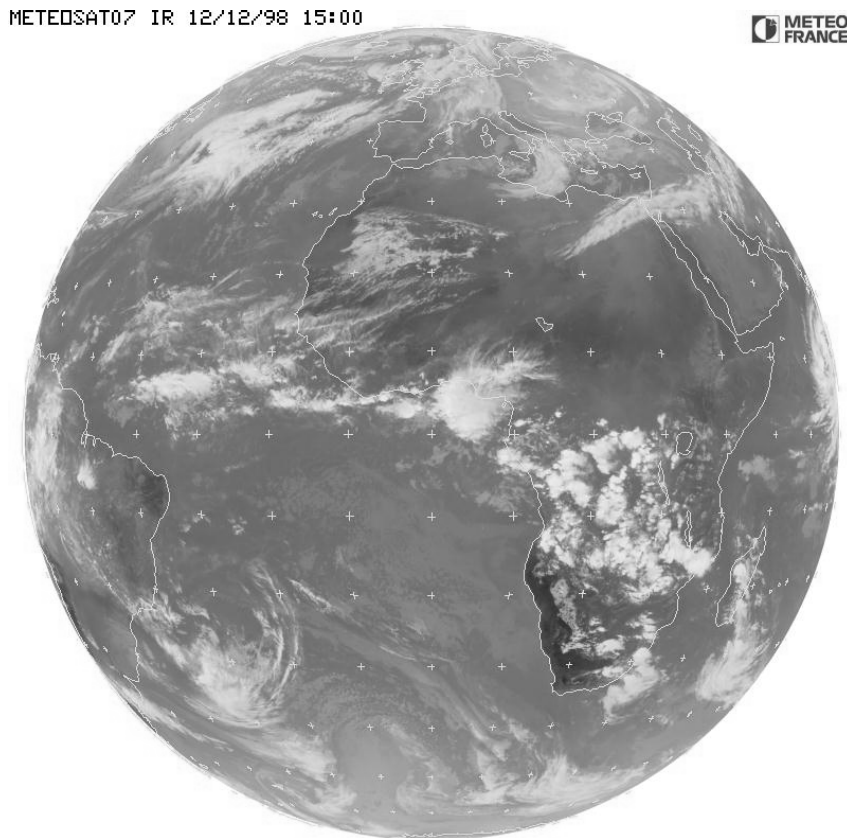


Figure 5.4: The Earth as seen from the infrared channel (10.5 to $12.5 \mu m$) of the main operational Meteosat satellite on December 12th 1998 at 15 UTC. Crosses indicate the intersections of every 10° latitude and longitude. The dark colors belong to the warmest and the light colors to the coldest infrared brightness temperatures. The picture was provided to the MOZAIC database by the Meteo France Space Center, Lannion.

All satellites are spin stabilized by rotating with a spin speed of 100 rpm. During each rotation one data line including 2500 pixels is scanned starting in the south-east corner of the viewing area. The following line is scanned to the north of the last one during the next rotation. With a total of 2500 lines to be scanned, a whole image scan takes 25 minutes, followed by a 5 minute retrace and stand-by period. The resulting 30 minutes time-frame for every image is called a slot. In the first years of the MOZAIC project the temporal resolution of the CDS images is lower with an image every three hours from 1994 until November, 15th 1995, and an image every hour from November, 15th 1995 to April, 21st 1997. Afterwards one image per slot is available. With 2500×2500 pixels a spatial resolution of about 5 km at the sub-satellite point is obtained. The image area is hemispherical, but in practice only a great circle of about 55° - 60° provides data without too much distortion (figure 5.5).

MPEF Segment Grid and Product Extraction Area

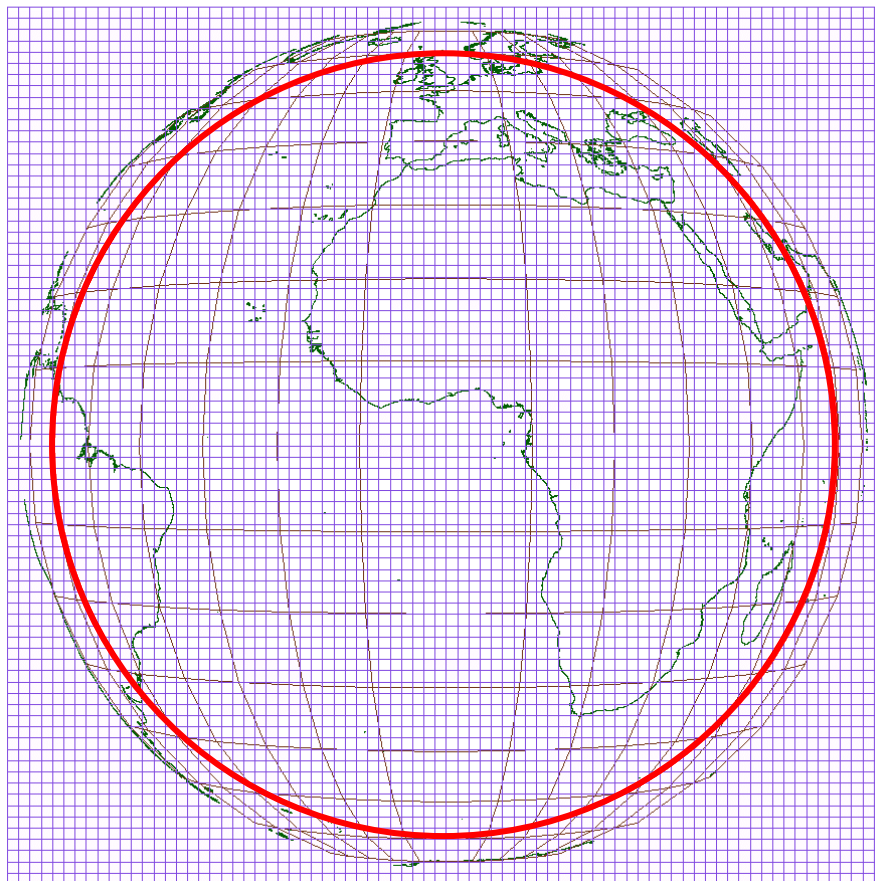


Figure 5.5: The area used for data retrieval from the Meteosat satellite (red circle) and the segment grid. Source: Eumetsat homepage <http://www.eumetsat.de>

The Earth's atmosphere is scanned with 4 sensors in 3 different wavebands. One sensor detects radiation that is emitted in the infrared waveband between 10.5 and 12.5 μm . The second is built for radiation from the strong water vapor absorption band between 5.7 and 7.1 μm . For the reflected visible light between 0.5 and 0.9 μm two sensors scan parallel lines with half of the viewing angle and at double read out speed leading to a resolution of 5000×5000 pixels corresponding to about 2.5 km at the sub-satellite point. Additionally to the original infrared channel count, a corrected infrared count (corir) is produced and provided with the data. It is corrected from the effects of the atmosphere above the measured surface and other distortions like semi-transparent clouds and clouds that do not cover a whole pixel. In addition to the direct images several meteorological products are produced at Eumetsat and archived at the Meteorological Archive and Retrieval Facility (MARF) which belongs to Eumetsat (<http://www.eumetsat.de>). The product used to obtain the cloud top temperature (CTT) data used in this work is the corir count from the CDS. As most of the other products it is processed in image segments, with one segment containing 32×32 pixels leading to 80×80 segments with a spatial resolution of about 160 km at the sub-satellite point (figure 5.5).

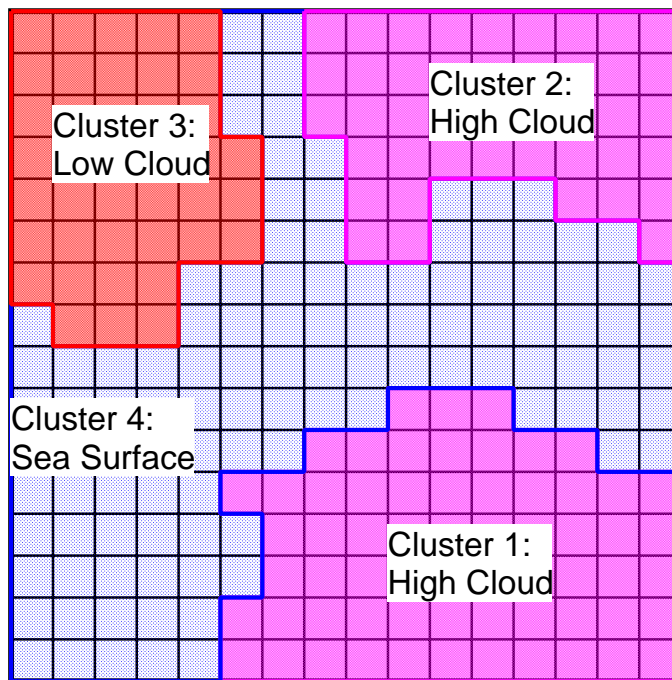


Figure 5.6: Example for one segment with four clusters of pixels with different optical properties. Only a quarter of a segment containing 16×16 pixels is represented. The actual segments contain 32×32 pixels.

For the CDS these segments are divided in up to 5 clusters of pixels corresponding to areas with discrete optical properties like different surfaces (e.g., sea, forest, or desert) or clouds in different altitude ranges (figure 5.6). The count for all pixels

with similar optical properties is averaged, and if there are more than 5 clusters the ones with similar optical properties are merged together. The merging procedure starts with similar surface properties. High cloud clusters are only merged if there are still more than 5 clusters after all other clusters have been merged. Nevertheless, there is the possibility for information about high clouds being lost in this merging procedure. For each cluster the number of pixels included is given together with the mean pixel count, the corresponding standard deviation, and several other parameters. Calibration information to calculate the CTT from the pixel count is also available. The calibration is performed by using cloud free segments over the ocean to obtain a sea surface temperature count and the space count (the part of the image outside the Earth's disc) as the two points to specify the calibration slope (Eumetsat, 1996). Theoretical radiances are obtained with the help of the NCEP sea surface temperature analysis (see also section 5.4) and atmospheric correction tables that are calculated using ECMWF forecast profiles.

5.4 Sea Surface Temperature

As an important indicator for global change, the sea surface temperature is monitored intensively. Ship measurements are carried out by regular trading ships mostly on the northern hemisphere and along the coastlines of the continents. There are few in the southern ocean, as well as in the tropical and eastern south Pacific. To close this gap in the measurements, drifting buoys have been deployed mostly in the tropical Pacific and the Southern Ocean. Nevertheless, the coverage by in situ measurements is not very dense especially on the southern hemisphere. In addition, the individual data can have large errors in temperature and position. Since 1985 these measurements are complemented by satellite measurements. From the 5-channel Advanced Very High Resolution Radiometer (AVHRR) on board the NOAA -7, -9, -11 and -14 polar orbiting satellites sea surface temperatures are derived on an operational basis. The satellite data provide an almost global coverage. There are, however, drawbacks, for example there are no measurements possible below clouds and even in clear-sky areas the water vapor content influences the derived sea surface temperature value as well as an increased aerosol content does, e.g. after significant volcanic activity.

Neither the in situ data nor the satellite data provide global coverage or are on a regular grid. Therefore, a real-time global sea surface analysis is produced operationally at the Climate Analysis Center of the National Center for Environmental Prediction (NCEP) (formerly NMC)/NOAA (Reynolds, 1988). The in-situ data and the satellite data are smoothed individually and then blended together. Where enough in situ data are available, they are used, and if there are not enough, the gradients of the satellite field are used. This way, the good spatial coverage of the

satellite data can be exploited and biases can be avoided. In order to improve the resolution of the global SST fields in time and space Reynolds and Smith (1994) applied the method of optimum interpolation to the data. From $1^\circ \times 1^\circ$ averages a weekly analysis is produced.

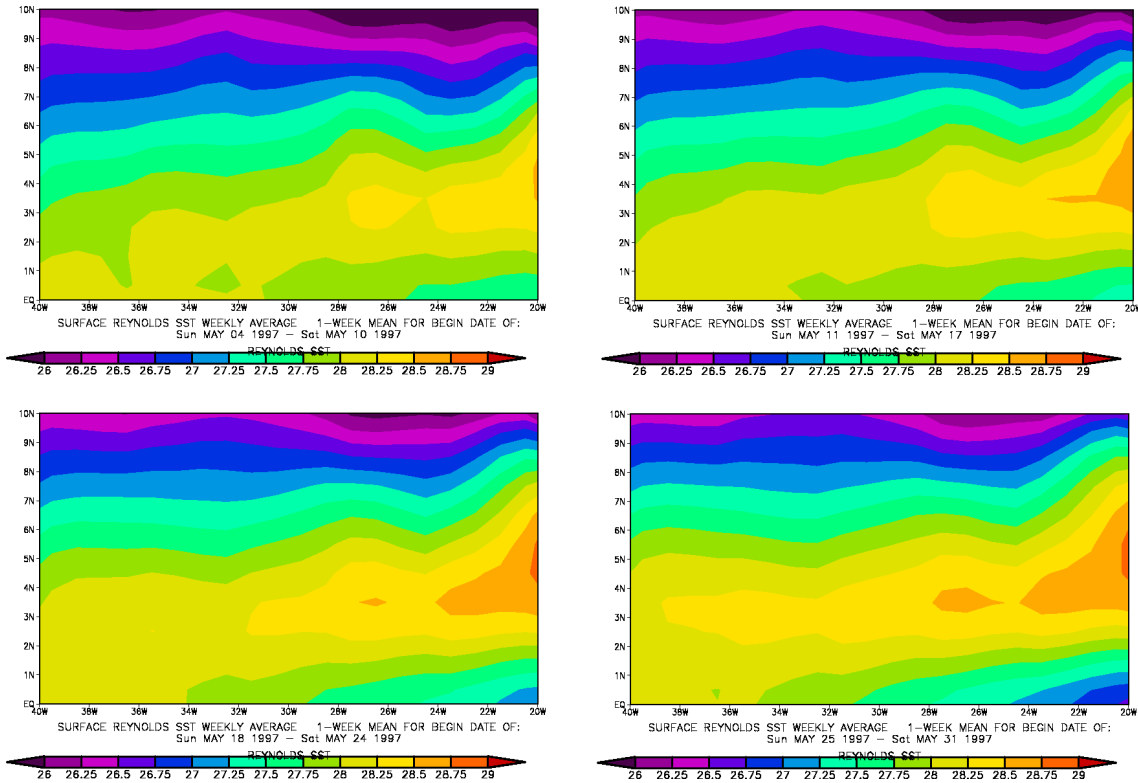


Figure 5.7: Weekly Reynolds analysis of SST between the equator and 10°N and 40°W to 20°W for 4 subsequent weeks during May 1997. Source: NOAA-Cires/Climate Diagnostics Center homepage <http://www.cdc.noaa.gov/>

Figure 5.7 shows the weekly Reynolds SST analysis for 4 subsequent weeks. Only minor changes from week to week can be found, whereas there is a larger difference between the first and the last week. The weekly average are therefore superior to monthly averages and provide a sufficient time resolution. As the flight corridor to South America is collocated with the main trade shipping route the availability of in-situ measurements and thus the quality of the SST data in this region is very high. It is somewhat lower towards the southern central part of the Northern Atlantic. The SST analysis error averaged over the whole tropics is less than 0.1°C (Reynolds and Smith, 1994). These SST data are provided by the NCEP through their website (<ftp://ftp.ncep.noaa.gov/pub/cmb/sst/oisst>).

5.5 Tracing Convective Clouds Along the Trajectories

In this section the method developed to trace the convective origin of the measured air is presented. With this method the actual convective cloud the air parcel originates from can be identified, even if it is not the nearest convective cloud.

The CDS data are reduced such that from every segment only clusters with clear sky over sea or with cloud cover are used. For all clusters with the same optical property class (i.e., sea surface, low, middle, or high clouds) in one segment the temperatures are calculated separately from the corrected infrared channel count with the help of the calibration tables. From these temperatures a weighted mean by number of pixels per cluster is calculated for each group of clusters with the same optical properties. For every MOZAIC averaged (one minute) data point (date, time, latitude, longitude, pressure, temperature (from ECMWF, section 4.6)) there is a set of nine trajectory points (latitude, longitude, pressure, temperature), which indicate the coordinates of the measured air parcel for two days prior to the measurement at 0:00, 6:00, 12:00, and 18:00 UTC as calculated from ECMWF wind fields. That means that the time difference between the MOZAIC data point and the first trajectory point varies. This results in trajectory points at all time distances from the MOZAIC data points and not only on fixed intervals. A spline interpolation is then applied to obtain trajectory locations for every half hour, consistent with the Meteosat slots. As the temperature varies almost linearly with the logarithm of the pressure in the tropics below the tropopause, it can be interpolated as well.

To allow the search for high clouds along the trajectory the CTT values of the segment at the location of the trajectory at the given time are added to the dataset. The lowest CTT that is available in each segment from the averages of all property classes is taken. This way the whole area of the segment will be identified as cloud even if the segment is only partly cloud-covered. Therefore, no cloud will be missed, but there is a possibility that the trajectory actually originates from a cloud at a greater distance. The corresponding SST from the weekly Reynolds analysis data is also added.

The convective origin of the trajectories (figure 5.8) is identified by searching backwards along each trajectory for the first point with clouds with a CTT of less than 240K ($CTT < 240K$). This corresponds to an altitude of approximately 10km in the tropics and is often used as a threshold to identify deep convection (Kley et al., 1997). It is also the approximate temperature at the minimum altitude the MOZAIC aircraft use, and as we expect the air to subside outside the clouds, air from lower clouds could not reach the aircraft. In addition, the temperature at the location of the trajectory T_{Tr} has to be higher than the CTT ($T_{Tr} > CTT$) in order to make sure that the trajectory has not passed above the cloud. This criterion does only

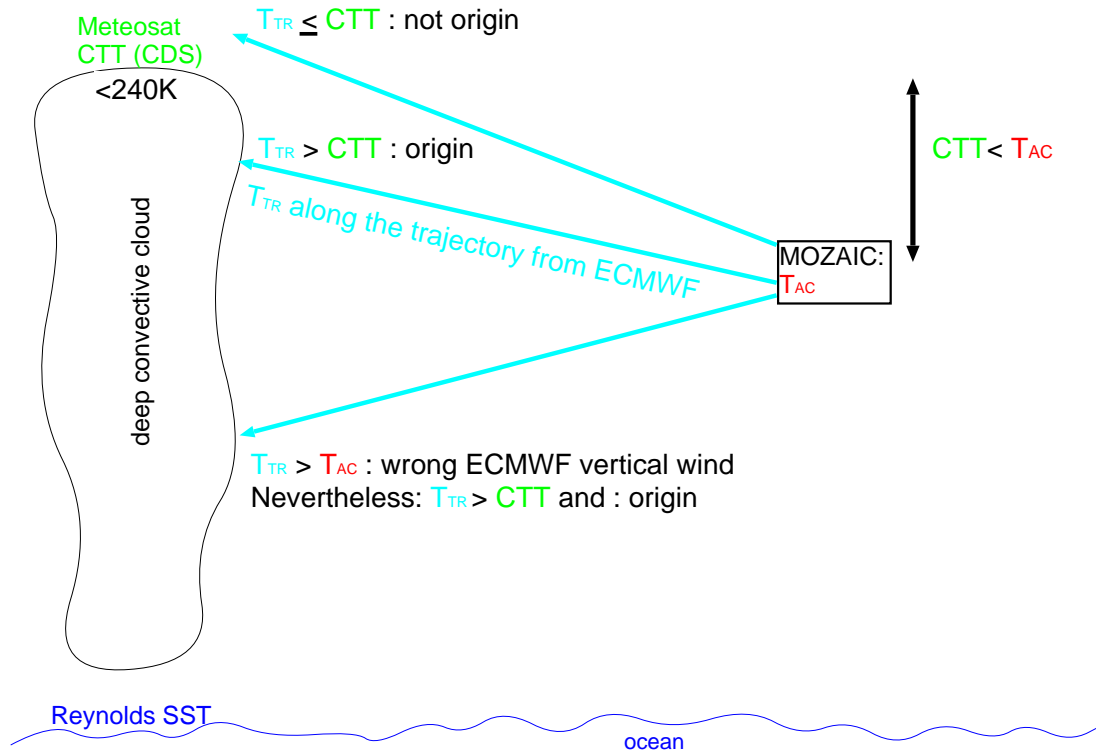


Figure 5.8: Examples of trajectory with different vertical motion to illustrate the different criteria. Only clouds where all criteria are fulfilled are interpreted as the convective origin of the measured air.

affect trajectories that subside corresponding to the ECMWF vertical motion. It is always valid for trajectories that are lifted in the analysis model with a wrong T_{TR} . But most of the time the latter originate from the middle of a convective region and are not very likely to have passed above a cloud. As the air subsides in cloud free regions due to radiative cooling, the top of the cloud from which the trajectory originates has to be in a higher altitude than the aircraft. To ensure this in spite of the uncertainties of the vertical movement of the trajectory, the third criterium used is $T_{AC} > CTT$ where T_{AC} is the local temperature at the location of the aircraft. This criterium is stronger than the above mentioned $CTT < 240K$ criterion as the temperature at the aircraft is below 240K for 98% of all measurements.

During the search additional parameters are determined along the trajectory, e.g., the length of time that is needed to get from the cloud to the aircraft as well as the path length of the trajectory. All these parameters are added to each MOZAIC data record. The resulting dataset consists of the MOZAIC measurements with a related distance to the originating convection for each measurement. The originating convection in this context is only defined through the CTT criterion explained above. No distinction can be made between hot towers, high altitude anvils, or

cirrus clouds. The resolution of the CTT dataset does not allow the identification of single hot towers that cover only a typical area of 10km^2 , anyway.

5.6 The Origin of the Measured Air from the Trajectory Analysis

The influence of the data limitations and some general features of the trajectories derived from the method described in the previous section are presented in this section.

5.6.1 Influence of Trajectory Length and Satellite Field of View

Theoretically, almost every air parcel in the tropics has been lifted from the surface through convection in its history, and thus every trajectory should originate from a convective cloud when it is calculated backwards in time far enough. The trajectories are only two days long. Therefore, some of them never reach the convective origin, especially in the subtropical high pressure belts, where there is few local convective activity.

Another factor possibly limiting the number of trajectories encountering convective clouds is the limited data retrieval area of Meteosat (red circle in figure 5.5). Its influence on the trajectories is shown in figure 5.9. As soon as the trajectories leave the field of view of Meteosat no CTT data are available and convection cannot be identified. Figure 5.10 shows the fraction of trajectories with convection by latitude band. The purple line with crosses denotes the total number of trajectories for each latitude band. It is consistent with the total number of measurements inside the troposphere for each latitude band. The fraction of trajectories that end inside the field of view of Meteosat, which is approximately a great circle of 60° around the origin of the geographic coordinate system, is shown by the green dashed line with stars. This fraction is almost 100% in the region around the equator with low large-scale horizontal winds and around 75% elsewhere. That means that the limitation due to the restricted field of view is negligible in the inner tropics and not very significant outside. The red dashed line shows the fraction of trajectories with convection relative to all trajectories that end inside the Meteosat field of view. Except for the subtropical high pressure belt between 20°N and 40°N , between 70% and 80% of the trajectories that do not leave the field of view encounter convection. Only 20% of the trajectories that end inside the field of view between 20°S and 20°N do not encounter deep convection within 2 days, and are limited due to their length. In this region longer trajectories would not improve the amount of data significantly. In chapters 6 and 7 only trajectories with a convective origin in this innertropical

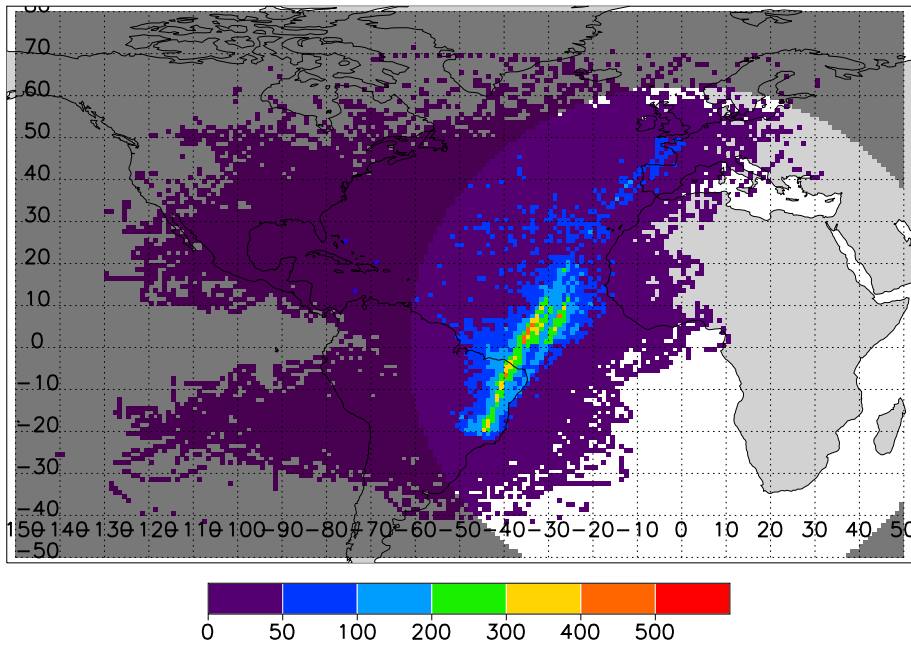


Figure 5.9: Endpoints of all backward trajectories. Number per $1^\circ \times 1^\circ$ grid box. 'Endpoints' means the location of the backward trajectory either 2 days before the MOZAIC measurement or at the high cloud in case one was encountered along the way. The area where no CDS data are available is shaded. The same, but only for trajectories with convection: see appendix.

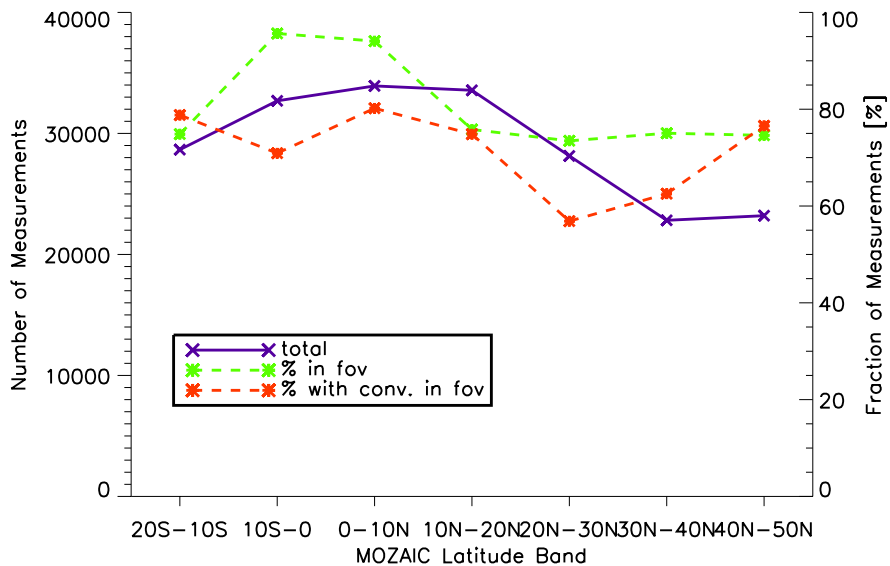


Figure 5.10: Total number of trajectories (blue), fraction of trajectories that end inside the Meteosat field of view (green, dashed), and trajectories with convection as a fraction of the ones that end inside the field of view (red, dashed) by MOZAIC measurement latitude band.

region are used.

5.6.2 Identifying Source Regions

The source region of the measured air presented in chapter 4 is identified with the help of the trajectories. Either the endpoint of the trajectory around two days before the measurement is assumed to be the source or, if convection is detected along the trajectory, the location of this convection is taken as the origin. Due to the restrictions of the trajectories and the satellites field of view this origin is just an estimate of the real origin of the trajectory. Convection that has happened more than two days before the measurement can not be identified although it might still influence the characteristics of the measured air.

For an organized approach to an analysis of the origin of the measured air, the complete area that is reached by the trajectories in two days (figure 5.9) is divided into different regions. A distinction is made between continents and oceans and the Atlantic ocean is further broken up into different parts. This distinction gives a more detailed view on the origin of the measured air although the real origin is uncertain outside the Meteosat field of view where convection cannot be identified. Table 5.1 gives the fraction of trajectories ending in different regions for all latitude bands. The table clearly shows that in all latitude bands the region or regions that

| | 20-10°S | 10°S-0° | 0-10°N | 10-20°N | 20-30°N | 30-40°N | 40-50°N |
|------------------------|-----------|-----------|-----------|-----------|-----------|-----------|-----------|
| S. America | 69 | 44 | 7 | 4 | < 1 | | |
| Africa | | < 1 | 2 | 4 | 5 | 2 | 1 |
| Europe | | | | | < 1 | 2 | 11 |
| N. America | | | < 1 | 2 | 3 | 6 | 8 |
| S. Pacific | 16 | 1 | < 1 | | | | |
| S. Atlantic | 14 | 34 | 8 | 1 | < 1 | | |
| Atl. 0°-10°N | 2 | 19 | 72 | 18 | 2 | | |
| Atl. 10°-20°N | | 1 | 7 | 47 | 22 | 3 | < 1 |
| Atl. 20°-30°N | | < 1 | 1 | 9 | 39 | 21 | 4 |
| N. Atlantic | | | < 1 | 2 | 16 | 59 | 71 |
| Caribbean | | < 1 | 2 | 13 | 13 | 8 | 5 |
| Number of Trajectories | 28660 | 32690 | 33925 | 33567 | 28140 | 22821 | 23201 |

Table 5.1: Fraction in percent of trajectories from the regions of origin with respect to the measurement latitude bands. The Caribbean region includes a few trajectories from the Pacific at the same latitude as the Caribbean. Fractions greater 10% are in bold face.

correspond to the flight corridor at the respective latitude are the major source of

the measured air. This is particularly striking for the ITCZ and South America, which will be the main regions of interest in the following chapters. Only a much smaller part comes from the directly neighboring regions and a minor part from other regions.

5.6.3 Distance Between Measurement and Cloud: Latitudinal and Seasonal Variations

The limited meridional exchange on the timescale of two days can also be seen in figures 5.11 and 5.12. They show the direct distance between the MOZAIC measurement point and the cloud that was found along the trajectory in latitude and longitude. Only trajectories that encounter convection are presented. The diagrams can be seen as if the aircraft would always be in the origin and the clouds encountered by the trajectories are the black dots.

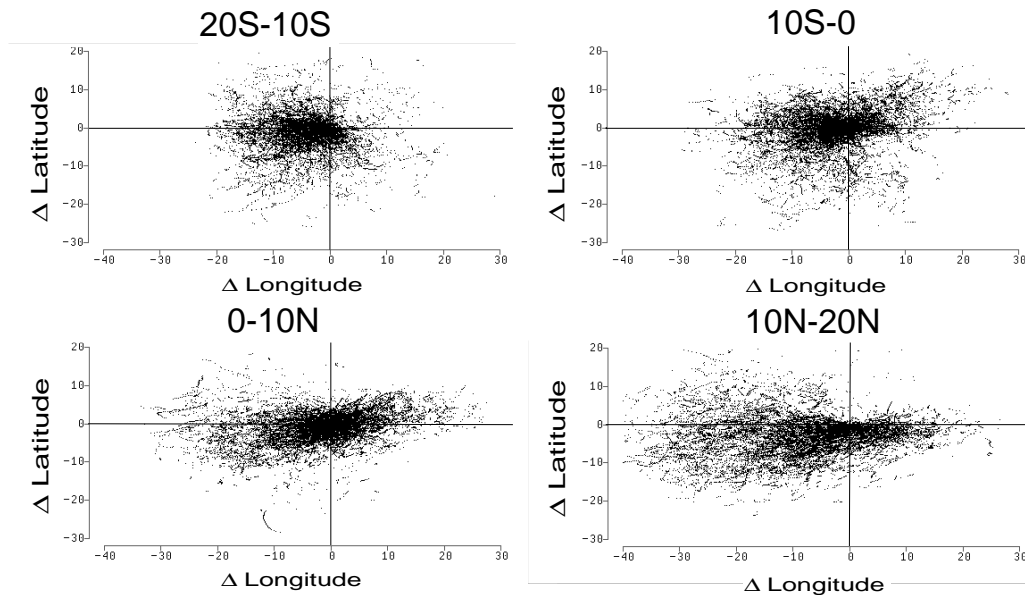


Figure 5.11: Distance of convection to measurement point in geographical degrees for measurements in different latitude bands.

Figure 5.11 is for different latitude bands. The whole MOZAIC period until June 2000 is presented. By far most trajectories do not reach further than 10° in the meridional direction and only very few further than 20° . In the zonal direction most trajectories especially on the southern hemisphere reach not farther than 20° , but on the northern hemisphere there is a significant part of trajectories reaching almost 40° . The region with the largest distances is between 10°N and 20°N . The limitation of the trajectory length on the southern hemisphere can be explained with the

restricted field of view of Meteosat as only trajectories that encounter convection are shown. These can only be relatively short over South America as the aircraft fly close to the edge of the field of view.

In order to illustrate the seasonal variations figure 5.12 presents the same diagram as figure 5.11 but only for data in the ITCZ between the equator and 10°N for different seasons. Although the seasons are not as marked as outside the tropics there are seasonal variations in the large-scale circulation that show up in the distribution of the trajectories. Generally large-scale winds in this latitude band are not very strong and the prevailing direction is southwest especially in winter. But in the summer months almost all trajectories come from the east indicating east to northeast as the dominant wind direction in this season.

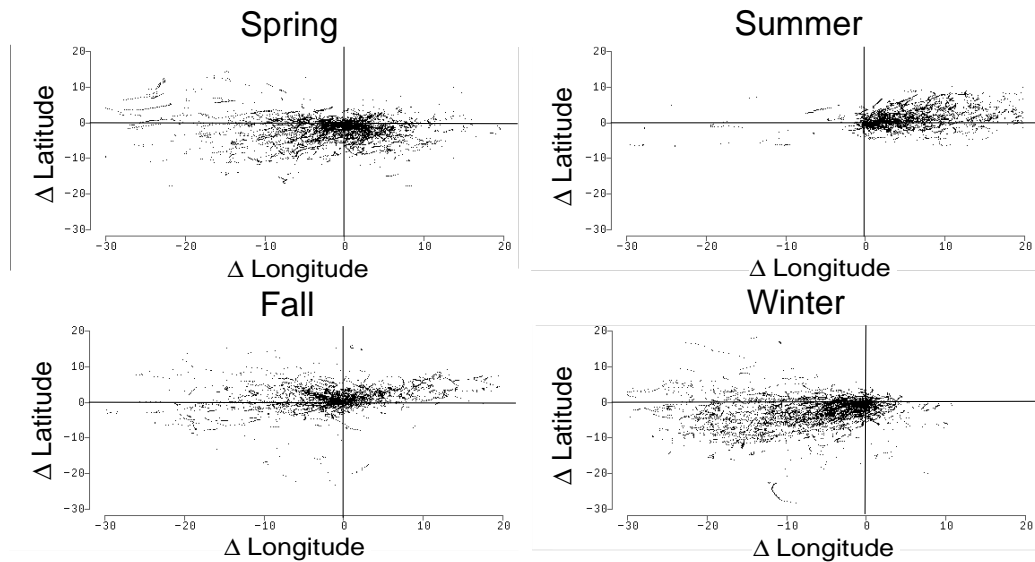


Figure 5.12: Seasonal variations in the distance of convection to measurement point in geographical degrees for measurements taken between the equator and 10°N .

Chapter 6

Convection and the Water Vapor Distribution

In this chapter the water vapor distribution and other characteristics of air masses of convective origin in cloud-free areas are studied with the help of the trajectories shown in chapter 5. Only trajectories that have encountered a convective cloud in two relatively uniform regions of high convective activity are used (figure 6.1). The first region is in the ITCZ between the equator and 10°N . Only trajectories with convection between 20°W to 40°W are taken to make sure that only convection over a remote area of the ocean will be dealt with. This part of the measurements with their origin in the ITCZ will be referred to as ITCZ in the rest of this work. The second one is the part of South America which lies inside the field of view of Meteosat.

As shown in section 5.6 many of the trajectories are relatively short and the aircraft

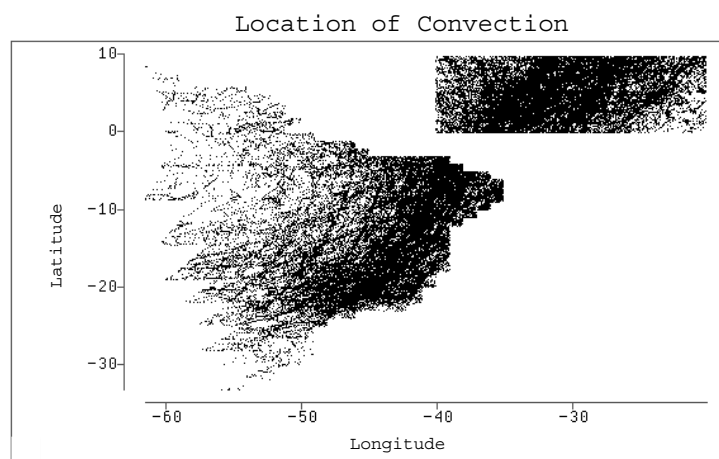


Figure 6.1: Locations of convection for the two regions studied further, ITCZ and South America.

are close to the convective clouds. More than 60% of the trajectories are shorter than 550km corresponding to 5 degrees in latitude or longitude, and 10% encounter convection immediately at the aircraft. But there are also trajectories encountering clouds only after 2 days (1.5%) or more than 2000km (4%). The distribution of the measurements onto the different pressure levels is not uniform in these two region. While in the ITCZ the 238hPa level and the 262hPa level dominate, there is also a significant number of measurements in the highest altitude pressure level at 197hPa over South America (figure 6.2).

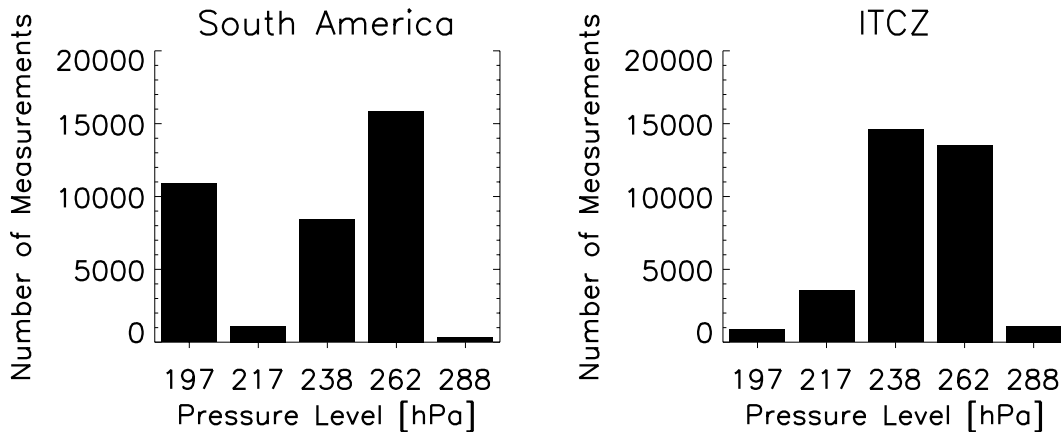


Figure 6.2: Histograms of the distribution of pressure levels for the ITCZ and South America.

In section 6.1 only measurements with very short trajectories with a length of less than 80km are taken to provide a comprehensive overview over the properties of air in the vicinity of convection. This choice corresponds to half the resolution of the CTT data. It includes approximately 40% data that have been measured inside a CTT segment with high clouds that satisfy the criterion. The rest of the measurements is taken in cloud-free segments that lie immediately downwind of a segment with high clouds. The next section 6.2 includes all trajectories sorted by length in time and space to study the change of air characteristics as the air is advected away from the convective region. Only different trajectories with different lengths related to the different MOZAIC measurements can be studied and not the real evolution along one single trajectory. It is assumed that in a statistical sense the trajectories encounter similar conditions as they move through the cloud-free areas away from the originating convection.

6.1 The Vicinity of Convective Clouds

In this section a climatology of measurements close to convective clouds is presented. In order to study the processes influencing the air as it is advected away from

the convection it is necessary to know how variable the humidity is close to the clouds with regard to, e.g., the pressure levels and seasons. Differences between the ITCZ and South America are shown and the dependence of the humidity close to convection on the underlying sea surface temperature is also studied. As indicated in section 5.3 the resolution of the CDS is approximately 160 km at the subsatellite point. Therefore, trajectory lengths of up to 80 km represent measurements close to convective clouds within this resolution. This threshold also includes enough measurements for this study as approximately 10% of the trajectories that find convection at all seem to encounter the convective cloud immediately, although the aircraft rarely fly very close to active convection.

6.1.1 Variability with Altitude

At first the measured parameters are examined regarding their variation with altitude. For this purpose relative humidity is plotted for all pressure levels (figure 6.3). Although the coverage per pressure level is not uniform, there are at least several

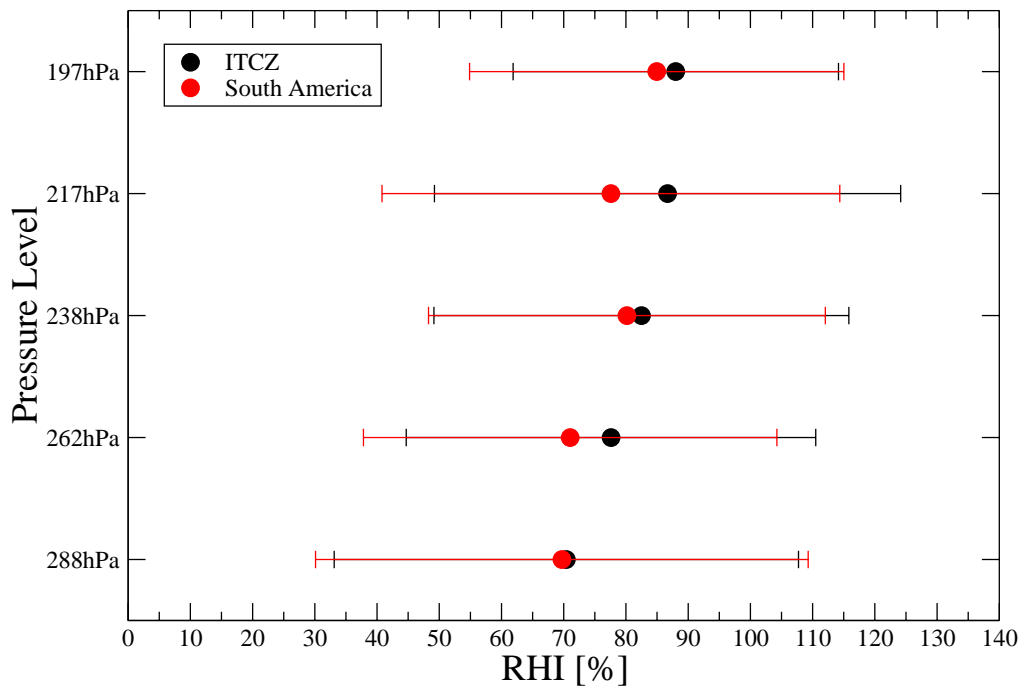


Figure 6.3: Relative humidity by pressure level near convection, mean and standard deviation.

hundred measurements on each. This way the statistical basis for all pressure levels is quite strong. A striking feature of the relative humidity measurements in figure 6.3 is the large standard deviation. Even in the vicinity of a convective cloud very low relative humidities are found apart from the expected ones near saturation (figure 6.4), although the relative fraction of dry measurements is much smaller than

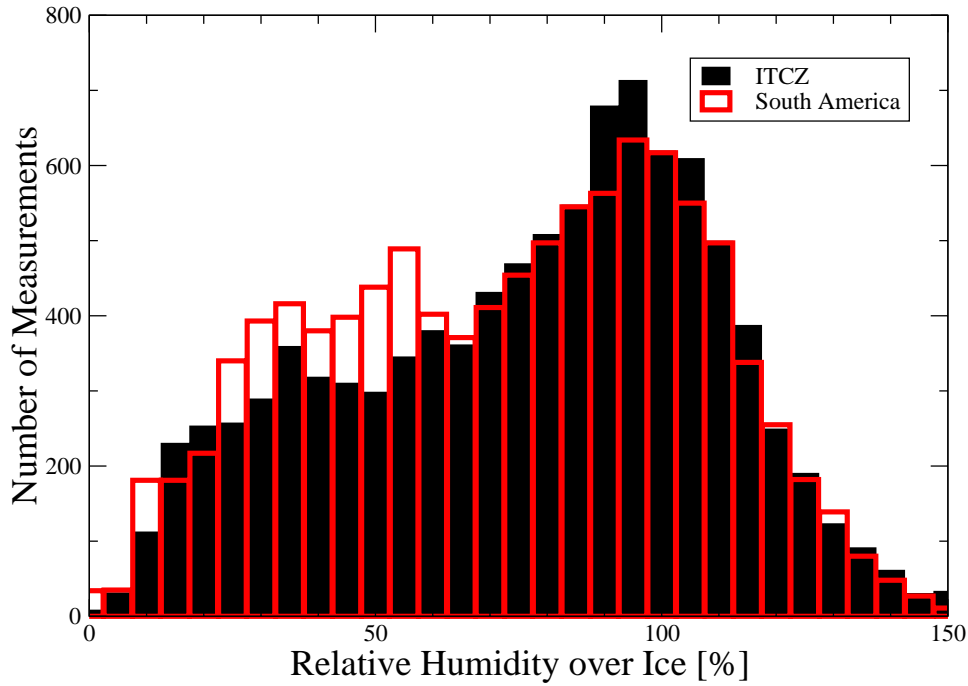


Figure 6.4: Histogram of the relative humidity with respect to ice near convection for all pressure levels.

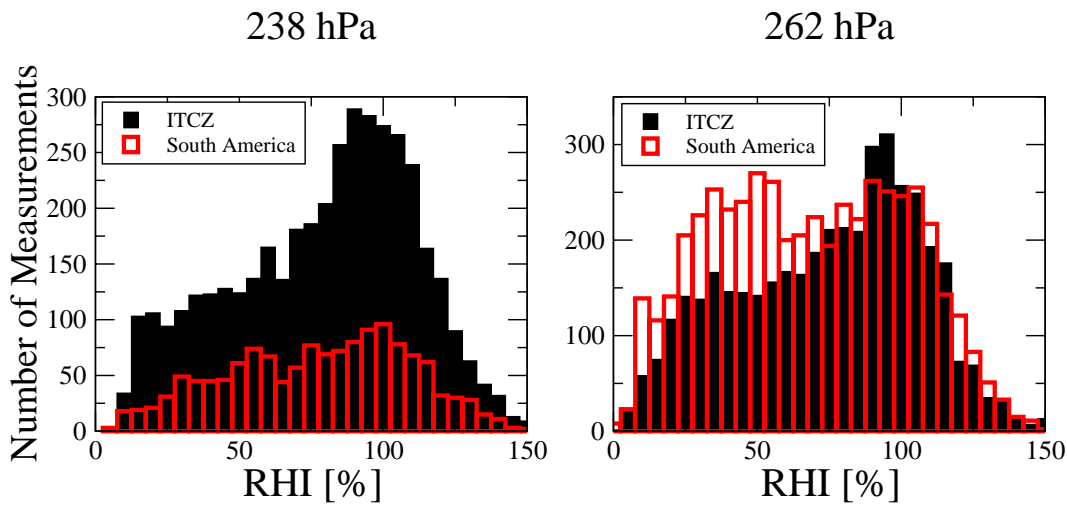


Figure 6.5: Histograms of the relative humidity with respect to ice near convection for the two main pressure levels.

for all measurements taken together. The distributions on the two main pressure levels are similar particularly in the ITCZ corresponding to the small variation of the mean value for the different pressure levels. The strong bimodality is statistically significant and does not depend on season or location within the ITCZ. For an interpretation it has to be remembered how the measurements are performed. The

MOZAIC dataset is a climatology in which the relation of data points in time, distance, SST dependence etc. is a purely statistical one. Any figure shows the state of the parameter in question at the time and location of the measurement. This means that the bimodality of the relative humidity is due to the aircraft encountering air masses that are either wet or dry. This is an unexpected result considering the fact that the measurements are taken in lee but close to a convective cloud segment, within the resolution of the CDS of 160km.

A reason for the low humidities close to a convective cloud may be convectively induced subsidence or convective downdrafts. These can be very dry due to the downward transport of air with lower specific humidities. Another reason could be the limited resolution of the CTT data. Convective hot towers cover typically only an area of 10km^2 (Riehl, 1979). The trajectories are assumed to have encountered a convective cloud as soon as they reach a CDS segment with only a fraction of high cloud cover even if the trajectory passes the cloud at a certain distance. Outside the convective hot towers the relative humidity can be low due to convective downdrafts and subsidence. A third reason for measurements of dry air may be that the measurements are taken below the non-precipitating anvil of a convective cloud. As the resulting distribution of relative humidity values is very broad, the standard variation gives only an impression of the range of values but is no indicator of the significance of the mean value. The resulting mean relative humidity varies between 70% and 90% with lower values in lower altitudes and there are no significant differences between the ITCZ and South America. In the two main pressure levels in the ITCZ it is very close to 80%.

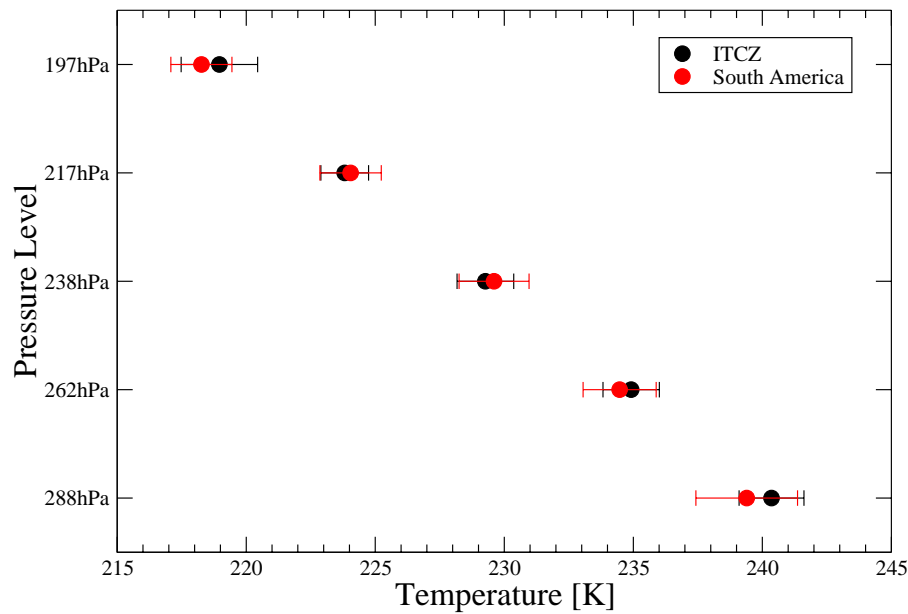


Figure 6.6: Temperature by pressure level near convection.

The difference between the mean temperatures of the highest and lowest pressure level is 21K and the temperature does not vary much on single pressure levels (figure 6.6). As a result the specific humidity difference is almost one order of magnitude although the relative humidity is almost constant (figure 6.7). The difference between the ITCZ and South American humidity is small compared to the difference between the pressure levels. As for the relative humidity the standard deviation on each pressure level is about 50% of the mean value.

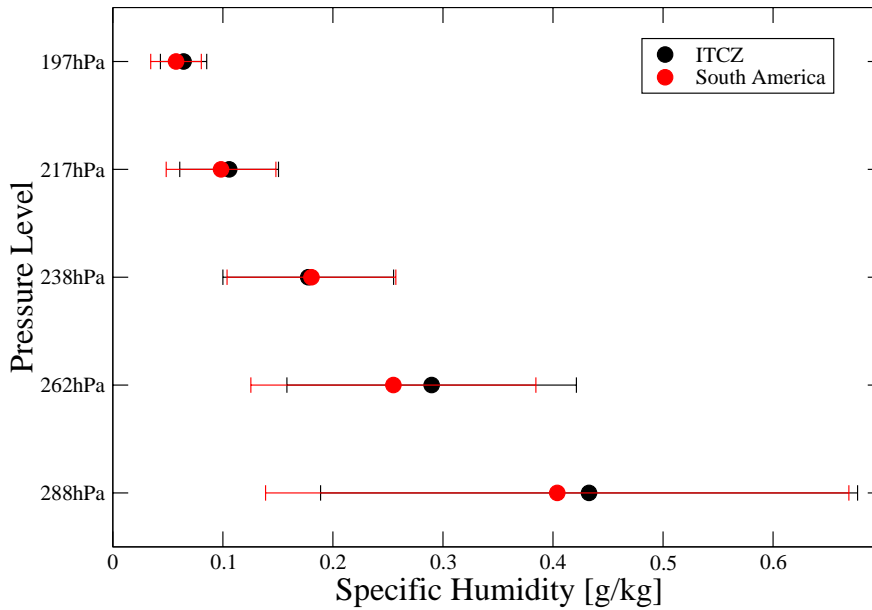


Figure 6.7: Specific humidity by pressure level near convection.

6.1.2 Seasonal Variability

The overall mean values presented above include seasonal variations. This is even more important as the sampling is not uniform seasonally, particularly over South America. Figure 6.8 shows the proportion of measurements per season for the 262hPa pressure level. This proportion varies from pressure level to pressure level and is more even for all pressure levels taken together. All seasonal values given here are the sum or mean for the three months of all years that form the respective northern hemisphere (N.H.) season, according to the meteorological definition.

Despite the fact that all aircraft fly over both regions the number of measurements differ (figure 6.8). The difference can be explained by the differences in local convective activity. Only measurements close to convection are taken and the seasonal distribution of convection is more uniform in the ITCZ than over South America. The seasonal variability of the mean relative humidity (figure 6.9) is relatively low. Comparing the ITCZ and South America, it is noticeable that the mean relative

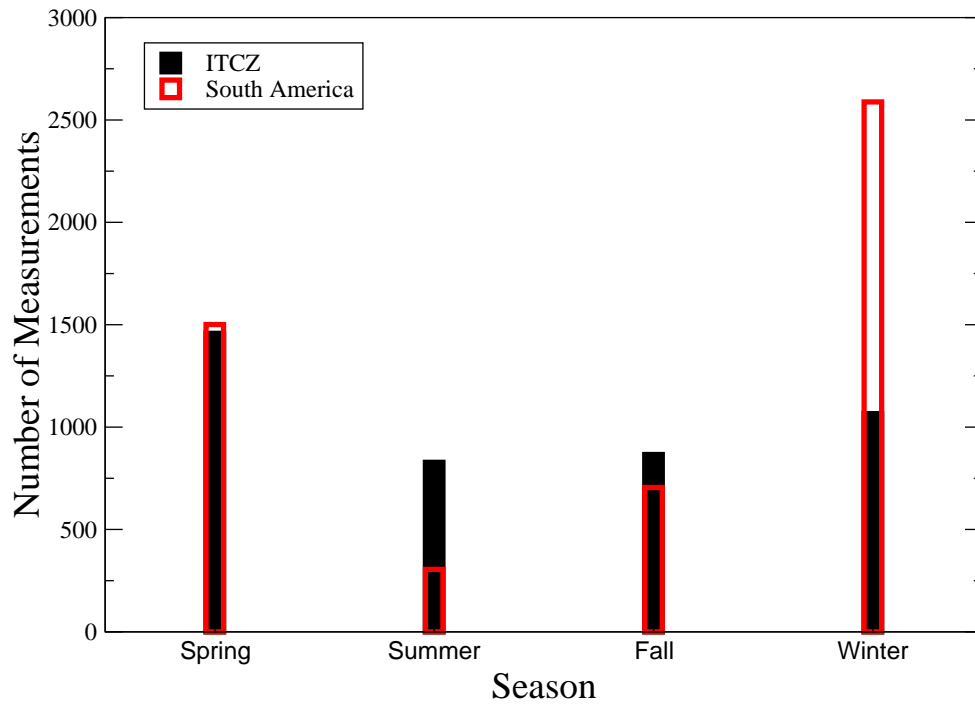


Figure 6.8: Seasonal number of measurements close to convection in the ITCZ and South America at 262 hPa.

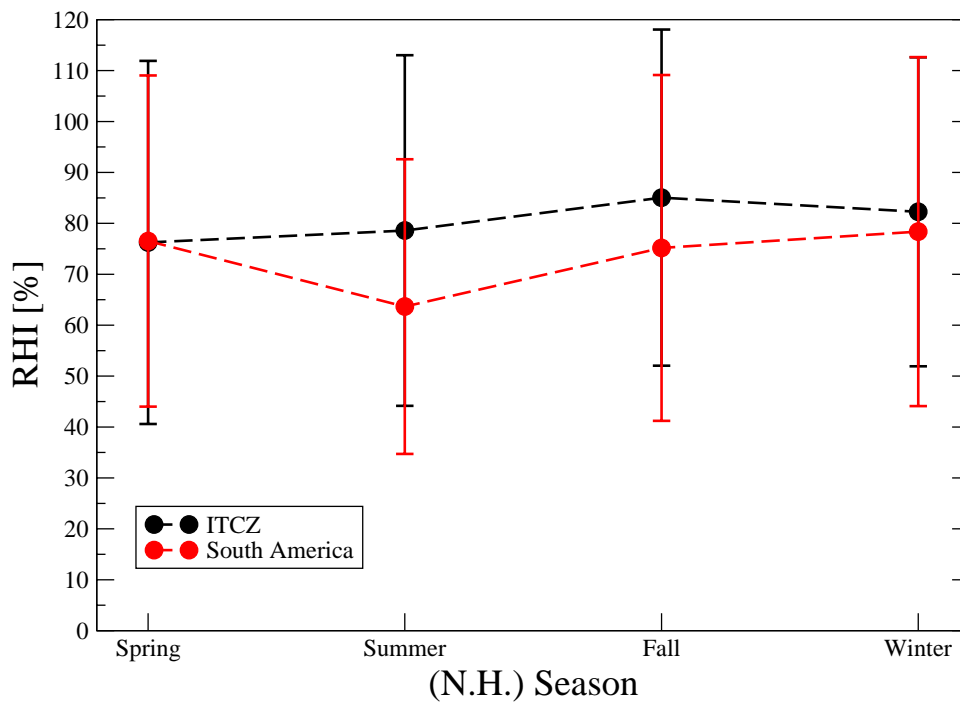


Figure 6.9: Seasonal variability of relative humidity near convection for all pressure levels.

humidity is similar in winter and spring when there is more convective activity over the latter, and lower in summer and fall.

The mean specific humidity on the 262 hPa level (figure 6.10) is also lower and more variable above South America throughout the seasons. This corresponds to the overall mean value being lower in the two lower altitude pressure levels.

The lower humidity found above the continent can be related to the different na-

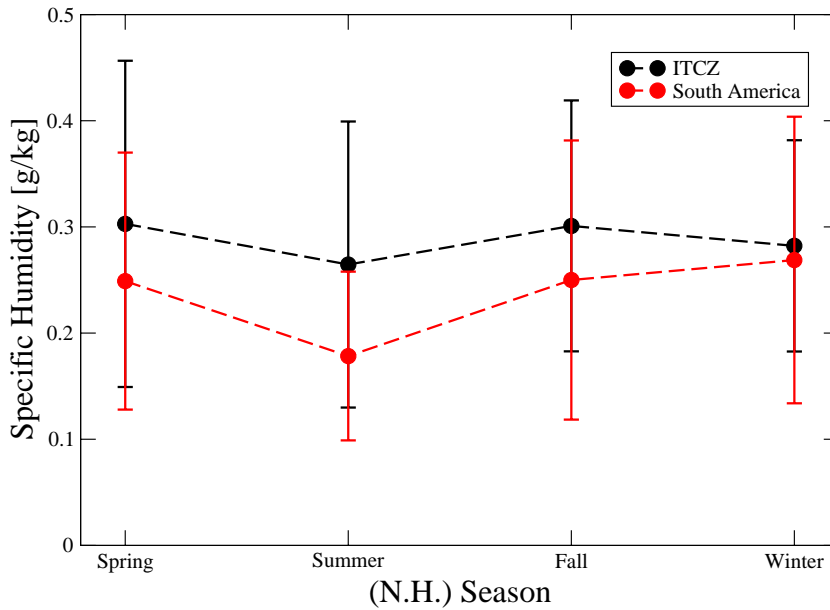


Figure 6.10: Seasonal variability of specific humidity measured at 262 hPa near convection.

ture of the convection over the ocean and the continent. In order to illustrate the characteristics of the convective activity over both regions the OLR is chosen (see also section 5.2). The seasonal mean of the OLR averaged from 1995 to 2000 (figure 6.11) is always near $220 W/m^2$ in some parts of the ocean region studied here, but never much lower. Over the continent in contrast, there are seasons with very high mean OLR over the whole area, but if there is convection and low OLR in winter and spring it is below $210 W/m^2$ almost everywhere. This means that the convection over the continent is restricted to certain times of the year, but reaches higher altitudes than the convection over the ocean. The high altitude convection could lead to drier air in the low altitude pressure levels either due to less detrainment in these levels or through downdrafts of very dry air from above in the vicinity of convection. For the ITCZ, where the evolution of the humidity as the air is transported away from the convection is studied in detail in chapter 7, seasonal variations of the relative and specific humidity are negligible.

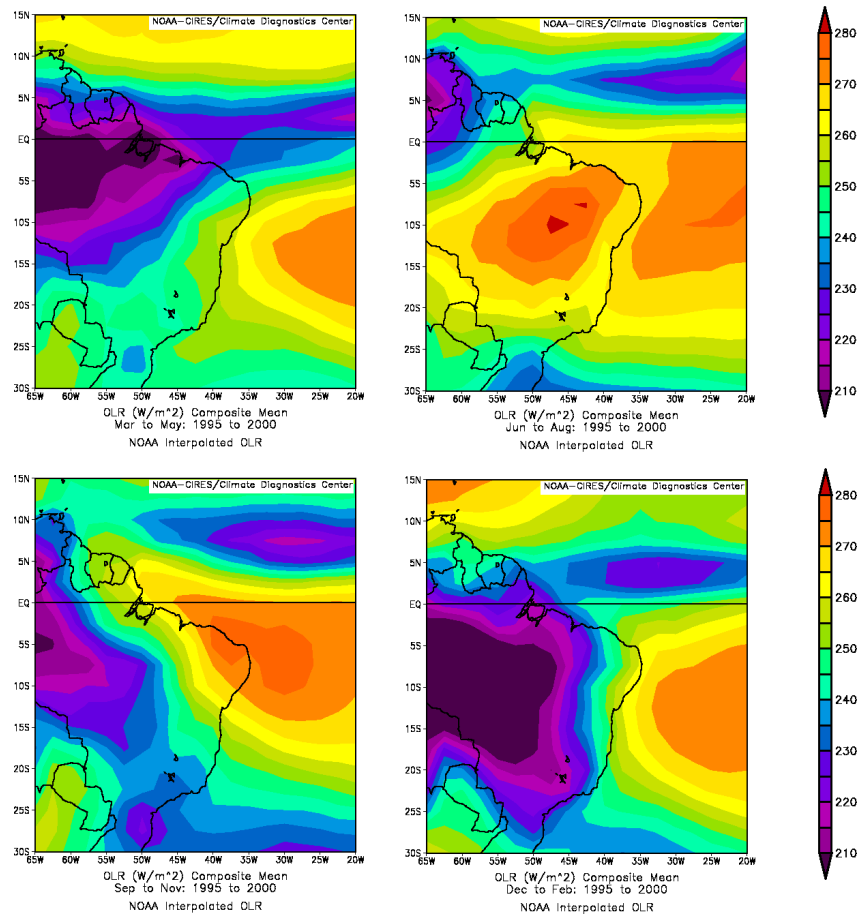


Figure 6.11: Multi-year mean of OLR (in Wm^{-2}) for the four northern hemisphere seasons, 1995 to 2000. The relevant part of South America and the ITCZ are shown. Spring: upper left, summer: upper right, fall: lower left, and winter: lower right. Source: NOAA-Cires/Climate Diagnostics Center homepage <http://www.cdc.noaa.gov/>

6.1.3 Ozone Variability

The ozone distribution is unimodal and has a distinct maximum particularly in the ITCZ (figure 6.12). The standard deviation of the ozone measurements is still almost 50% of the mean value (figure 6.13). In the ITCZ the mean is almost constant, increasing only very slightly with height at about 35 ppbv. Over South America the ozone mean shows no clear behavior with height at about 43 ppbv. The lower values over the remote ocean area are expected as most of the air that is transported into the upper troposphere stems from the boundary layer and the remote marine boundary layer is ozone depleted (see section 2.3). The higher values as compared to the values found directly at the ocean surface can be explained by entrainment of air with larger ozone mixing ratios during the convective ascent (Kley et al., 1999)(see also section 2.3).

The mean ozone mixing ratio (figure 6.14) is almost constant throughout the year in the ITCZ, but slightly lower in spring. The situation over South America is different. While the mean value is not that different from the ITCZ in most seasons, it is about 50% higher in fall. This outstanding high value can be explained with the biomass burning in southern hemisphere spring at the end of the dry season (see section 2.3).

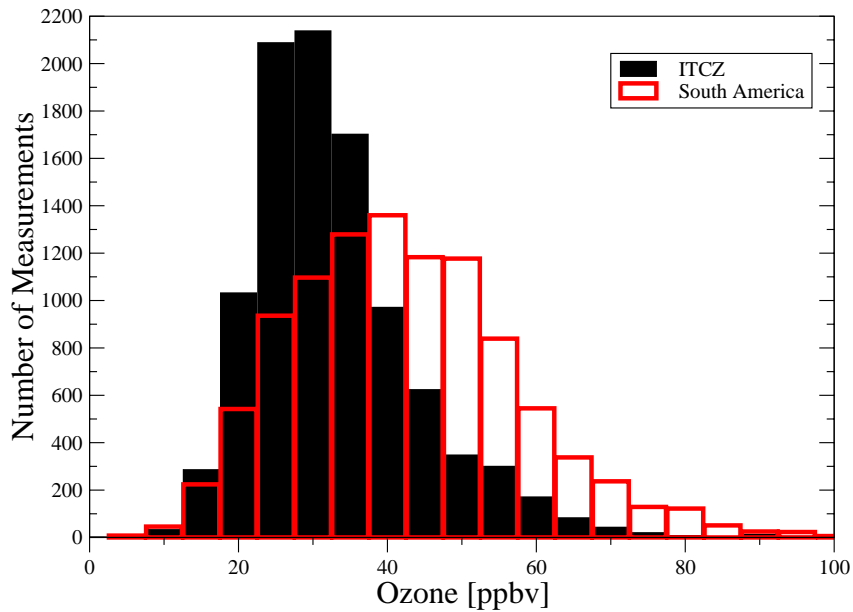


Figure 6.12: Histogram of ozone mixing ratios close to convection.

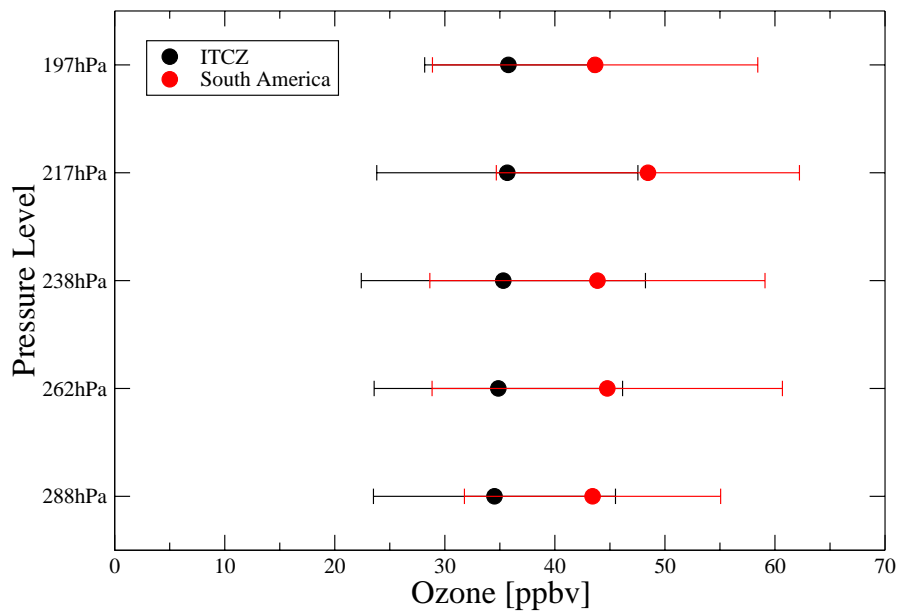


Figure 6.13: Ozone by pressure level near convection, mean and standard deviation.

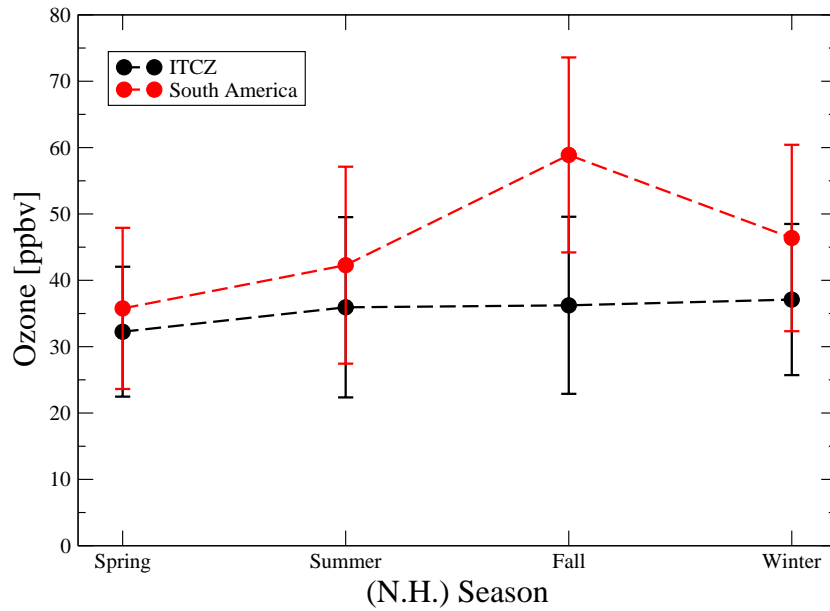


Figure 6.14: Seasonal variability of ozone near convection for all pressure levels.

6.1.4 Influence of the Sea Surface Temperature on Deep Convection

In this section the influence of the sea surface temperature on deep convection is studied using measurements close to the convection over the ITCZ. If there is a feedback mechanism based on the coupling between upper tropospheric humidity and the sea surface temperature through convection, it should be represented by a dependence of the humidity near convection on the sea surface temperature in the first place. The distribution of the SST below the convection that was identified with the Meteosat CTT data is narrow (figure 6.15). There are very few data below 300K which is the necessary minimum temperature for deep convection (Gadgil et al., 1984; Graham and Barnett, 1987), and there are very few measurements above 302K as well. This is consistent with findings by Waliser et al. (1993) that sea surface temperatures in excess of about 302.5K occur only under diminished convection. Therefore, these SSTs can not be found in this dataset containing only SSTs below deep convective clouds.

There is an increase of the relative humidity within the SST range from 300K to approximately 302K and a decrease at higher SSTs (figure 6.16). The increase in mean relative humidity from about 70% at 300K to about 90% at 302K is larger than any mean seasonal variation or the differences between the pressure levels. Therefore, it can not be due to seasonal or altitude related biases. The higher mean relative humidity arises from a larger proportion of relative humidities near or above

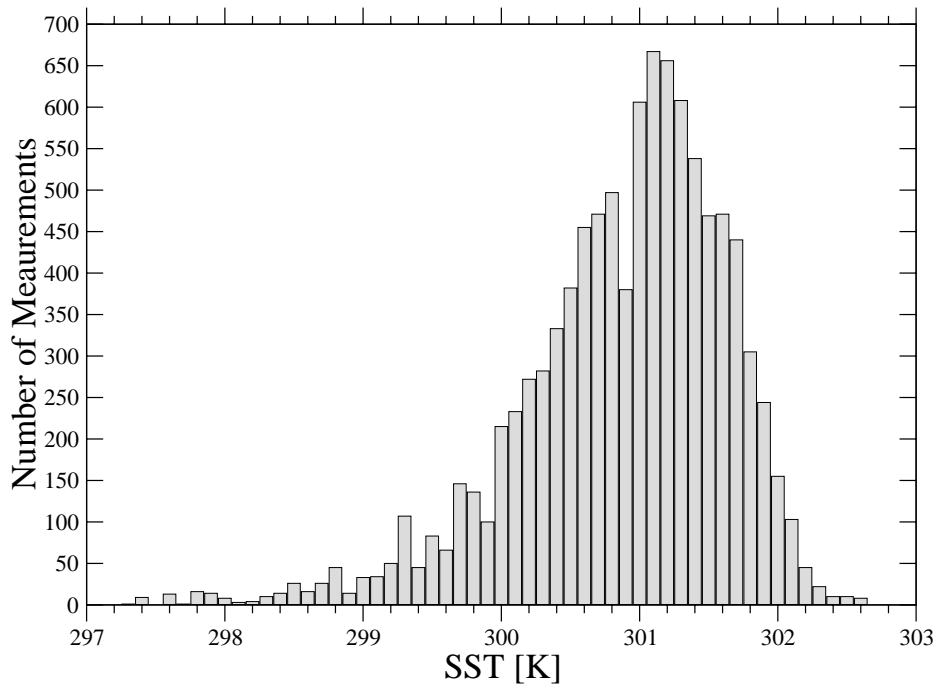


Figure 6.15: Histogram of the sea surface temperature below the convective cloud in 10th of a degree SST bins.

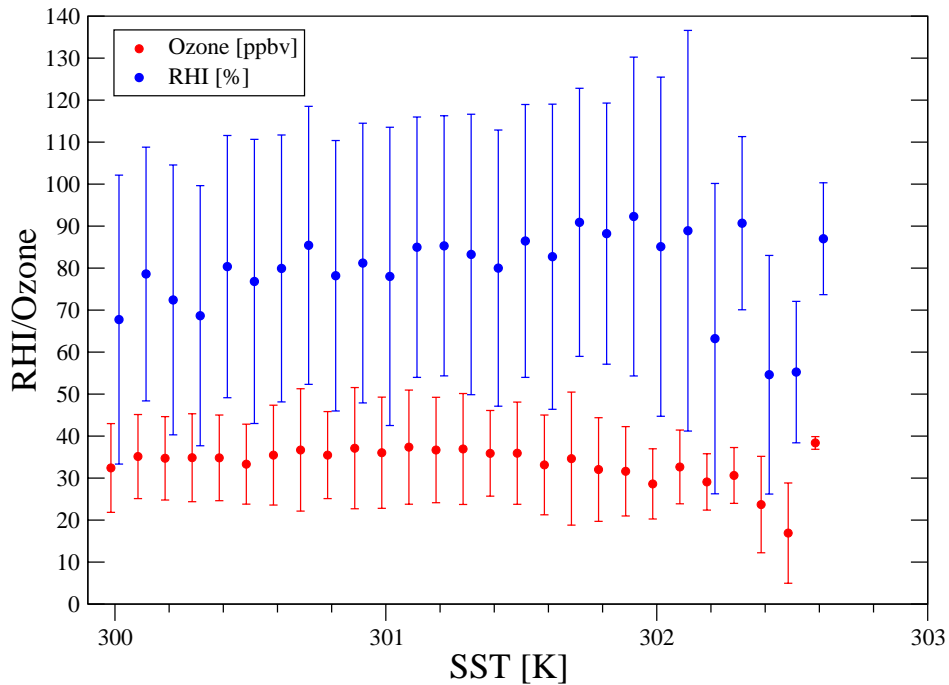


Figure 6.16: Relative humidity with respect to ice and ozone versus SST in 10th of a degree SST bins.

saturation in the data at higher SST. However, the decrease in the relative humidity for SSTs above 302.2K is not significant. All data above 302.2K originate from only 11 flights, and more than 60% from only 2 different flights.

As the distribution of relative humidity is not unimodal (figures 6.4 and 6.5), the decrease in the mean value can be due to either a change in the humidity in each mode or a change in the fraction of measurements in each mode. In order to separate the two modes the measurements were divided into three parts, under the assumption that the distribution is strictly bimodal. Measurements with relative humidities represent the dry mode with a maximum around 30%, and measurements above 70% relative humidity represent the moist mode with a maximum close to saturation. The third part includes the equivocal overlap region of both modes between 50% and 70% relative humidity.

The fraction of measurements in each mode is shown in figure 6.17. With increasing SST the percentage of the dry mode decreases while that of the moist mode increases. The percentage of measurements in the intermediary range stays roughly constant. The mean relative humidity for each mode is shown versus SST in figure

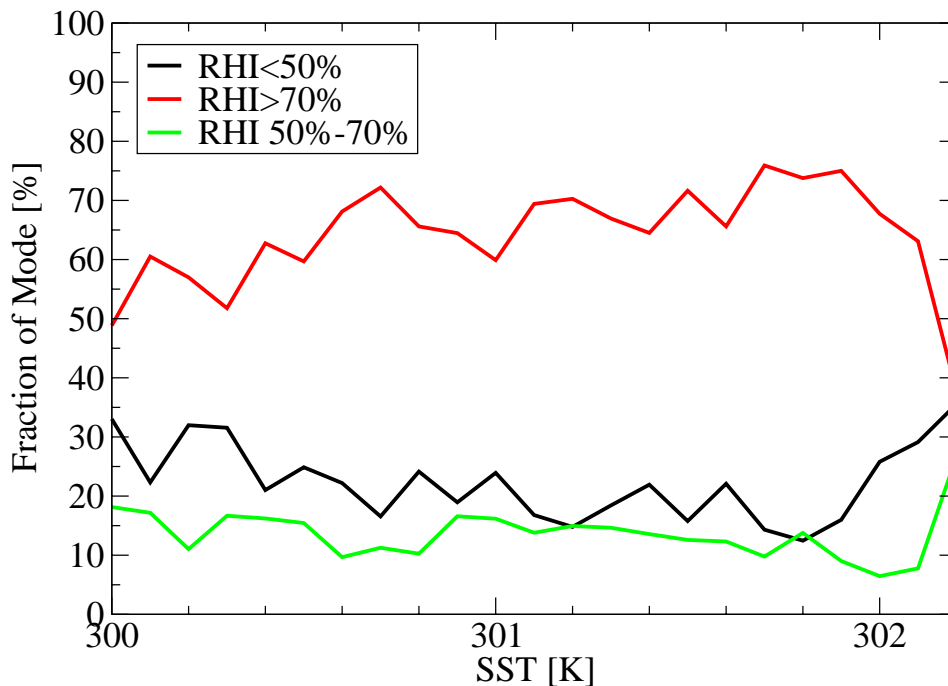


Figure 6.17: Percentage of measurements in each mode versus SST.

6.18. The mean of the moist mode is 100% at 300K SST. It increases slowly to approximately 110% at higher SSTs. Conversely, the mean relative humidity in the dry mode is about 35% at lower SSTs and decreases very slightly towards 302K. Therefore, the increase in the overall relative humidity mean is partly due to the

increase in the moist mode mean relative humidity and also to the increase in the relative number of measurements in this mode.

The mean ozone mixing ratio versus SST is also shown in figure 6.16. It is almost constant at about 35ppbv up to 301.5K SST and decreases from there to slightly below 30ppbv at 302K. Seen separately for the two relative humidity modes (figure 6.18) the ozone mixing ratio in the dry mode is slightly higher than that in the moist mode. The decrease at SSTs above 301.5K occurs in both modes but is stronger in the dry mode.

The mean specific humidity for each relative humidity mode versus SST for the two main pressure levels is presented in figure 6.19. On both pressure levels the specific humidity in the moist mode increases by about 30% between 300K and 302K SST. The dry mode mean specific humidity stays close to constant at most SSTs on both pressure levels with a peak between 301.5K and 302K at 262hPa.

Correspondingly, the temperature is presented in figure 6.20. In both pressure levels the mean temperature in the dry mode is slightly higher than that of the moist mode. All temperatures increase approximately according to the SST increase indicating that the lapse rate does not change. Together with the minor change in the relative humidity the temperature increase leads to the increase in the specific humidity with increasing SST.

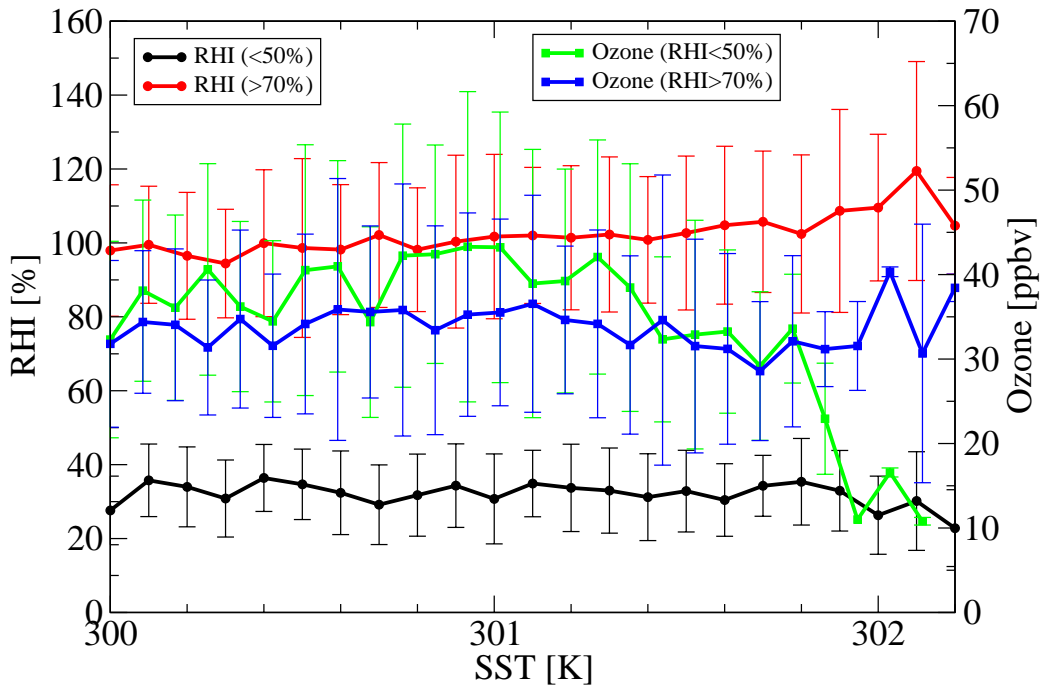


Figure 6.18: Mean relative humidity and ozone mixing ratio for both modes.

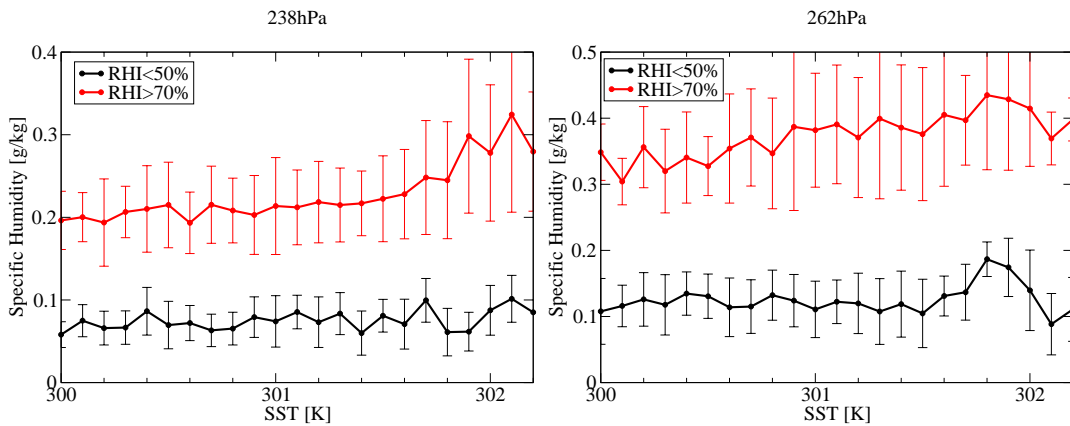


Figure 6.19: Specific humidity versus SST for 238hPa (left) and 262hPa (right), separated into the relative humidity modes.

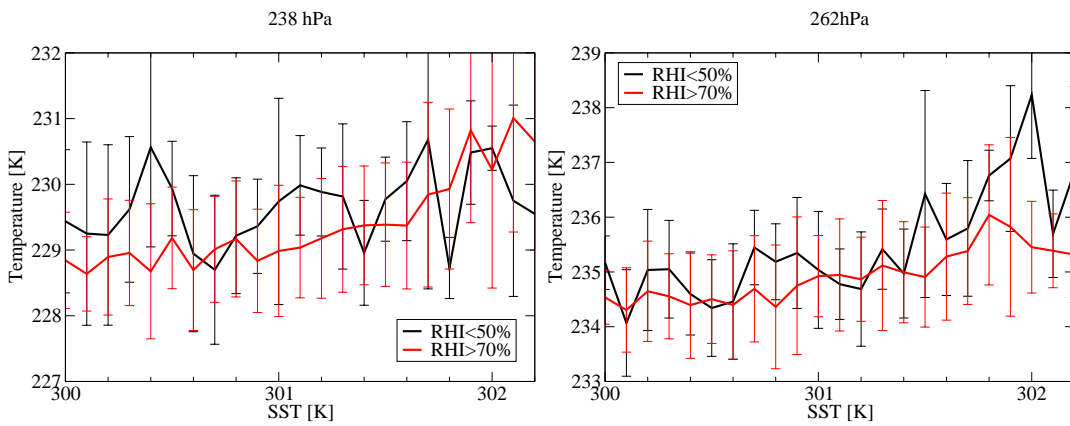


Figure 6.20: Temperature versus SST for 238hPa (left) and 262hPa (right), separated into the relative humidity modes.

6.2 Advection Away From Convective Regions

The development of the relative and specific humidities and also the ozone concentration for different trajectory lengths is studied in this section. It is distinguished between trajectory lengths in time and in space. At first, the dependence of the different parameters on the trajectory length in time will be shown, because time, not space, is the crucial parameter for radiative processes that play the most significant role during the transport of the air.

It must be stressed, that it is not possible to follow the development of the humidity along a single trajectory. Measurements are taken along the flight track of the aircraft, and the trajectories are used to trace the air parcel, the measurement was

taken in, back to the convective cloud that is located closest in the upwind direction. Every hourly bin includes a sample of mostly independent measurements that happen to have the same distance in time to their closest deep convective cloud. The resulting evolution of the relative humidity with distance from the convection represents a mean picture that certainly includes trajectories that have been influenced by different processes.

In order to study the dependence of the different parameters on the trajectory length in time the MOZAIC data are binned in groups per hour of trajectory length. The distribution of the data on these bins is shown in figure 6.21. About 20% of the

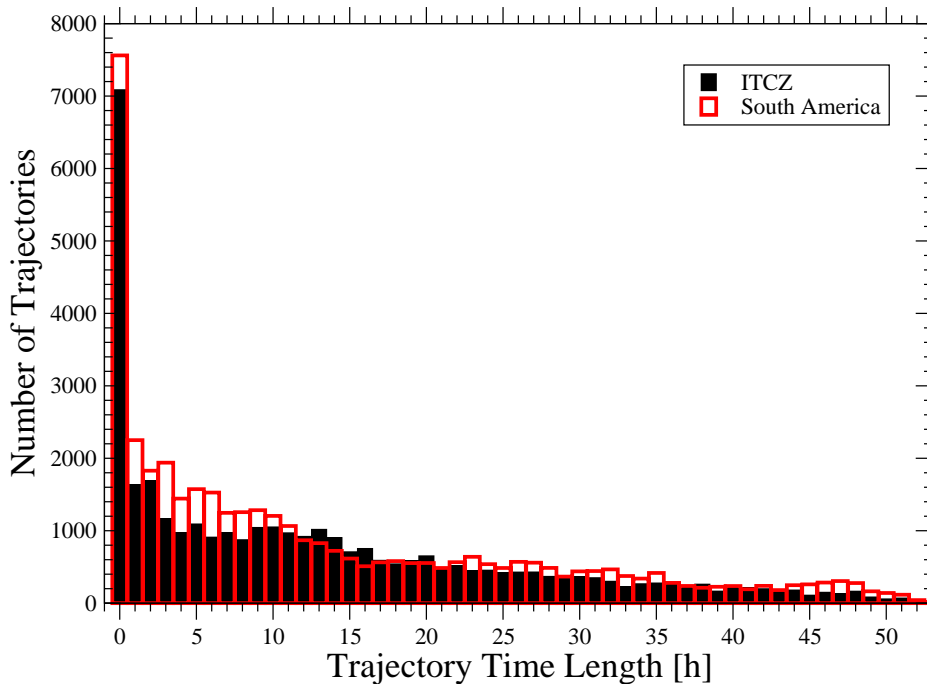


Figure 6.21: Histogram of trajectory length in hours.

trajectories encounter a convective cloud within the first hour. The number of measurements with one to two hours of trajectory length is only 5%, and it decreases slowly from there. Between 48 and 49 hours of trajectory length there are only 0.5% left. But these measurements are taken on more than 30 different flights for the convection found in the ITCZ alone and include samples from all years and all seasons. After 49 hours the number of measurements drops faster, as the trajectories are only calculated for approximately 2 days.

6.2.1 Development of Humidity

The relative humidity decreases with increasing trajectory length (figure 6.22). This decrease is similar over South America and the ITCZ. From the mean humidity of

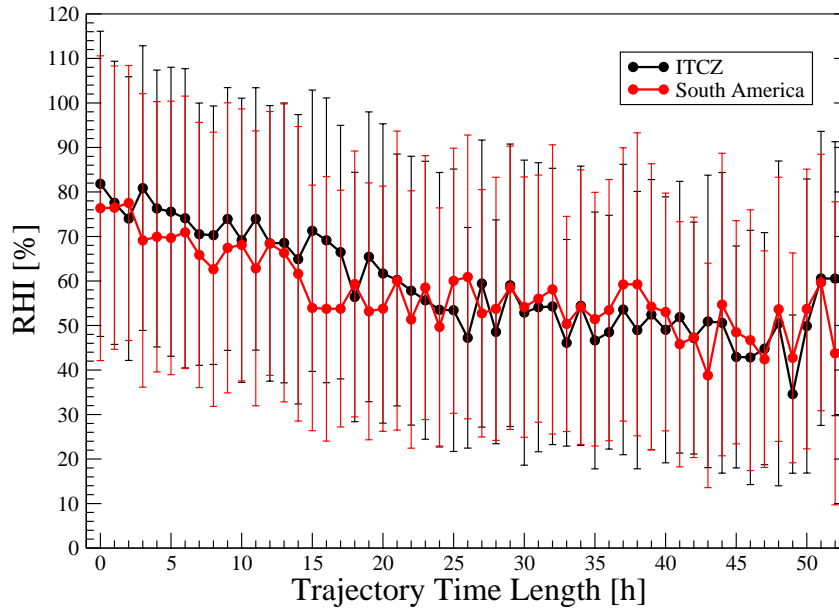


Figure 6.22: Relative humidity by trajectory length in hours for all pressure levels.

about 80% close to the convection it falls off to around 45% after 48 hours. The large standard deviations included as error bars in this plot are again only an indicator for the wide range of humidity values found in each bin. In order to examine whether the change in the mean relative humidity is due to a change in the humidity in each mode or a change in the fraction of measurements in each mode, the humidity measurements for each hourly bin are splitted into two parts (see section 6.1.4). The mean relative humidity of both modes (figure 6.23, left) does not change significantly

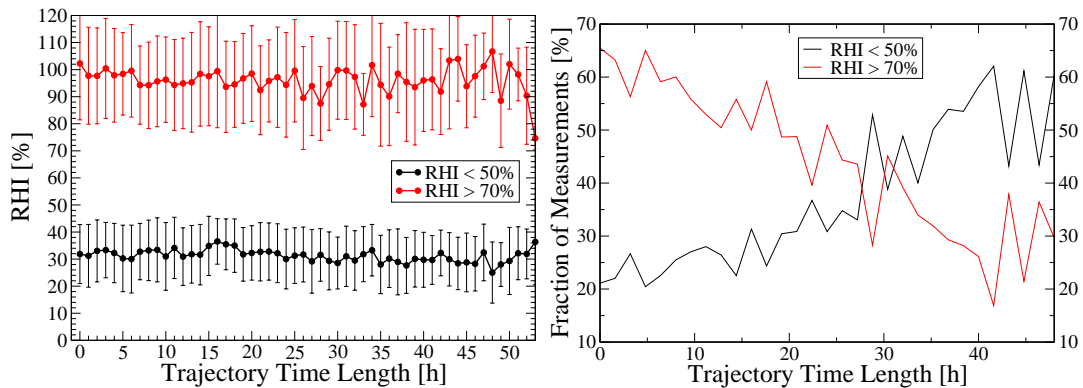


Figure 6.23: Relative humidity (left) and fraction of measurements (right) for both modes by trajectory length in hours for all pressure levels. Only measurements with trajectories originating in the ITCZ are shown.

for the different trajectory lengths. On the other hand, the fraction of measurements with relative humidities above 70% decreases from 60% to approximately 25% after

two days, while the fraction of measurements with relative humidities below 50% increases accordingly. Therefore, the change in the mean relative humidity is due to the proportion of the two modes.

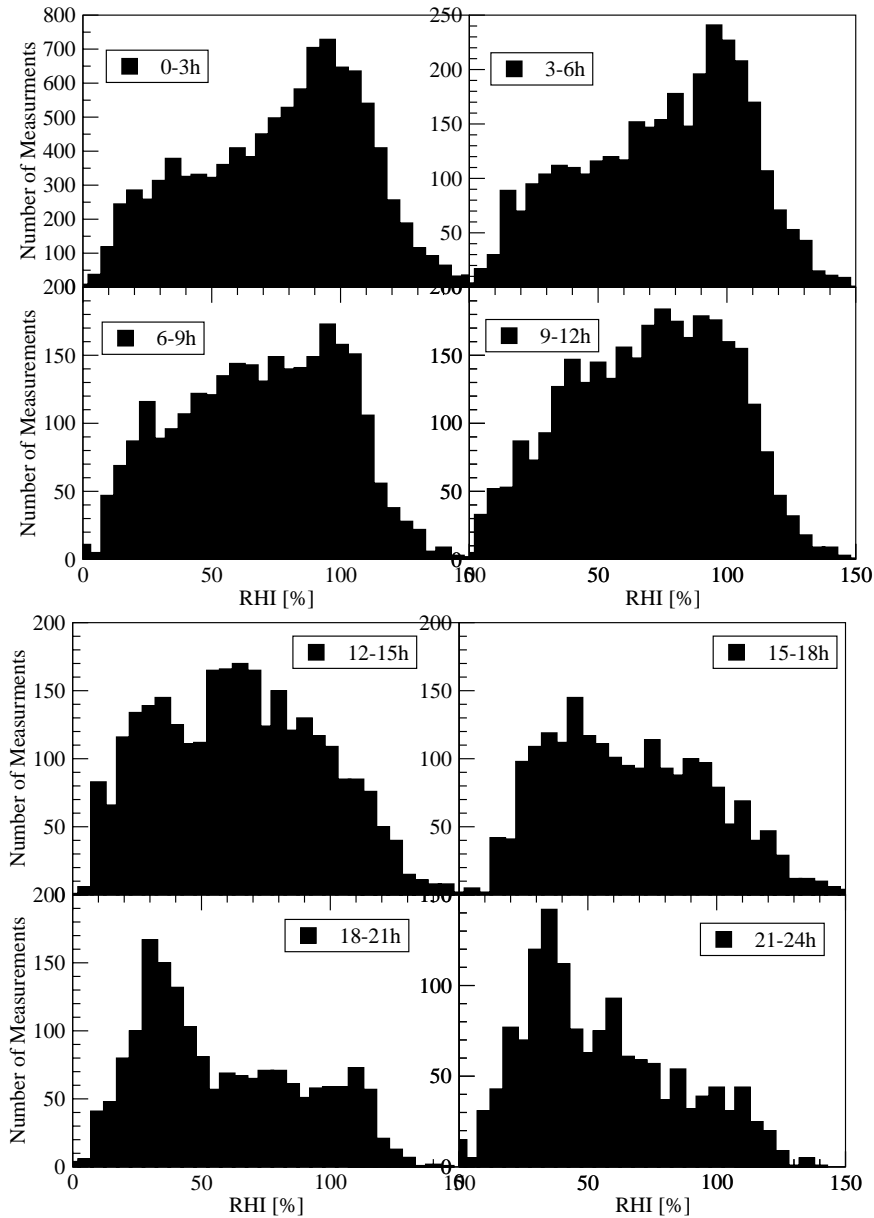


Figure 6.24: Histograms of relative humidity with respect to ice for every 3h of trajectory length. Shown is only the first day.

The distribution changes from a bimodal distribution with a primary maximum near saturation and a secondary maximum in the lower humidities close to the convection to a distribution which is dominated by a peak at very low humidities but has a large tail up to saturated values farther away from the convection (figure 6.24).

This happens entirely during the first day with the strongest change between 12h and 15h, when the distribution is intermediary. Up to 12h of trajectory length the saturated mode clearly dominates and after 15h the dry mode dominates. Between 12h and 15h the overlap region between the two modes dominates the distribution. There is only a minor further change during the second day (figure 6.25).

The question whether the decrease in relative humidity can be explained exclusively by radiative cooling and subsidence is addressed in chapter 7 for measurements of airparcels originating in the ITCZ.

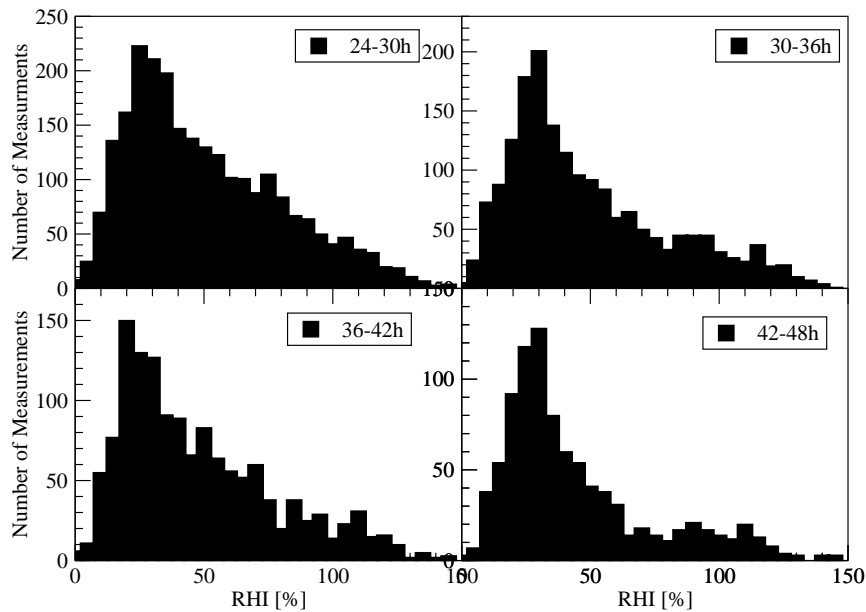


Figure 6.25: Histograms of relative humidity with respect to ice for every 6h of trajectory length during the second day.

6.2.2 Development with Spatial Distance

In order to examine the spatial distribution of the humidity relative to the distance from the convection, the mean relative humidity in 100km bins of trajectory length is shown next. In figure 6.26 the number of measurements per 100km bin is presented. About one third of all measurements are within 100km of a convective cloud and fall into the first bin. From there the number of measurements per bin falls off much more quickly relative to the maximum distance than the number of measurements per hour does relative to the 54 hours maximum duration. The reason for this behavior are the weak horizontal winds in the regions of high convective activity. Due to the small number of measurements at greater distances from convection the data basis is only sufficient to build reliable mean values up to a trajectory length of about 2000 km or even less for trajectories originating in the ITCZ.

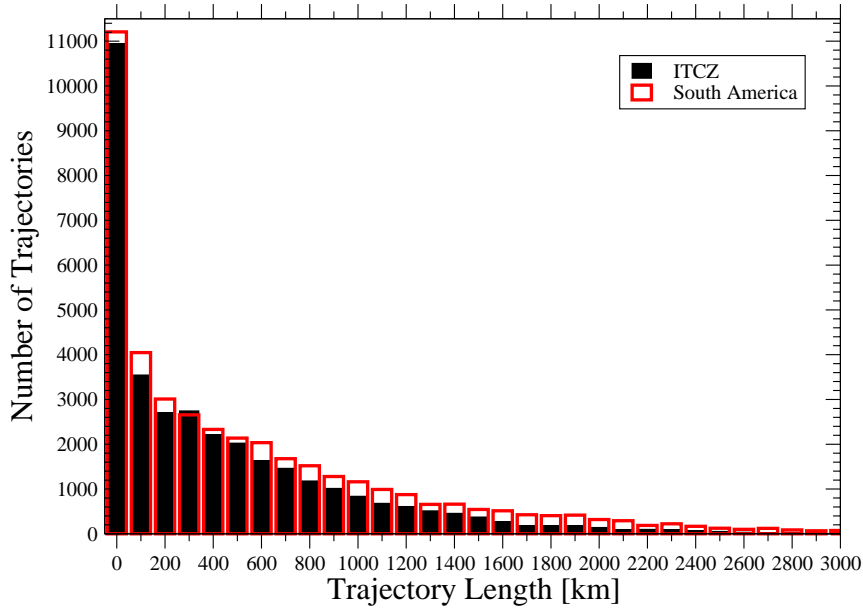


Figure 6.26: Histogram of trajectory length in km. The bins are every 100km.

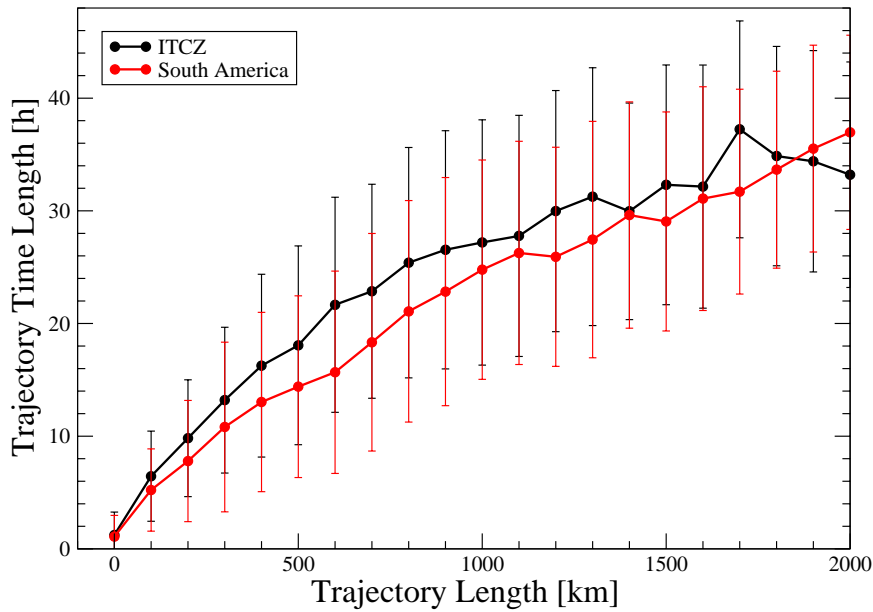


Figure 6.27: Trajectory time length mean and standard variation for 100km bins.

Figure 6.27 shows the mean trajectory time length for every 100km bin. The trajectories over the ITCZ take longer to reach a certain distance than the ones over South America except for those around 2000km length. The relative humidity decreases with spatial trajectory length similarly as with temporal trajectory length (figure 6.28). The difference is that the mean values stay higher than they do in figure 6.22

throughout the 2000km with sufficient data coverage. The South America values do not fall below about 50% and the ITCZ values stay at 55% after about 800 km and even rise at distances of more than 1500 km, where there are even fewer samples in the ITCZ than over South America. At these distances the mean time length of the ITCZ trajectories is almost constant and even decreases for distances larger than 1700km. This indicates that from the ITCZ only trajectories experiencing relatively high horizontal wind speeds reach these distances. Therefore, the slightly increasing relative humidities are connected to trajectories relatively short in time.

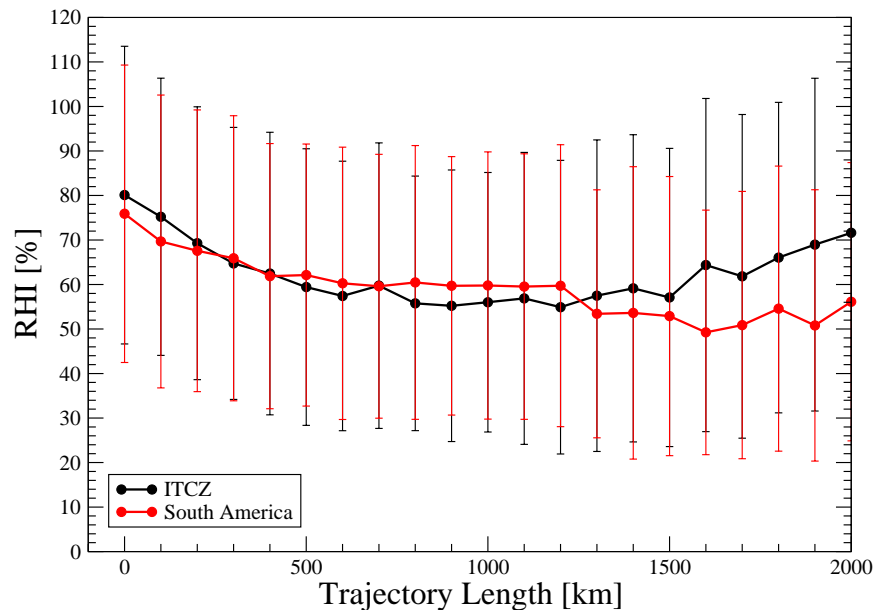


Figure 6.28: Relative humidity by trajectory length in km. 100 km bins like in figure 6.26.

6.2.3 Development of Ozone

The development of the ozone mixing ratio with trajectory time length (figure 6.29) is different over South America and over the ITCZ. Over South America it decreases from its initial value near 45ppbv to approximately 41ppbv after 1 hour. From there it increases to around 50ppbv after 48h. Over the ITCZ the mixing ratio starts at 36ppbv staying almost constant during the first 17h. Afterwards it increases slowly showing a higher variability on the second day. As the lifetime of ozone in the tropical upper troposphere is approximately 100 days (see section 2.3) chemical production or loss during two days is negligible. Therefore, the constant low level on the first day is an indicator that there is few small scale mixing not resolved by the trajectories. On the second day, the ozone concentration increases pointing to mixing processes. Unfortunately, the ozone gradients are not high enough to allow

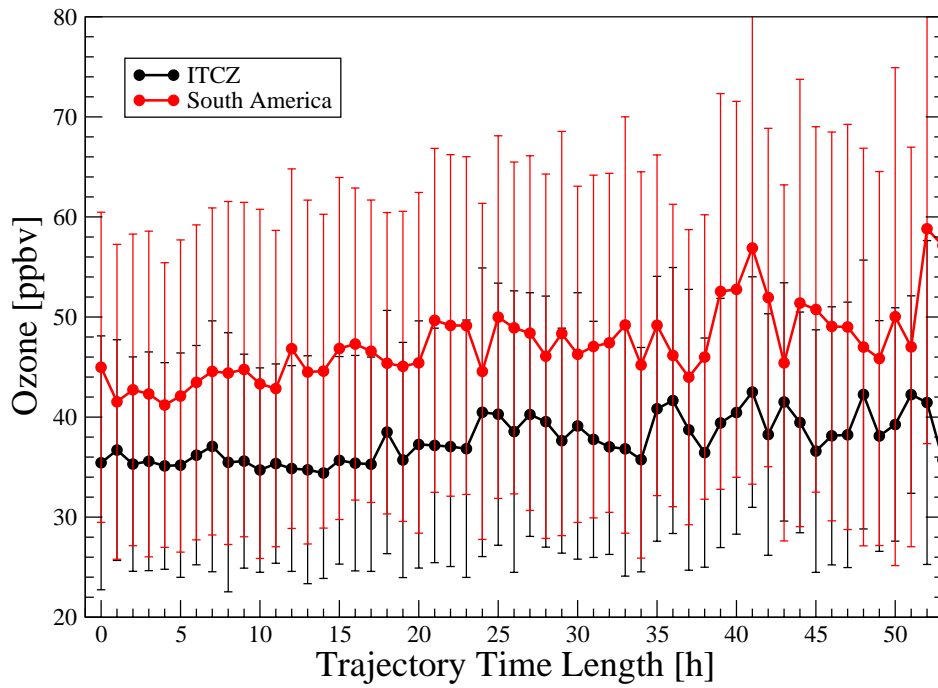


Figure 6.29: Ozone mixing ratio by trajectory length in hours for all pressure levels.

small scale mixing to make a significant difference in the mean ozone concentration. This makes it difficult to obtain a quantitative estimate of these mixing processes.

Chapter 7

Processes Influencing the Humidity of Convective Outflow

7.1 Introduction

In this chapter the dynamic and thermodynamic processes that are able to change the properties of an airparcel during the advection away from a convective region are studied in more detail. Only measurements in airparcels originating in the ITCZ are used to allow for the use of ozone as an indicator for mixing processes (section 2.3).

The key question is whether the decrease of the relative humidity along the trajectory (figure 6.22) is consistent with drying through subsidence induced by radiative cooling and the resulting adiabatic warming. Only the evolution of the mean relative humidity by time is examined as radiative processes depend on time. For a closer view at the relative humidity development the same data for the ITCZ as in figure 6.22 are presented in figure 7.1 without the standard deviation and with a 3 hours running mean added. From the starting value of approximately 80% near the cloud the relative humidity drops below 50% during the 48h of trajectory length. The decrease happens almost completely during the first 24h and the mean humidity is almost constant for all measurements with a trajectory length between 24h and 48h. This is consistent with the development of the distribution of the relative humidity (figure 6.25) that does not change significantly during the second day of trajectory length. The mean behavior during the first day of trajectory length is also consistent with the distribution of the relative humidity (figure 6.24). During the first 15h, while the distribution has its dominant mode near saturation, the mean relative humidity decreases only by 10%. After the distribution has changed, being dominated by dry measurements, the decrease is faster.

An indicator that the rate of decrease in mean relative humidity may not be consistent with clear-sky subsidence are the model results presented by Mapes (2001)

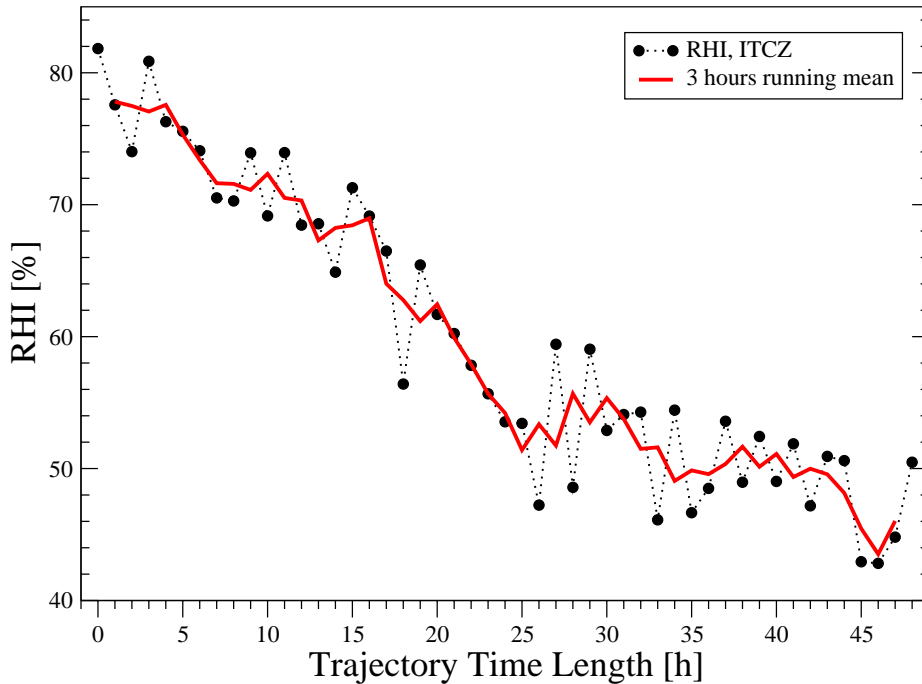


Figure 7.1: Mean relative humidity with respect to ice with distance (in hours) from convection (as in figure 6.22, but without the standard deviation). The red line indicates the 3 hours running mean.

(figure 2.3). The effect of radiative cooling is strongest in the MOZAIC measurement region around 11km altitude. After one day the relative humidity has already dropped to about half of its initial value. It is thus lower than the mean relative humidity from the MOZAIC measurements two days after the convection, although the mean starting relative humidity close to the convection is similar to that used by Mapes. Unfortunately, there is no other model study that presents the development of the relative humidity as Mapes does. What can be compared are results of radiative heating rates found with other models and different humidity data (Doherty and Newell, 1984; Clough et al., 1992; Ramsey and Vincent, 1995; Sherwood, 1996; Zhang and Chou, 1999; Hartmann et al., 2001).

In order to be able to compare the measurements with the literature values of radiative cooling rates, these rates have to be determined from the measurements. As the vertical motion in the ECMWF model is not reliable (section 5.2) it is determined from a conceptual model, because it is important for thermodynamical processes. In section 7.2 it is assumed that the air undergoes no mixing along the trajectory and the specific humidity stays constant. At least for measurements with less than one day of trajectory length this assumption is supported by the development of the ozone concentration (figure 6.29). From this assumption the temperature and pressure at the location of detrainment from the cloud is deduced under the condition

that the relative humidity at that location is known. The temperature difference between the point of detrainment and the MOZAIC aircraft is then determined to give the vertical velocity along the trajectory. This vertical velocity and the radiative cooling rate that is derived from it are compared in section 7.3 with the model results.

7.2 Subsidence During Large-Scale Advection

The air, that is advected away from the convective area, loses energy by emitting long-wave radiation. This radiative cooling leads to a sinking motion during which the air is compressed adiabatically and thus warmed. In the warming air the relative humidity is lowered very quickly. This way large parts of the tropical upper troposphere are filled with relatively dry air. The amount of water vapor in this air depends almost solely on the altitude at which it was detrained from the cloud. At that point the air is saturated and the relative humidity is close to 100%. The specific humidity depends on the local temperature and pressure.

During advection and subsidence the specific humidity of the air does not change, unless it is mixed with moister or drier air or hydrometeors evaporate. The relative humidity is then diminished according to the rising local temperature. Under the assumption that the air has a specified relative humidity at the point it left the cloud and that there was no mixing along the trajectory so that the specific humidity stays constant, the temperature and pressure at the point where the trajectory left the cloud can be determined. From this temperature and the temporal length of the trajectory the vertical velocity of the air can be calculated. The assumption that there is no mixing was made by others studying the influence of tropical convection on the humidity in the tropical upper troposphere (Udelhofen and Hartmann, 1995; Salathé and Hartmann, 1997). As a possible mixing would most likely be with drier air, this assumption gives an estimate of the maximum vertical velocity.

q_C as the specific humidity at the cloud edge is equal to q_A (in g/kg), the specific humidity calculated from the relative humidity and temperature measured at the aircraft, in the case without mixing. The specific humidity (or mixing ratio, see chapter 3) can be calculated from the local air pressure p_C and the local partial pressure of water vapor over ice $e_{I,C}$, both at the cloud edge (Curry and Webster, 1999):

$$q_A = q_C = 622 \frac{e_{I,C}}{p_C - e_{I,C}}. \quad (7.1)$$

As $e_I \ll p$,

$$q_A = 622 \frac{e_{I,C}}{p_C}. \quad (7.2)$$

With $\mathcal{H}_{I,C}$, the relative humidity with respect to ice (in %), the saturation vapor pressure $e_I(T_C)$ at the temperature at the cloud edge is:

$$e_I(T_C) = \frac{q_A p_C}{6.22 \mathcal{H}_{I,C}} \quad (7.3)$$

$e_I(T_C)$ can be calculated with the help of the Goff-Gratch formula (3.1). This way, $e_I(T_C)$ is eliminated from equation (7.3), which is then iteratively solved for T_C . For this purpose p_C is calculated from the pressure at the aircraft p_A and the temperature difference with the help of the local lapse rate $\gamma = dp/dT = 4hPa/K$ deduced from MOZAIC measurements at different pressure levels in the tropical region (dp/dT being nearly linear between 288hPa and 197hPa):

$$p_C = p_A + \gamma (T_C - T_A) \quad (7.4)$$

$$T_C = A / \left(\ln \left(\frac{q_A (p_A + \gamma(T_C - T_A))}{6.22 \mathcal{H}_{I,C}} \right) - (B + C T_C + D T_C^2 + E \ln T_C) \right) \quad (7.5)$$

For the relative humidity $\mathcal{H}_{I,C}$ the value 80% is taken, which is the mean from the measurements that were taken very close to convection.

A typical vertical velocity induced by radiative cooling is 22hPa/d (Sherwood, 1996). This would result in a temperature difference of only 5.5K per day. Therefore, the temperature at the aircraft T_A is chosen as the starting value to calculate T_C from equation (7.5). The iteration is stopped when the resulting temperature differs by less than 0.01K from the previous one. The pressure can then be calculated from the lapse rate as indicated above, cf. equation (7.4). The resulting temperature T_C and pressure p_C are merged with the MOZAIC and trajectory data so that the temperature difference between the aircraft and the cloud edge can be assigned to the time length of the trajectory. The vertical velocity is then determined by building means of the temperature difference for bins of one hour of trajectory time length as in section 6.2 (figure 7.2). A linear regression is applied to the three regions of different behavior in the development of the relative humidity distribution, the first 15 hours, hours 16 to 24 and the second day. The slope gives the subsidence rate for each region in K/h which is converted into km/d by using the lapse rate. The lapse rate is obtained from the MOZAIC measurements. The climatological mean value from measurements over the ITCZ in cruise altitude is 8.6 K/km. Comparison with single profiles over South America, where the aircraft start or land, shows similar values. In addition, data from balloon soundings on board the Polarstern along 30°W longitude (Smit et al., 1991) and in the scope of the SHADOZ (Southern Hemisphere ADditional OZonesondes) project (Thompson et al., 2002) in Natal (Brazil), Paramaribo (Surinam), and Ascension Island were taken into account and showed good agreement with the MOZAIC climatological mean value.

The mean vertical velocity calculated from the determined temperature difference between aircraft and cloud edge over 48h and the respective values for the three

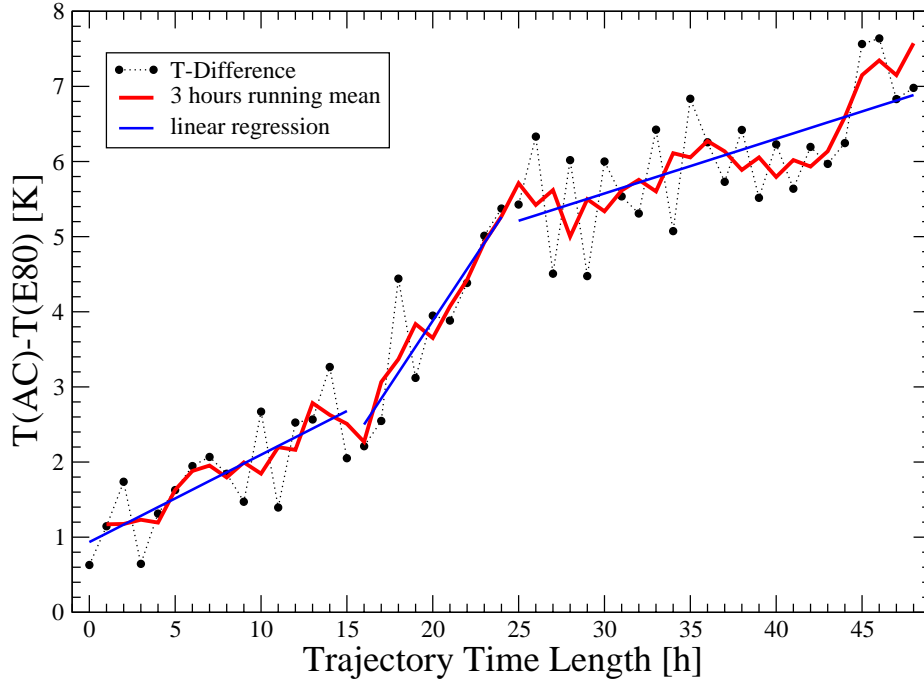


Figure 7.2: Mean temperature difference between the aircraft ($T(\text{AC})$) and the air at the point where the trajectory leaves the cloud ($T(\text{E80})$) under the assumption that the relative humidity at the cloud is 80 %. The red line indicates the 3 hours running mean and the blue lines show a piecewise linear regression for an estimate of the subsidence rate. The temperature difference is equivalent to the vertical displacement during the time of the trajectory length.

regions are presented together with the resulting radiative cooling rates in table 7.1. To calculate the rate of radiative cooling from the vertical velocity the hydrostatic energy equation is used (e.g., Holton (1992)):

$$\left(\frac{\partial T}{\partial t} + u \frac{\partial T}{\partial x} + v \frac{\partial T}{\partial y} \right) + (\Gamma - \gamma) w = J/c_p \quad (7.6)$$

with Γ being the dry adiabatic lapse rate, γ the actual lapse rate both in K/km , w the vertical velocity $w = dz/dt$, and J the radiative cooling rate. The specific heat c_p is $1.004J/(gK) \approx 1J/(gK)$, and the first term can be neglected as in the tropics horizontal temperature variations are very small and the variations in time are negligible on the timescales concerned. Therefore,

$$J = w(\Gamma - \gamma) \quad (7.7)$$

The radiative cooling rates given in table 7.1 are calculated with the MOZAIC climatological mean lapse rate of 8.6 K/km.

| Time Range | Slope [$\Delta T/h$] | Vertical Velocity [km/d] | Cooling Rate [K/d] |
|------------|------------------------|--------------------------|--------------------|
| 0 – 48 h | 0.14 ± 0.02 | 0.38 ± 0.07 | 0.46 ± 0.08 |
| 0 – 15 h | 0.12 ± 0.13 | 0.32 ± 0.36 | 0.38 ± 0.43 |
| 16 – 24 h | 0.35 ± 0.30 | 0.96 ± 0.84 | 1.15 ± 1.01 |
| 25 – 48 h | 0.07 ± 0.07 | 0.19 ± 0.20 | 0.23 ± 0.24 |

Table 7.1: Slope determined by linear regression from the derived mean temperature difference between cloud and aircraft by trajectory length, mean vertical velocities and radiative cooling rates. Shown are different ranges of trajectory lengths. The vertical velocities and cooling rates are calculated with the MOZAIC climatological mean lapse rate of 8.6 K/km. The standard deviations originate from the linear regression that includes the standard variations of the hourly mean temperature differences.

Except for the mean cooling rate over two days the determined radiative cooling rates have large standard deviations of approximately 100% of the mean value for the different time ranges. These standard deviations originate from the linear regression where the standard deviations of the hourly mean values are taken into account. Nevertheless, these numbers are based on a strong statistical background. In each hourly bin contributing to the mean values the slope is determined from, there are more than 130 measurements taken on more than 40 flights in all years and all seasons. The number of flights sampled with trajectory length of up to one day even exceeds 100 in every hourly bin.

7.3 Analysis of the Processes Influencing the Humidity

In this section the results from the previous section are discussed. The comparison with model results allows to draw conclusions about processes involved in the observed development of humidity with distance from the convection.

7.3.1 Comparison with Model Results

Radiative cooling rates from different radiative transfer models are presented in table 7.2. All the model calculations are made for clear-sky conditions. The numbers are taken from graphs which all show a significant gradient in the radiative cooling rate between 300 and 200hPa. The numbers presented are valid approximately at 220hPa. More than 75% of the measurements are taken below that level so that the cooling rates would be rather higher than the numbers given here. The cooling rates calculated by Ramsey and Vincent (1995) and Zhang and Chou (1999) were

| Source | Humidity Data | Model | Cooling Rate |
|--------------------------|-----------------------------------------------|----------------------------------------------------------|--------------------------------------------------------------------|
| Doherty and Newell, 1984 | Dopplick (1974) scaled standard profile | Dopplick (1970) | 1.25-1.4 K/day |
| Clough et al., 1992 | ICRCCM (WMO intercomparison study) | line-by-line radiance model FASCODE | 1.2 K/day |
| Ramsey and Vincent, 1995 | ECMWF | Harshvardhan, 1987 | 1.2 K/day only IR |
| Sherwood, 1996 | ECMWF + CEPEX (above 300 hPa) | LOWTRAN (LW) CCM2 (SW) | 22 mb/day (vert. vel.) \cong 0.71 K/day (with $\gamma=8.6$ K/km) |
| Zhang and Chou, 1999 | TOGA COARE | Chou and Suarez, 1994 | 1.5 K/day only IR |
| Hartmann, et al. 2001 | McClatchey, 1971 standard tropical atmosphere | Delta-four-stream scheme (Liou, 1988; Fu and Liou, 1992) | 1 K/day |
| Mapes, 2001 | RHI= 85 % RHI= 40 % | CCM2 | 1.4 K/day 0.8 K/day |

Table 7.2: Radiative cooling rates found in the literature from different radiance models with different humidity data for clear-sky situations near 220hPa.

only calculated for infrared radiation. As most of the flights take place in the early morning hours and the trajectories are not influenced by solar radiation for at least the first 8 hours, these values are still applicable during that time (figure 7.3).

All radiative cooling rates found in the literature (table 7.2) are higher than the derived mean value for the whole two days (table 7.1) by about a factor 2. Only the rate during the second period from 16 to 24 hours trajectory length is in the range of the data given by the model. The derived cooling rate on the second day is much lower and the one in the first 15 hours is also clearly smaller than the model results. The derived cooling rates are obtained from measurements of relative humidity alone under the assumption of no mixing and thus a constant specific humidity. Therefore, no distinction can be made between an additional source of energy not accounted for in the radiative transfer models (e.g., an additional absorber) or an additional source of humidity not accounted for in the conceptual model (e.g., hydrometeors) as the reason for the difference between the models and the derived values.

The most obvious reason for an inconsistency between the model results and the derived cooling rates is the possibility that the numbers are based on inconsistent conditions. Radiative cooling rates depend strongly on humidity. Therefore, the source of the humidity data used in the model influences the calculated values. As

the humidity profiles for the model calculations are based on conventional humidity techniques they are subject to the same limitations as discussed in section 2.5. The only model result with reliable upper tropospheric water vapor measurements is the one from Sherwood (1996). He obtains the lowest radiative cooling rate. Mapes (2001) on the other hand, who starts with a constant relative humidity of 85% on all altitude levels finds a much higher initial radiative cooling rate with partly the same model as Sherwood. His initial relative humidity is not too far from the mean values found in the MOZAIC climatology, although it certainly does not reflect the real humidity distribution.

All model calculations are carried out under clear-sky conditions and along the trajectories no high clouds are found from the Meteosat CDS. But although this dataset even includes a correction for semi-transparent clouds that would appear as being lower than in reality, there is still the possibility that thin cirrus are not detected as high clouds or even not detected at all. This could happen either if the radiative influence of the cloud is so small that the algorithms used to detect clouds fail or if the horizontal extend of the cloud is so small that the weighted average with other high clouds (see section 5.3) leads to an overestimate of the cloud top temperature. An upper estimate for the detection threshold of Meteosat are the properties of cirrus that are usually referred to as 'subvisible'. These clouds are abundant near the tropopause particularly over the Pacific ocean (e.g., Gierens et al. (2000); Mc-

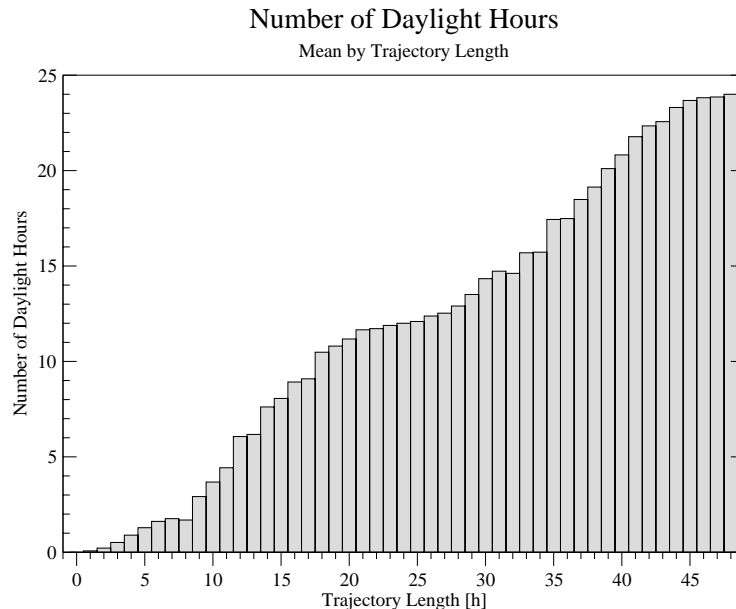


Figure 7.3: Mean number of daylight hours per 1 hour trajectory length bin. Daylight hours are all hours between 8:00 and 20:00 UTC, which is about 6:00 to 18:00 local time in the ITCZ. The solar zenith angle and temporal shifts for trajectories covering large zonal distances were not taken into consideration.

Farquhar et al. (2000)). They could have no influence on the cooling rate between 300hPa and 200hPa from there, though, as their radiative influence is confined locally (e.g., Ackerman et al. (1988); Sherwood (1999); McFarquhar et al. (2000)). In addition, their maximum ice water content of 0.002gm^{-3} (Ackerman et al., 1988) is too low to have an impact through precipitation to lower levels. At 197hPa and 218K, 0.002gm^{-3} are equivalent to a specific humidity of 0.006g/kg while the specific humidity at this level is at least 10 times higher.

A third possibility discussed by Sherwood (1996) as an explanation for the vertical velocities he finds in ECMWF analysis that are lower than his model results is the existence of an absorber of solar radiation not accounted for in the models. This can be excluded for this study at least for the inconsistency in the first 15 hours, due to the minor influence of sunlight during that time (figure 7.3).

7.3.2 The First Half of the First Day

From figure 6.24 it is known that a significant amount of measurements with trajectory length lower than 15h is near or above saturation. The percentage of measurements with a relative humidity above 100% relative to the number of all measurements in each hourly bin decreases from nearly 30% for shorter trajectories to about 15% (figure 7.4). In comparison with measurements from the Stratospheric

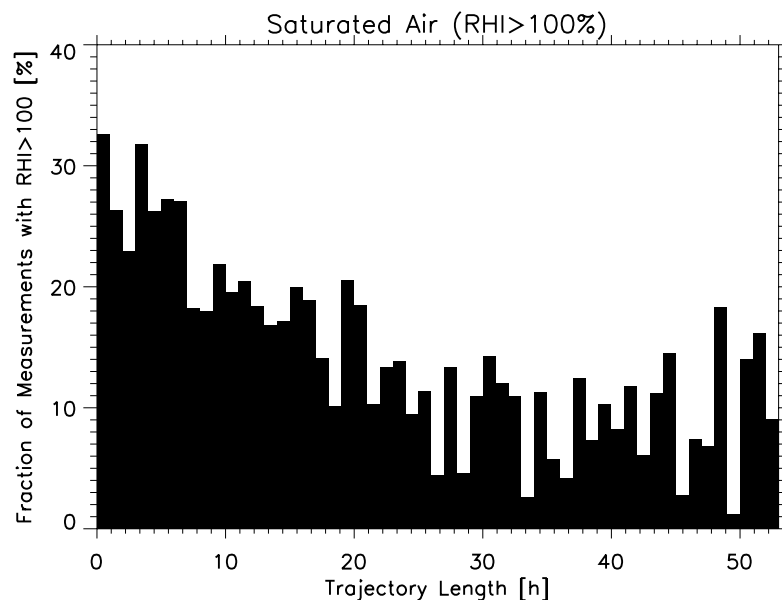


Figure 7.4: Fraction of measurements above 100% relative humidity with respect to ice by trajectory length in hours.

Aerosol and Gas Experiment (SAGE II) Gierens et al. (2000) show a connection between the areas of MOZAIC measured supersaturation and subvisible cirrus. The

frequency of occurrence of these clouds over the tropical Atlantic at an altitude of 10.5km (corresponding to the MOZAIC cruise altitude) from SAGE II measurements is also 20%-30%. Even in this altitude the evaporation of cloud particles alone could not explain the slower subsidence as the ice water content is in the same order of magnitude as for subvisible clouds at the tropopause (Gierens et al., 2000). However, radiative effects can have a significant influence. Heating rates induced by subvisible clouds are estimated to approximately the same size as the radiative cooling rates in clear-sky environment or even larger (e.g., Ackerman et al. (1988); McFarquhar et al. (2000)). They could balance the radiative cooling and thus prevent subsidence. Therefore, the air would not warm adiabatically and the relative humidity would be higher than in the surrounding, sinking air. Sherwood (1999) shows in a model study with cirrus clouds in different altitudes and with different optical depths that the absorption of radiation has an influence on the humidity up to an order of magnitude stronger than the evaporation of cloud particles. It is strongest for optically thin clouds between 200hPa and 300hPa. He also finds an enhancement of the lifetime of the clouds.

A similar model study by Dobbie and Jonas (2001) also shows a significant increase in cloud lifetime due to radiative processes. In addition, they find an enhancement of inhomogeneity and turbulence inside the cloudy layer. Turbulence could be an explanation for the measured supersaturation even after the air is transported away from a convective cloud for 12h and in the presence of ice particles.

7.3.3 The Second Half of the First Day

After 15h away from the convection the distribution of relative humidity changes to a mode in the dry range near 30% relative humidity. The decrease in mean relative humidity during the following hours is faster than in the other periods and the derived cooling rate is in the range of the model results. This is an indication for the presence of clear-sky conditions. Once the thin cirrus fall below a critical limit of optical depth due to wind shear the pumping mechanism fails and the clouds dissipate rapidly (Sherwood, 1999).

7.3.4 The Second Day

The very low subsidence rate on the second day are more difficult to explain. The influence of cirrus clouds on that second day is unlikely as the fraction of saturated air is rather low then. In addition, there is the period of faster sinking between hours 16 and 24 which would point to a disintegration of the cirrus detrained from the convective cloud by then. One possible reason for the low vertical velocity could be small-scale mixing processes playing a bigger role on the second day. This would

be confirmed by the development of the ozone concentration along the trajectory (figure 6.29). While it is rather constant and low on the first day it becomes more variable with larger mixing ratios on the second day. Unfortunately, an estimate of the order of magnitude of these mixing processes with the help of the ozone measurements is difficult, as the ozone concentration throughout the whole ITCZ is rather low and uniform.

Soden (1998) gives another confirmation of this phenomenon, though. He finds that the characteristics of the water vapor structures he follows to obtain trajectories become weaker after one day and points to small-scale mixing processes as an explanation. This would also lead to a reduced accuracy of the trajectories themselves possibly resulting in wrong trajectory lengths. Another reason could be the origin of the air farther away from the convection from higher altitudes. This air, that is very dry after the detrainment from the clouds has lower radiative cooling rates and therefore lower vertical velocities right from the beginning of the trajectory.

7.4 Conclusion

A summary of the results of this chapter is given in figure 7.5. It can be concluded

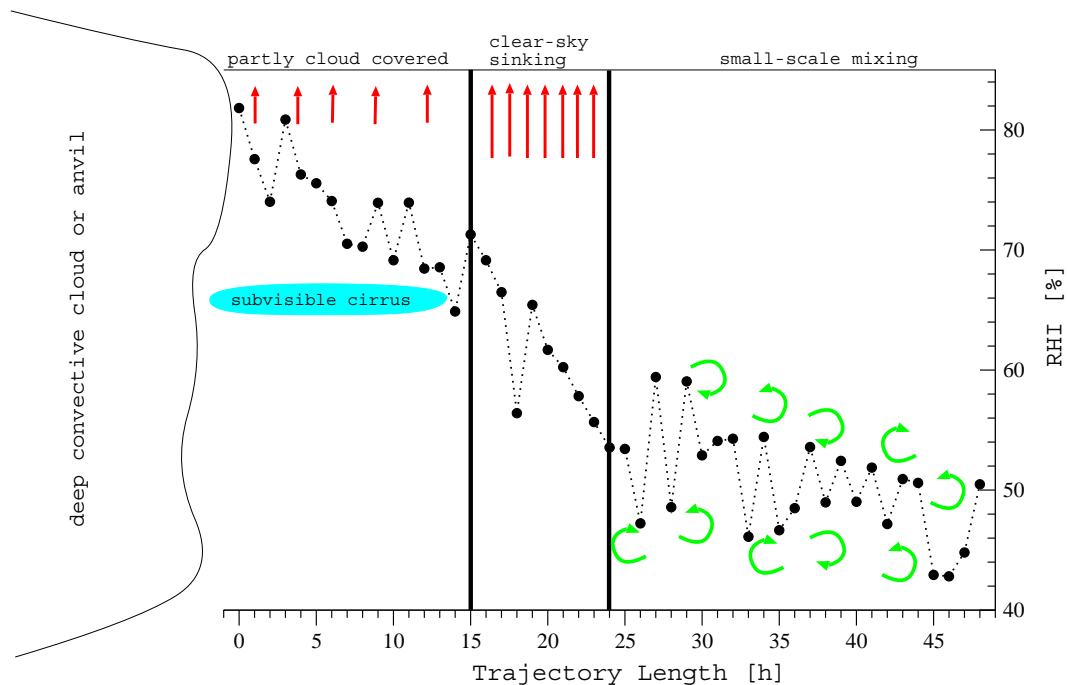


Figure 7.5: Summary of the results. The processes most likely involved in the slow decrease of the relative humidity are indicated relative to the trajectory length. The red arrows represent the radiative cooling.

that large portions of the cloud-free upper troposphere over the tropical Atlantic do not behave as expected from clear-sky radiative transfer models. This process can only apply to about 30% of the convective outflow as this is the fraction of supersaturated air near the cloud and also the average subvisible cirrus cover in the ITCZ above the tropical Atlantic. If 70% of the air does sink as expected under clear-sky conditions the radiative effect from clouds in the other 30% must be significant to result in a determined cooling rate of less than half of the clear-sky value. A quantitative estimate of this effect is difficult. Due to the sampling method it can not be distinguished whether the air parcel the measurements was taken in was supersaturated or even part of a subvisible cloud any time prior to the measurement. Therefore, the development of single air parcels can not be reconstructed.

The development of the mean relative humidity on the second day shows that the influence of convection and convective outflow in this region does not extend much farther than about one day or 1000km. After that, the mean humidity does not change much further most likely due to small scale mixing processes.

With regard to the question to what extent deep convection influences the humidity of the surrounding air it can be concluded, that the drying effect of the subsidence is not as strong as expected from clear-sky radiance models at least in the ITCZ over the Atlantic. In addition, the effect of single convective clouds does not reach very far, particularly not into the subtropical dry regions, which might be due to the abundance of convection in the ITCZ.

Chapter 8

Summary and Outlook

In this study, the extensive MOZAIC dataset was used to study the water vapor distribution over the Atlantic ocean and processes influencing the development of the humidity of tropical deep convective outflow during the transport away from the convection. A more than 4 year climatology of accurate in-situ measurements taken on board commercial aircraft on flights between Europe and South America in a cruise altitude between 10 and 12km is presented first. The water vapor distribution is highly variable in space and time. The highest humidities are found in midlatitudes and in the ITCZ which is always located between the equator and 10°N but moves within these latitudes during the seasonal cycle. It also shows seasonal and interannual variations in monthly mean humidity.

An interesting feature of the tropical atmosphere is the distribution of the relative humidity. Inside the ITCZ and above the warm ocean south of it, the distribution is bimodal. In addition to a maximum at very low humidity values there is a secondary maximum near saturation and also a significant amount of measurements above saturation. This secondary maximum becomes the primary one for measurements taken in the vicinity of convection while it almost vanishes farther away from convection and in particular in the subtropical region between 20°N and 30°N .

A comparison with ECMWF humidities interpolated to the same points the measurements were taken shows that the secondary maximum is not as pronounced as in the measured data. In addition, the amount of supersaturated air is much smaller. This leads to a dry bias of the ECMWF analysis compared to the measurements.

With the help of backward trajectories and satellite data of cloud top temperatures the origin of the measured air was traced back to areas of deep convection. It is shown that the meridional exchange is not very strong. For most measurements the convection is not more than 10 degrees of latitude away. Particularly in the ITCZ there is also only a very weak zonal circulation so that most measurements are taken very close to the originating convection. This means also that the distances between

convective clouds can not be very large. The analysis of air that was measured close to convective clouds shows that the mean relative humidity with respect to ice lies near 80% on all pressure levels and in all seasons as well over the South American continent as over the ITCZ. In contrast, the distribution of measured relative humidities is relatively wide with a significant number of measurements below 50%. This is most likely due to the limited extend of deep convective hot towers and the limited resolution of the CDS, so that the trajectories do not actually originate from the cloud but from the surrounding subsiding region. There are no significant altitudinal or seasonal variations in the mean relative humidity close to the convective cloud.

However, there is a variation in this mean relative humidity related to the sea surface temperature. In the sea surface temperature range where deep convective clouds are observed, between approximately 300K and 302K, the mean relative humidity increases from 70% to 90%. This increase in the mean of the bimodal distribution is mainly due to an increase in the relative amount of moist air near saturation and only partly due to an increase in the mean relative humidity of the moist mode. The temperature in the upper troposphere increases according to the increase in the sea surface temperature indicating no change in lapse rate. Due to this temperature increase, the specific humidity on a given pressure level increases with increasing sea surface temperature.

The development of the measured parameters during the transport away from the convection is studied by sorting the measurements by trajectory time length. Then mean values for every hour of trajectory length are taken as the mean state of the air at a given distance from the convection. The relative humidity with respect to ice decreases from its initial mean value of 80% to around 50% during the first day. After that it decreases only very slowly. The decrease is caused solely by a shift in the distribution. The relative number of measurements in the dry range increases while the percentage of measurements with higher relative humidity decreases. The specific humidity on single pressure levels does also decrease, and the ozone concentration stays constant on a low level in the ITCZ and a somewhat higher level over South America during the first day and increases slightly afterwards.

The central question addressed in this work is whether the decrease in relative humidity can be explained alone by radiative cooling and the resulting subsidence and adiabatic warming. For this purpose a radiative cooling rate is determined from the humidity data by assuming that the relative humidity at the convective origin of the air is 80%, and that there is no mixing along the trajectory so that the specific humidity stays constant. This cooling rate is compared to the published results from several different radiative transfer models. The comparison shows agreement between the data and the model only on the second half of the first day between 16 and 24 hours after the convection. In the first 15h the determined cooling rate is less

than half the value of most model results, and on the second day it is even smaller. The discrepancy in the first 15 hours can be explained with the existence of subvisible cirrus clouds in the vicinity of deep convective clouds. This is supported by the large number of measurements of saturated air even after more than 12 hours. The main effect of these clouds lies not in the evaporation of cloud particles, but in their efficient absorption of infrared radiation that can compensate for the radiative cooling. This absorption also increases the lifetime of the clouds and leads to inhomogeneities and turbulence causing areas of supersaturation even in the presence of ice particles.

The most plausible explanation for the small determined cooling rate on the second day is small scale mixing. The development of the mean ozone concentration that is constant on the first day, and becomes more variable and higher on the second day, gives an indication for this. The main conclusions are that the drying effect of the subsidence is not as strong as expected from radiance models and the influence of convection and convective outflow from the ITCZ does not extend much farther than about one day or 1000km.

The features that might be important to take into account in climate models are the bimodal distribution of the relative humidity and the larger fraction of supersaturated air as found in other datasets, for example in the ECMWF analysis. The effect of subvisible cirrus clouds on the humidity and thus their longer lifetime should be considered as well. It would be helpful to extend this work to a larger area of the Atlantic as well as to other parts of the world. Unfortunately, the latter could only be achieved by an extension of the MOZAIC project. An interesting region that could be studied with the existing data is the Caribbean sea if CTT data from GOES were used.

Cloud top temperature data at higher resolution would be necessary for a detailed analysis of the situation close to the convective cloud and a distinction between different types of clouds like mesoscale convective clusters, single hot towers, or anvils. Larger amounts of data could make further analysis possible such as a study of the dependence of the development of the relative humidity by trajectory length on the SST. A more quantitative analysis of the processes involved in the dynamics of the tropical upper troposphere could be accomplished with the help of a radiative transfer model driven with realistic humidity data.

Appendix A

Additional Graphs

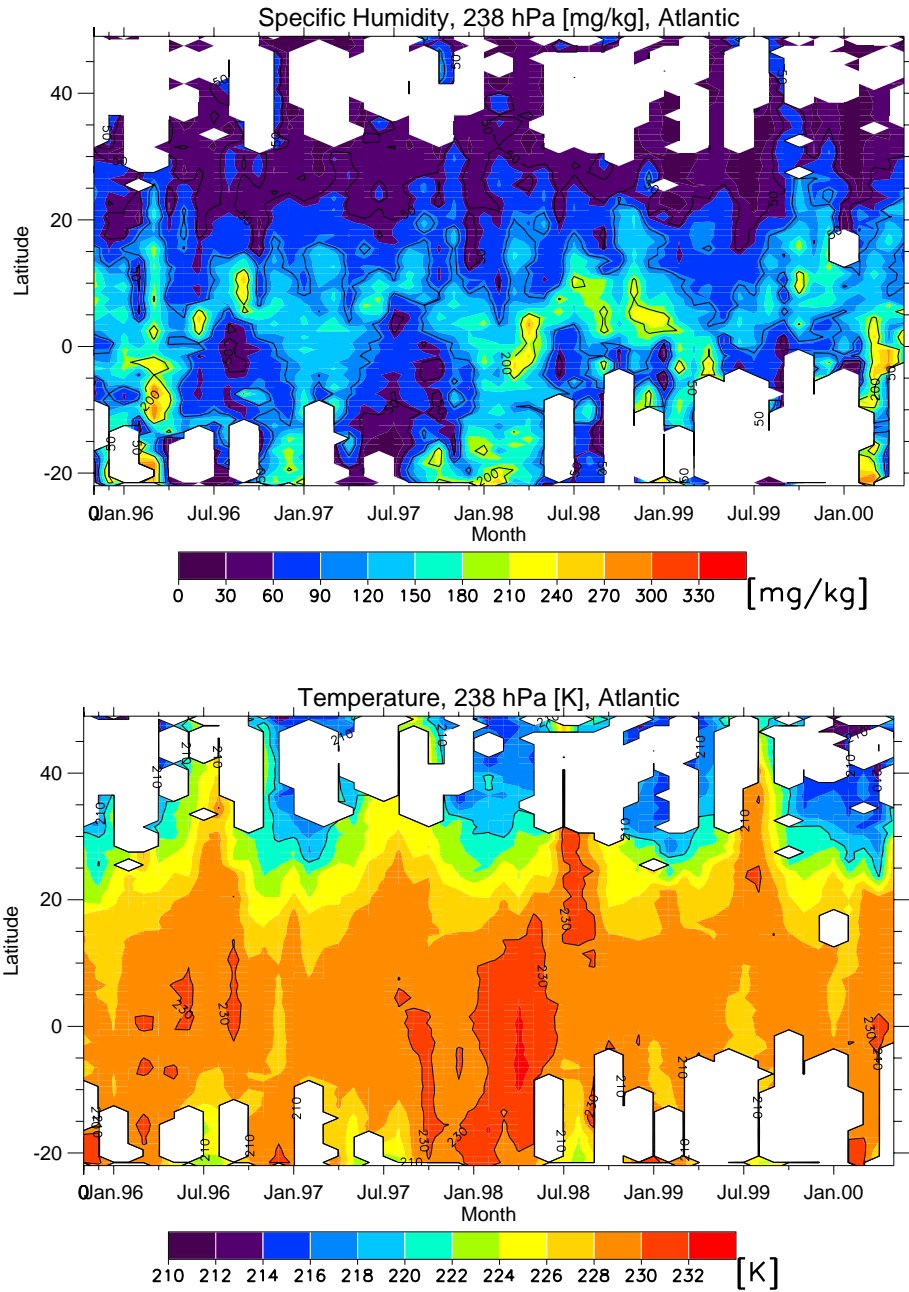


Figure A.1: Specific humidity and temperature from November 1995 to May 2000. Monthly mean by latitude for 238hPa pressure level. Same as figure 4.7.

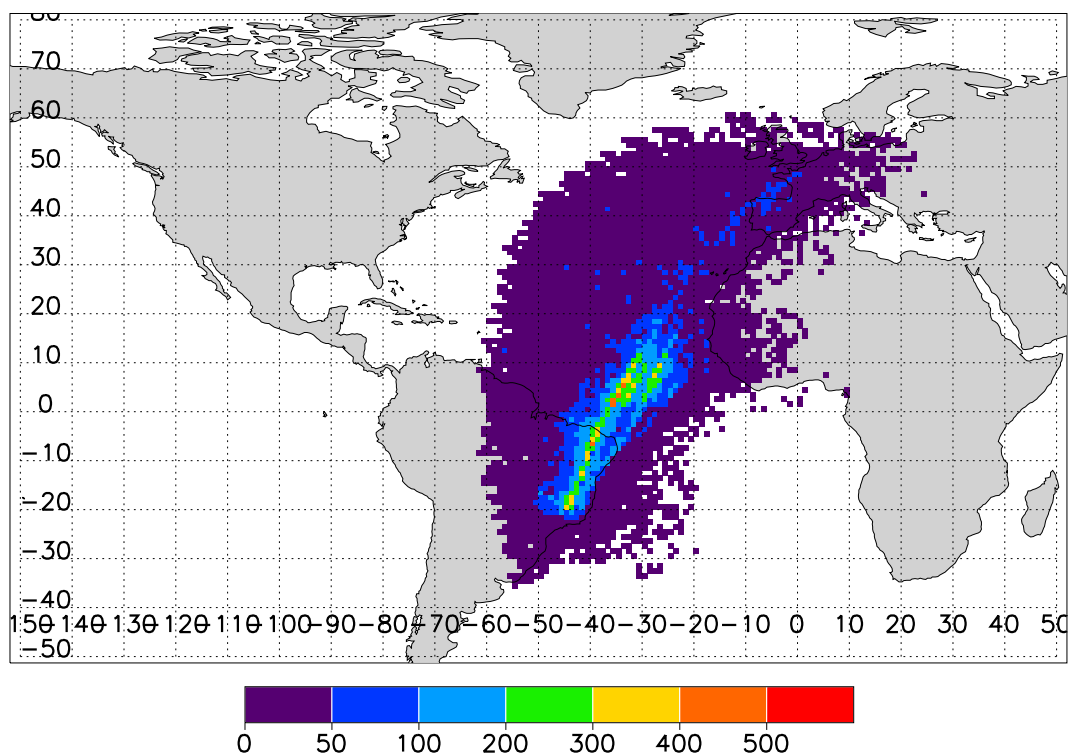


Figure A.2: Endpoints of trajectories that encounter a cloud. Number per $1^\circ \times 1^\circ$ grid box. Corresponding to figure 5.9.

Bibliography

- Ackerman, T. P., K.-N. Liou, F. P. J. Valero, and L. Pfister, Heating Rates in Tropical Anvils. *J. Atmos. Sci.*, **45**, 1606–1623, 1988.
- Anderson B. E., W. B. Grant, G. L. Gregory, E. V. Browell, J. E. Collins, G. W. Sachse, D. R. Bagwell, C. H. Hudgins, B. R. Blake, and N. J. Blake, Aerosols from biomass burning over the tropical South Atlantic region: Distributions and impacts. *J. Geophys. Res.*, **101**, 24,117–24,137, 1996.
- Arking, A., The radiative effects of clouds and their impact on climate. *Bull. Amer. Meteor. Soc.*, **71**, 795–813, 1991.
- Baede, A. P. M., E. Ahlonsou, Y. Ding, and D. Schimel, The Climate System: an Overview. In: *Climate Change 2001: The Scientific Basis. Contribution of Working Group I to the Third Assessment Report of the Intergovernmental Panel on Climate Change* [Houghton, J. T., Y. Ding, D. J. Griggs, M. Noguer, P. J. van der Linden, X. Dai, K. Maskell, and C. A. Johnson (eds.)] Cambridge University Press, 2001.
- Betts, A. K., Greenhouse warming and the tropical water budget. *Bull. Amer. Meteor. Soc.*, **71**, 1464–1465, 1990.
- Bony, S., J.-P. Duvel, and H. Le Treut, Observed dependence of the water vapor and clear-sky greenhouse effect on sea surface temperature: comparison with climate warming experiments. *Clim. Dyn.*, **11**, 307-320, 1995.
- Bony, S., K.-M. Lau, and Y. C. Sud, Sea Surface Temperature and Large-Scale Circulation Influences on Tropical Greenhouse Effect and Cloud Radiative Forcing. *J. Climate*, **10**, 2055-2077, 1997.
- Bouttier, F. and G. Kelly, Observing-system experiments in the ECMWF 4D-Var data assimilation system. *Q. J. R. Meteor. Soc.*, **127**, 1469–1488, 2001.
- Chen, M., R. B. Rood, and W. G. Read, Seasonal variations of upper tropospheric water vapor and high clouds observed from satellites. *J. Geophys. Res.*, **104**, 6193–6197, 1999.

- Chiang, J. C. H., S. E. Zebiak, and M. A. Cane, Relative Roles of Elevated Heating and Surface Temperature Gradients in Driving Anomalous Surface Winds over Tropical Oceans. *J. Atmos. Sci.*, **58**, 1371-1394, 2001.
- Chou, M.-D. and M. J. Suarez, An efficient thermal infrared radiation parameterization for use in general circulation models. NASA Tech. Memo. 104606, Vol. 3, 85pp., 1994.
- Clark, H. L., R. S. Harwood, P. W. Mote, and W. G. Read, Variability of water vapor in the tropical upper troposphere as measured by the microwave limb sounder on UARS. *J. Geophys. Res.*, **103**, 31695-31707, 1998.
- CLIMAP, The surface of the ice-age earth. *Science*, **191**, 1131-1144, 1976.
- Clough, S. A., M. J. Iacono, and J.-L. Moncet, Line-by-line calculations of atmospheric fluxes and cooling rates: Application to water vapor. *J. Geophys. Res.*, **97**, 15761-15785, 1992.
- Curry, J. A. and P. J. Webster, *Thermodynamics of Atmospheres and Oceans*. Academic Press, San Diego, 1999.
- Dessler, A. E. and S. C. Sherwood, Simulations of tropical upper tropospheric humidity. *J. Geophys. Res.*, **105**, 20155-20163, 2000.
- Dobbie, S. and P. Jonas, Radiative influence on the structure and lifetime of cirrus clouds. *Q. J. R. Meteor. Soc.*, **127**, 2663-2682, 2001.
- Doherty, G. M. and R. E. Newell, Radiative effects of changing atmospheric water vapour. *Tellus*, **36B**, 149-162, 1984.
- Dopplnick, T. G., *Global radiative heating of the earth's atmosphere*. Planetary Circulations Project, Department of Meteorology, MIT, 1970.
- Dopplnick, T. G., Radiative heating in the atmosphere. In *The general circulation of the tropical atmosphere and interactions with extratropical latitudes*, R. E. Newell, J. W. Kidson, D. G. Vincent, and G. J. Boer, editors. Volume 2, chapter 6, pages 1-25, 1974.
- Duhnke, K., H. G. J. Smit, D. Kley, A. Marenco, P. Speth, and J. Wefers, *Untersuchung der in MOZAIC gemessenen Ozon- und Wasserdampfverteilung im polaren Strahlstrom über dem Nordatlantik*. Jül-Bericht 3593, Forschungszentrum Jülich, 1998.
- Elliott, W. P. and D. J. Gaffen, On the utility of radiosonde humidity archives for climate studies. *Bull. Amer. Meteorol. Soc.*, **72**, 1507-1520, 1991.

- Eumetsat Meteorological Products Extraction Facility, *Meteosat Transition Programme, Algorithms Specification Handbook, Issue 2.0*. Eumetsat, Darmstadt, 1996.
- Eumetsat Meteorological Archive and Retrieval Facility, *Meteosat Archive User Handbook, Issue 2.2*. Eumetsat, Darmstadt, 1999.
- Fu, Q. and K.-N. Liou, On the correlated k-distribution method for radiative transfer in nonhomogeneous atmospheres.. *J. Atmos. Sci.*, **49**, 2139–2156, 1992.
- Fu, R., A. D. Del Genio, W. B. Rossow, and W. T. Liu, Cirrus-cloud thermostat for tropical sea surface temperatures tested using satellite data. *Nature*, **358**, 394–397, 1992.
- Gadgil, S., P. V. Joseph, and N. V. Joshi, Ocean-atmosphere coupling over monsoon regions. *Nature*, **312**, 141–143, 1984.
- Giannini A., J. C. H. Chiang, M. A. Cane, Y. Kushnir, and R. Seager, The ENSO teleconnection to the tropical Atlantic Ocean: Contributions of the remote and local SSTs to rainfall variability in the tropical Americas. *J. Climate*, **14**, 4530–4544, 2001.
- Gierens K., U. Schumann, M. Helten, H. G. J. Smit, and P.-H. Wang, Ice-supersaturated regions and sub visible cirrus in the northern midlatitude upper troposphere. *J. Geophys. Res.*, **105**, 22746–22754, 2000.
- Goff, J. A. and S. Gratch, Low-pressure properties of water from -160 to 212 F. *Trans. Amer. Soc. Heat. Vent. Eng.*, **52**, 95–122, 1946.
- Graham, N. E. and T. P. Barnett, Sea surface temperature, surface wind divergence, and convection over tropical oceans. *Science*, **238**, 657–659, 1987.
- Guilderson, T. P., R. G. Fairbanks, and J. L. Rubenstone, Tropical temperature variations since 20,000 years ago: Modulating interhemispheric climate change. *Science*, **263**, 663–665, 1994.
- Hack, J. J., B. A. Boville, B. P. Briegleb, J. T. Kiehl, P. J. Rasch, and D. L. Williamson, Description of the NCAR community climate model (CCM2). *NCAR Tech. Note NCAR/TN-382+STR*, Natl. Cent. for Atmos. Res., Boulder, Colo., 1993.
- Handoh, I. C. and G. R. Bigg,, A self-sustaining climate mode in the tropical Atlantic, 1995-1997: Observations and modelling. *Q. J. R. Meteor. Soc.*, **126**, 807–821, 1999.
- Harshvardhan, R. Davies, D. A. Randall, and T. G. Corsetti, A fast radiation parameterization for atmospheric circulation models. *J. Geophys. Res.*, **92**, 1009–1016, 1987.

- Harrison, E. F., P. Minnis, B. R. Barkstrom, V. Ramanathan, R. D. Cess, and G. G. Gibson, Seasonal-variation of cloud radiative forcing derived from the Earth Radiation Budget Experiment. *J. Geophys. Res.*, **95**, 18687–18703, 1990.
- Hartmann, D. L. and M. L. Michelsen, Large-Scale Effects on the Regulation of Tropical Sea Surface Temperature. *J. Climate*, **6**, 2049–2062, 1993.
- Hartmann, D. L., J. R. Holton, and Q. Fu, The heat balance of the tropical tropopause, cirrus, and stratospheric dehydration. *Geophys. Res. Lett.*, **28**, 1969–1972, 2001.
- Hastenrath, S., *Climate Dynamics of the Tropics*. Kluwer Academic Publishers, 1991.
- Held, I. M. and B. J. Soden, Water vapor feedback and global warming. *Annu. Rev. Energy Environ.*, **25**, 441–475, 2000.
- Helten, M., H. G. J. Smit, W. Sträter, D. Kley, M. Zöger, R. Busen, and P. Nedelec, Calibration and performance of automatic compact instrumentation for the measurement of relative humidity from passenger aircraft. *J. Geophys. Res.*, **103**, 25643–25652, 1998.
- Helten, M., H. G. J. Smit, D. Kley, J. Ovarlez, H. Schlager, R. Baumann, U. Schumann, P. Nedelec, and A. Marengo, In-flight comparison of MOZAIC and POLINAT water vapor measurements. *J. Geophys. Res.*, **104**, 26087–26096, 1999.
- Heymsfield, A. J., L. M. Miloshevich, C. Twohy, G. Sachse, and S. Oltmans, Upper-tropospheric relative humidity observations and implications for cirrus ice nucleation. *Geophys. Res. Lett.*, **25**, 1343–1346, 1998.
- Holton, J. R., *An introduction to dynamic meteorology*. Academic Press, San Diego, 1992.
- Inamdar, A. K. and V. Ramanathan, Physics of Greenhouse Effect and Convection in Warm Oceans. *J. Climate*, **7**, 715–731, 1994.
- Inamdar, A. K. and V. Ramanathan, Tropical and global scale interactions among water vapor, atmospheric greenhouse effect, and surface temperature. *J. Geophys. Res.*, **103**, 32177–32194, 1998.
- Jacob, D. J., B. G. Heikes, S.-M. Fan, J. A. Logan, D. L. Mauzerall, J. D. Bradshaw, H. B. Singh, G. L. Gregory, R. W. Talbot, D. R. Blake, and G. W. Sachse, Origin of ozone and NO_x in the tropical troposphere: A photochemical analysis of aircraft observations over the South Atlantic basin. *J. Geophys. Res.*, **101**, 24235–24250, 1996.

- Jensen, E. J., W. G. Read, J. Mergenthaler, B. J. Sandor, L. Pfister, and A. Tabazadeh, High humidities and subvisible Cirrus near the tropical tropopause. *Geophys. Res. Lett.*, **26**, 2347–2350, 1999.
- Kiehl, J. T., J. J. Hack, and B. P. Briegleb, The simulated Earth radiation budget of the National Center for Atmospheric Research community climate model CCM2 and comparisons with the Earth Radiation Budget Experiment (ERBE). *J. Geophys. Res.*, **99**, 20815–20827, 1994.
- Kiehl, J. T. and K. E. Trenberth, Earth's annual global mean energy budget. *Bull. Amer. Meteor. Soc.*, **78**, 197–208, 1997.
- Kley, D. and E. J. Stone, Measurements of water vapor in the stratosphere by photodissociation with Ly α (1216 Å) light. *Rev. Sci. Instrum.*, **49**, 691–697, 1978.
- Kley, D., E. J. Stone, W. R. Henderson, J. W. Drummond, W. J. Harrop, A. L. Schmeltekopf, T. L. Thompson, and R. H. Winkler, *In situ* measurements of the mixing ratio of water vapor in the stratosphere. *J. Atmos. Sci.*, **36**, 2513–2524, 1979.
- Kley, D., P. J. Crutzen, H. G. J. Smit, H. Vömel, S. J. Oltmans, H. Grassl, and V. Ramanathan, Observations of near-zero ozone concentrations over the convective pacific: Effects on air chemistry. *Science*, **274**, 230–233, 1996.
- Kley, D., H. G. J. Smit, H. Vömel, H. Grassl, V. Ramanathan, P. J. Crutzen, S. Williams, J. Meywerk, and S. J. Oltmans, Tropospheric water-vapor and ozone cross-sections in a zonal plane over the central equatorial Pacific ocean. *Q. J. R. Meteorol. Soc.*, **123**, 2009–2040, 1997.
- Kley, D., H. G. J. Smit, and V. Ramanathan, Regulation of deep convection through advection and entrainment of subtropical upper tropospheric air. *Proceedings of 23rd Conference on Hurricanes and Tropical Meteorology, Dallas, Texas*, American Meteorological Society, Boston, 1999.
- Klinker, E., F. Rabier, G. Kelly, and J.-F. Mahfouf, The ECMWF operational implementation of four-dimensional variational assimilation. III: Experimental results and diagnostics with operational configuration. *Q. J. R. Meteor. Soc.*, **126**, 1191–1215, 2000.
- Lau, K.-M., H.-T. Wu and S. Bony, The role of large-scale atmospheric circulation in the relationship between tropical convection and sea surface temperature. *J. Climate*, **10**, 381–392, 1997.
- Lindzen, Richard S., Some coolness concerning global warming. *Bull. Amer. Meteor. Soc.*, **71**, 288–299, 1990.

- Lindzen, R. S., M.-D. Chou, and A. Y. Hou, Does the earth have an adaptive infrared iris? *Bull. Amer. Meteor. Soc.*, **82**, 417–432, 2001.
- Liou, K.-N., *Radiation and cloud processes in the atmosphere*. Oxford University Press, New York, 1992.
- Liou, K.-N., Q. Fu, and T. P. Ackerman, A simple formulation of the delta-four-stream approximation for radiative transfer parametrizations. *J. Atmos. Sci.*, **45**, 1940–1947, 1988.
- Madden, R. A. and P. R. Julian, Description of a 40-50 day oscillation in the zonal wind in the tropical Pacific. *J. Atmos. Sci.*, **28**, 702–708, 1971.
- Madden, R. A. and P. R. Julian, Observations of the 40-50-day tropical oscillation – a review. *Mon. Wea. Rev.*, **122**, 814–837, 1994.
- Mahfouf, J.-F., Influence of physical processes on the tangent-linear approximation. *Tellus*, **51A**, 147–166, 1999.
- Mahfouf, J.-F. and F. Rabier, The ECMWF operational implementation of four-dimensional variational assimilation. II: Experimental results with improved physics. *Q. J. R. Meteor. Soc.*, **126**, 1171–1190, 2000.
- Manabe, S. and R. T. Wetherald, Thermal equilibrium of atmosphere with a given distribution of relative humidity. *J. Atmos. Sci.*, **24**, 241, 1967.
- Mapes, B., Water’s two height scales: the moist adiabat and the radiative troposphere. *Quart. J. Roy. Meteor. Soc.*, **127**, 2353–2366, 2001.
- Marenco, A., V. Thouret, P. Nédélec, H. G. J. Smit, M. Helten, D. Kley, F. Karcher, P. Simon, K. Law, J. Pyle, G. Poschmann, R. von Wrede, C. Hume, and T. Cook, Measurement of ozone and water vapor by Airbus in-service aircraft: The MOZAIC airborne program, An overview. *J. Geophys. Res.*, **103**, 25,631–25,642, 1998.
- McClatchey, R. A., R. W. Fenn, J. E. A. Selby, F. E. Volz, and J. S. Garing, *Optical properties of the atmosphere*. Air Force Geophysics Lab, 1971.
- McCormack, J. P., R. Fu, and W. G. Read, The influence of convective outflow on water vapor mixing ratios in the tropical upper troposphere: An analysis based on UARS MLS measurements. *Geophys. Res. Lett.*, **27**, 525–528, 2000.
- McFarquhar, G. M., A. J. Heymsfield, J. Spinhirne, and B. Hart, Thin and subvisual tropopause tropical cirrus: Observation and radiative impacts. *J. Atmos. Sci.*, **57**, 1841–1853, 2000.
- Newell, R. E., Climate and the ocean. *Am. Sci.*, **67**, 405-416, 1979.

- Newell, R. E., Y. Zhu, W. G. Read, and J. W. Waters, Relationship between tropical upper tropospheric moisture and eastern tropical Pacific sea surface temperature at seasonal and interannual time scales. *Geophys. Res. Let.*, **24**, 25-28, 1997.
- Philander, S. G., *El Niño, La Niña, and the Southern Oscillation*. Academic Press, 1990.
- Pierrehumbert, R. T., Thermostats, radiator fins, and the local runaway greenhouse. *J. Atmos. Sci.*, **52**, 1784–1806, 1995.
- Pierrehumbert, R. T., Lateral mixing as a source of subtropical water vapor. *Geophys. Res. Let.*, **25**, 151–154, 1998.
- Pierrehumbert, R. T. and R. Roca, Evidence for control of Atlantic subtropical humidity by large scale advection. *Geophys. Res. Let.*, **25**, 4537–4540, 1998.
- Pruppacher H. R., *Microphysics of clouds and precipitation*. Kluwer, Dordrecht, 1997
- Rabier, F., H. Järvinen, E. Klinker, J.-F. Mahfouf, and A. Simmons, The ECMWF operational implementation of four-dimensional variational assimilation. I: Experimental results with simplified physics. *Q. J. R. Meteor. Soc.*, **126**, 1143–1170, 2000.
- Ramanathan, V. and W. Collins, Thermodynamic regulation of ocean warming by cirrus clouds deduced from observations of the 1987 El Niño. *Nature*, **351**, 27–32, 1991.
- Ramsey, P. G. and D. G. Vincent, Computation of vertical profiles of longwave radiative cooling over the equatorial Pacific. *J. Atmos. Sci.*, **52**, 1555–1572, 1995.
- Raval, A. and V. Ramanathan, Observational determination of the greenhouse effect. *Nature*, **342**, 758–761, 1989.
- Read, W. G., J. W. Waters, D. L. Wu, E. M. Stone, Z. Shippony, A. C. Smedley, C. C. Smallcomb, S. Oltmans, D. Kley, H. G. J. Smit, J. L. Mergenthaler, and M. K. Karki, UARS MLS upper tropospheric humidity measurement: method and validation. *J. Geophys. Res.*, **106**, 32,207-32,258, 2001.
- Reynolds, R. W., A real-time global sea surface temperature analysis. *J. Climate*, **1**, 75–86, 1988
- Reynolds, R. W. and T. M. Smith, Improved global sea surface temperature analysis using optimum interpolation. *J. Climate*, **7**, 929–948, 1994
- Riehl, H., *Climate and Weather in the Tropics*, Academic Press, London, 1979.

- Salathé, E. P. and D. L. Hartmann, A trajectory analysis of tropical upper-tropospheric moisture and convection. *J. Climate*, **10**, 2533–2547, 1997.
- Scheele, M. P., P. C. Siegmund, and P. F. J. van Velthoven, Sensitivity of trajectories to data resolution and its dependence on the starting point: in or outside a tropopause fold. *Meteorol. Appl.*, **3**, 267–273, 1996.
- Sherwood, S. C., Maintenance of the free-tropospheric tropical water vapor distribution. Part I: Clear regime budget. *J. Climate*, **9**, 2903–2918, 1996.
- Sherwood, S. C., On moistening of the tropical troposphere by cirrus clouds. *J. Geophys. Res.*, **104**, 11,949–11,960, 1999.
- Simon, P., Ozone/Potential Vorticity correlations, pages 74–77. *MOZAIC-II technical final report*, 2000.
- Smit, H. G. J., S. Gilge, and D. Kley, *Ozone profiles over the Atlantic Ocean between 36°S and 52°N in March/April 1987 and September/October 1988*. Jül-Bericht 2567, Forschungszentrum Jülich, 1991.
- Smit, H. G. J., W. Sträter, M. Helten, and D. Kley, *Environmental simulation facility to calibrate airborne ozone and humidity sensors*. Jül-Bericht 3796, Forschungszentrum Jülich, 2000.
- Soden, B. J., Tracking upper tropospheric water vapor radiances: A satellite perspective. *J. Geophys. Res.*, **103**, 17069–17081, 1998.
- Soden, B. J. and J. R. Lanzante, An assessment of satellite and radiosonde climatologies of upper-tropospheric water vapor. *J. Climate*, **9**, 1235–1250, 1996.
- Spencer, R. W. and W. D. Braswell, How dry is the tropical free troposphere? implications for global warming theory. *Bull. Amer. Meteor. Soc.*, **78**, 1097–1106, 1997.
- Speth, P. and R. A. Madden, The observed General Circulation of the Atmosphere. *Landolt-Börnstein*, **4a**, Ch. 3, 1987.
- Stephens, G. L., On the relationship between water vapor over the ocean and the sea surface temperature. *J. Climate*, **3**, 634–645, 1990.
- Stocker, T. F., G. K. C. Clarke, H. Le Treut, R. S. Lindzen, V. P. Meleshko, R. K. Mugara, T. N. Palmer, R. T. Pierrehumbert, P. J. Sellers, K. E. Trenberth, J. Willebrand, Physical Climate Processes and Feedbacks. In: *Climate Change 2001: The Scientific Basis. Contribution of Working Group I to the Third Assessment Report of the Intergovernmental Panel on Climate Change* [Houghton, J. T., Y. Ding, D. J. Griggs, M. Noguer, P. J. van der Linden, X. Dai, K. Maskell, and C. A. Johnson (eds.)] Cambridge University Press, 2001.

- Stute, M., M. Forster, H. Frischkorn, A. Serejo, J. F. Clark, P. Schlosser, W. S. Broecker, and G. Bonani, Cooling of tropical Brazil (5°C) during the last glacial maximum. *Science*, **269**, 379–383, 1995.
- Sun, D.-Z. and R. S. Lindzen, Distribution of tropical tropospheric water vapor. *J. Atmos. Sci.*, **50**, 1643–1660, 1993a.
- Sun, D.-Z. and R. S. Lindzen, Water vapor feedback and the ice age snowline record. *Ann. Geophys.*, **11**, 204–215, 1993b.
- Thompson A. M., K. E. Pickering, D. P. McNamara, M. R. Schoeberl, R. D. Hudson, J. H. Kim, E. V. Browell, V. W. J. H. Kirchhoff, and D. Nganga, Where did tropospheric ozone over southern Africa and the tropical Atlantic come from in October 1992? Insights from TOMS, GTE TRACE A, and SAFARI 1992. *J. Geophys. Res.*, **101**, 24,251–24,278, 1996.
- Thompson, A. M., J. C. Witte, R. D. McPeters, S. J. Oltmans, F. J. Schmidlin, J. A. Logan, M. Fujiwara, V. W. J. H. Kirchhoff, F. Posny, G. J. R. Coetzee, B. Hoegger, S. Kawakami, T. Ogawa, B. J. Johnson, H. Vmel, and G. Labow, The 1998-2000 SHADOZ (Southern Hemisphere Additional Ozonesondes) Tropical Ozone Climatology: Comparisons with TOMS and Ground-based Measurements. *J. Geophys. Res.*, in press, 2002.
- Thouret, V., A. Marenco, J. A. Logan, P. Nédélec, and C. Grouhel, Comparison of ozone measurements from the MOZAIC airborne program and the ozone sounding network at eight locations. *J. Geophys. Res.*, **103**, 25,695–25,720, 1998.
- Tseng, L. and C. R. Mechoso, A quasi-biennial oscillation in the equatorial Atlantic ocean. *Geophys. Res. Let.*, **28**, 187–190, 2001.
- Udelhofen, P. and D. L. Hartmann, Influence of tropical cloud systems on the relative humidity in the upper troposphere. *J. Geophys. Res.*, **100**, 7423–7440, 1995.
- Vincent, D. G., A. Fink, J. M. Schrage, and P. Speth, High- and low-frequency intraseasonal variance of OLR on annual and ENSO timescales. *J. Climate*, **11**, 968–986, 1998.
- Waliser, D. E. and C. Gautier, A satellite-derived climatology of the ITCZ. *J. Climate*, **6**, 2162–2174, 1993.
- Waliser, D. E., N. E. Graham, and C. Gautier, Comparison of the highly reflective cloud and outgoing longwave radiation datasets for use in estimating tropical deep convection. *J. Climate*, **6**, 331–353, 1993.
- Waliser, D. E. and R. C. J. Somerville, Preferred latitudes of the Intertropical Convergence Zone. *J. Atmos. Sci.*, **51**, 1619–1639, 1994.

- Wallace, J. M. Effect of deep convection on the regulation of tropical sea surface temperature. *Nature*, **357**, 230–231, 1992.
- Winkler, P., Surface ozone over the Atlantic-ocean. *J. Atmos. Chem.*, **7**, 73-91, 1988.
- Zhang, C. and M.-D. Chou, Variability of water vapor, infrared radiative cooling, and atmospheric instability for deep convection in the equatorial western pacific. *J. Atmos. Sci.*, **56**, 711–723, 1999.
- Zhu, Y., R. E. Newell, and W. G. Read, Factors controlling upper-tropospheric water vapor. *J. Climate*, **13**, 836–848, 2000.

Danksagung/Acknowledgements

Ich danke Herrn Prof. Dr. D. Kley und Herrn Prof. Dr. P. Speth für die Vergabe des interessanten Themas, sowie die hilfreichen Diskussionen und Anregungen, und für die Begutachtung der Arbeit.

Herman Smit danke ich für viele aufschlussreiche Gespräche und Diskussionen, und für die Durchsicht der Rohfassung dieser Arbeit.

Für die Bereitstellung der MOZAIC-Daten bedanke ich mich bei den Mitarbeitern des MOZAIC-Projektes am Forschungszentrum Jülich, insbesondere Dr. Manfred Helten und Wolfgang Sträter, und auch bei den Mitarbeitern von CNRS/Toulouse und MeteoFrance/Toulouse, vor allem für die Bereitstellung der Trajektorien. Das MOZAIC Projekt wird von der Europäischen Kommission gefördert. Die Fluggesellschaften Lufthansa, Air France, Austrian Airlines und Sabena unterstützen das Projekt durch den kostenlosen Transport der Messinstrumente.

Sabine Schröder danke ich für ihre wertvolle Hilfe bei der Aufbereitung der CDS Daten, und Thomas Heil für die technische Unterstützung.

Ich möchte ausserdem allen weiteren Kolleginnen und Kollegen danken, die das ICG-2 (und II) zu einem angenehmen Arbeitsplatz gemacht haben.

Die CDS Daten wurden von Eumetsat, Darmstadt, kostenlos zur Verfügung gestellt. Ich danke Stephen Tjemkes und insbesondere Dr. Marianne König für die Programme, die mir das Lesen der Daten erleichtert haben, und für die prompte Beantwortung aller Fragen, die ich bezüglich der Daten hatte.

The NOAA Climate Diagnostics Center provides the Reynolds SST analysis on their Web site at <http://www.cdc.noaa.gov/>.

I also want to thank Rinus Scheele at KNMI, Netherlands for his introduction to the KNMI trajectory model and the trajectories for May 1995 that were very useful.

Thanks to Claude Boutron, Michèle Poinot, and all the other people who made

ERCA 2000 so very motivating and enjoyable.

Ich danke ausserdem Birgit Fischer und den (ehemaligen) DoktorandInnen, die mir geholfen haben durchzuhalten: Lars Hoppe, Astrid John, Dagmar Klasen, Bitu Kolaghar und Arnd Heiden, Johanna Kowol-Santen, Katja Mannschreck, Dorle Teuchert, Elmar Uherek.

Ganz besonders bedanke ich mich bei meinen Eltern und meiner Familie, die immer an mich geglaubt, und mich weit mehr als nur finanziell unterstützt haben.

Und Jan danke ich für seine Geduld und Unterstützung und natürlich auch für das sorgfältige Lesen der Rohfassung dieser Arbeit.

Zusammenfassung

Wasserdampf ist eines der wichtigsten atmosphärischen Spurengase mit bedeutendem Einfluss auf Chemie und Energiehaushalt der Atmosphäre und damit das Klima. Von grossem Interesse ist dabei die Wasserdampfverteilung in der oberen Troposphäre, insbesondere in den Tropen, da dort die meiste Sonnenergie aufgenommen wird, bevor sie dann in mittlere und hohe Breiten transportiert wird. Wasserdampf liefert ausserdem den wichtigsten Beitrag zum natürlichen Treibhauseffekt. Die mit dem atmosphärischen Wasserdampf zusammenhängenden Rückkopplungseffekte verursachen die grössten Unsicherheiten in heutigen Modellen zur Klimavorhersage.

Die wichtigste Wasserdampfquelle für die tropische obere Troposphäre ist tropische Konvektion. Grossräumigen Absinken, das seine Ursache sowohl in der Dynamik als auch im Strahlungshaushalt hat, gleicht die konvektive Aufwärtsbewegung aus, und transportiert dabei relativ trockene Luft in tiefere Luftschichten. Das Zusammenspiel dieser beiden Prozesse ist nicht gut verstanden, vor allem wegen des Mangels an zuverlässigen Messungen in dieser Region.

Von besonderem Interesse ist die Frage, welchen Einfluss tropische Konvektion auf die Feuchte der Umgebung hat. Für mögliche Rückkopplungseffekte spielt dabei vor allem die Abhängigkeit dieses Einflusses von der Oberflächentemperatur eine Rolle. Bei bisherigen Untersuchungen zu diesem Thema wurden Feuchte-Daten verwendet, die aus Satellitenmessungen bestimmt wurden. Solche Daten haben verschiedene Nachteile. Insbesondere ist die vertikale Auflösung meistens sehr grob. Dies führt dazu, dass aus der relativen Feuchte kein Zusammenhang zur spezifischen Feuchte hergestellt werden kann, da dieser stark von der Temperatur abhängt. Ausserdem erlauben die vorhandenen Satellitendaten nur eine rechnerische Bestimmung der Feuchte aus der gemessenen Strahlung. Die dabei verwendeten Algorithmen enthalten bereits Annahmen über die Eigenschaften der Atmosphäre, die die Berechnung der Feuchte beeinflussen können.

In dieser Arbeit werden der Wasserdampfgehalt und die Mechanismen, die für die Wasserdampfverteilung in der oberen tropischen Troposphäre verantwortlich sind, mithilfe eines grossen Datensatzes von in-situ Feuchtemessungen untersucht. Die Messungen wurden auf Linienflugzeugen grosser europäischer Fluggesellschaften im

Rahmen des EU Projektes MOZAIC durchgeführt (**M**easurements of **O**zone and **W**ater Vapor by **A**irbus In-Service **A**ir**C**raft; Messungen von Ozon und Wasserdampf auf Airbus Linienflugzeugen). Der einzige tropische Ozean, der regelmässig überflogen wurde, ist der tropische Atlantik. Dort gibt es seit Ende 1995 jeden Monat 10-20 Flüge.

Eine Klimatologie der gemessenen Parameter über dem tropischen Atlantik zeigt, dass die Feuchte auf allen Zeit- und Längenskalen sehr variabel ist. Durch die bimodale Verteilung mit sehr vielen Messungen extrem niedriger relativer Feuchte, aber auch einem hohen Anteil ge- und sogar übersättigter Luft, unterscheidet sich die Feuchte in den Tropen ausserdem deutlich von der Verteilung in den Sub- oder Extra-Tropen. In den Subtropen wird hauptsächlich sehr trockene Luft gemessen, während deren Anteil in mittleren Breiten niedrig ist. Darüberhinaus werden die Prozesse, die die Wasserdampfverteilung in den Gebieten mit absinkender Luft bestimmen, genauer untersucht. Der konvektive Ursprung der Luft wird dabei mithilfe von Rückwärts-Trajektorien, die im Rahmen des MOZAIC-Projektes von Meteo France (Toulouse) berechnet wurden, ausgehend von den MOZAIC-Messpunkten zurückverfolgt, und die konvektiven Wolken entlang der Trajektorien werden unabhängig davon mit METEOSAT Satelliten-Messungen der Wolkenoberflächentemperatur identifiziert.

Es zeigt sich, dass die konvektiven Wolken insbesondere in den inneren Tropen relativ nah an den Messungen liegen. Besonders der meridionale Austausch ist sehr schwach. In der Nähe von konvektiven Wolken liegt die mittlere relative Feuchte bei 80%. Sie variiert nur schwach mit der Höhe oder Jahreszeit. Die Verteilung der relativen Feuchte ist allerdings bimodal. Es werden zwar hauptsächlich hohe relative Feuchten nahe der Sättigung und auch darüber gemessen, ein deutlicher Anteil der Messungen liegt aber auch im trockenen Bereich um 20%-30%. Dieser hängt wahrscheinlich mit der geringen Ausdehnung der konvektiven Cumulonimbus-Türme zusammen. Ausserhalb dieser Türme sinkt die Luft ab und hat daher eine niedrige relative Feuchte. Durch die begrenzte Auflösung der Wolkenoberflächentemperatur-Daten kann nicht unterschieden werden, ob die Luft tatsächlich unmittelbar aus einer hohen Wolke kommt oder abgesunken ist.

Betrachtet man die Abhängigkeit von der Meeresoberflächentemperatur, bemerkt man einen Anstieg der mittleren relativen Feuchte mit dieser Temperatur. Konvektive Wolken werden für Meeresoberflächentemperaturen im Bereich von 300K bis 302K beobachtet. In diesem Temperaturintervall nimmt die relative Feuchte von 70% auf 90% zu, was hauptsächlich durch eine Zunahme der Anzahl sehr feuchter Messungen verursacht wird. Die Temperatur steigt etwa entsprechend der Meeresoberflächentemperatur an. Dies deutet darauf hin, dass sich der Temperaturgradient nicht ändert. Durch die lokale Temperaturzunahme steigt auch die spezifische Feuchte in der oberen Troposphäre mit der Meeresoberflächentemperatur.

Das Hauptthema dieser Arbeit ist die Untersuchung der Entwicklung der relativen Feuchte während des Transports von einer konvektiven Wolke in die Umgebung. Dazu werden die MOZAIC Messungen entsprechend der zugehörigen Trajektorienlänge sortiert. Es wird eine Abnahme der mittleren relativen Feuchte mit zunehmender Trajektorienlänge beobachtet, die durch eine Abnahme des Anteils von Messungen sehr feuchter Luft verursacht wird. Ob diese Abnahme allein durch ein strahlungsbedingtes Absinken der Luft mit nachfolgender adiabatischer Erwärmung erklärt werden kann, wird mit Hilfe eines Vergleichs mit Strahlungsmodellen untersucht. In der Luft, die von den konvektiven Wolken wegzieht und absinkt, nimmt im Mittel die relative Feuchte langsamer ab, als es aus Ergebnissen von Strahlungsmodellen, die ein rein strahlungsbedingtes Absinken unter wolkenlosen Bedingungen voraussetzen, erwartet würde. Man kann dabei in Bezug auf die Verteilung der relativen Feuchte drei zeitliche Bereiche unterscheiden. In den ersten 15 Stunden sinkt die Luft nur etwa halb so schnell wie in den Strahlungsmodellen. Nur zwischen Stunden 16 und 24 sinkt die Luft ungefähr so ab wie in den Modellen beschrieben, während am zweiten Tag das Absinken am langsamsten ist. Es gibt Hinweise darauf, dass optisch dünne Cirrus-Wolken in der Nähe der konvektiven Türme einen bedeutenden Einfluss auf das Strahlungsbudget haben. Dabei ist deren Einfluss durch Absorption von Strahlung wesentlich größer als durch die Verdampfung von Wolkenteilchen. Nach etwas einem Tag der Advektion von der konvektiven Wolke bleibt die relative Feuchte fast konstant, sehr wahrscheinlich aufgrund kleinskaliger Mischungsprozesse. Die trocknende Wirkung des grossräumigen Absinkens ist also im Mittel kleiner als bisher angenommen. Ausserdem erstreckt sich der Einfluss der Konvektion über dem tropischen Atlantik nur über eine Entfernung, die etwa einem Tag Transport entspricht.

Lebenslauf

Persönliche Daten

Name: Susanne Monika Nawrath
Geburtsdatum: 24. Dezember 1970
Geburtsort: Köln
Eltern: Franz Nawrath
Helga Nawrath geb. Kasper
Familienstand: ledig

Schulbildung

1977 - 1981 Johannes-Schule, Frechen-Königsdorf
1981 - 1990 Georg-Büchner-Gymnasium, Köln-Weiden
Mai 1990 Abitur

Hochschulstudium

Sept. 1990 Immatrikulation an der Universität zu Köln
Studiengang : Diplom-Geophysik
Oktober 1992 Diplom-Vorprüfung, Universität zu Köln
Mai 1995 mündliche Diplom-Hauptprüfung, Universität zu Köln
Juni 1995 - Juni 1997 Anfertigung der schriftlichen Diplomarbeit am
Institut für Geophysik und Meteorologie bei Prof. Dr. A. Ebel,
Thema: *Dynamik der Mesosphäre und unteren Thermosphäre,
untersucht mit Messungen des High Resolution Doppler Imager
auf dem Upper Atmosphere Research Satellite*

Dissertation

Nov. 1998 Beginn der Promotion an der Universität zu Köln
Institut für Geophysik und Meteorologie, Prof. Dr. P. Speth
seit Nov. 1998 Anfertigung dieser Dissertation am Forschungszentrum Jülich,
Institut für Chemie der belasteten Atmosphäre, Prof. Dr. D. Kley

berufliche Tätigkeiten

Jan. 1993 - Juni 1997 Studentische Hilfskraft (ab Januar 1997 Aushilfskraft) am
Institut für Geophysik und Meteorologie der Universität zu Köln
Sept. 1997 - Aug. 1998 "guest employee" und ab Mai 1998 "scientific assistant"
am Argonne National Laboratory, Argonne, USA
Environmental Reserch Division,
Atmospheric Section, Leiter: Dr. M. L. Wesely.
Nov. 1998 - Febr.. 2002 Wissenschaftliche Hilfskraft am Forschungszentrum Jülich,
Institut für Chemie der belasteten Atmosphäre, Prof. Dr. D. Kley

Ich versichere, dass ich die von mir vorgelegte Dissertation selbständig angefertigt, die benutzten Quellen und Hilfsmittel vollständig angegeben und die Stellen der Arbeit – einschließlich Tabellen, Karten und Abbildungen –, die anderen Werken im Wortlaut oder dem Sinn nach entnommen sind, in jedem Einzelfall als Entlehnung kenntlich gemacht habe; dass diese Dissertation noch keiner anderen Fakultät oder Universität zur Prüfung vorgelegen hat; dass sie – abgesehen von unten angegebenen Teilpublikationen – noch nicht veröffentlicht worden ist sowie, dass ich eine solche Veröffentlichung vor Abschluss des Promotionsverfahrens nicht vornehmen werde. Die Bestimmungen dieser Promotionsordnung sind mir bekannt. Die von mir vorgelegte Dissertation ist von Prof. Dr. P. Speth betreut worden.

Köln, den 15. März 2002

Susanne Nawrath

Keine Teilpublikationen